LIQUID CHROMATOGRAPHY COUPLED TO MASS SPECTROMETRY REVEALS THAT AGING AFFECTS LIPID DROPLET COMPOSITION

A DISSERTATION
SUBMITTED TO THE FACULTY OF THE GRADUATE SCHOOL
OF THE UNIVERSITY OF MINNESOTA
BY

MARZIEH RAMEZANI

IN PARTIAL FULFILLMENT OF THE REQUIREMENTS
FOR THE DEGREE OF
DOCTOR OF PHILOSOPHY

EDGAR A. ARRIAGA, ADVISOR

JULY, 2019

Acknowledgements

I would like to express my sincere gratitude to my advisor, Dr. Edgar A. Arriaga for his patience, motivation, and guidance over the years.

I would like to thank past and present graduate students and post-docs in the Arriaga group who contributed to this research.

I would like to thank the rest of my thesis committee, Dr. Michael T. Bowser, Dr. Timothy J. Griffin, and Dr. Danni Li for their insightful feedback for the thesis work presented here.

I would like to thank my manager, Stephen Andrichak for his understanding and encouragement in completing this work.

Finally and most importantly, I would like to thank my family. I would like to thank my husband and my best friend, Alireza, who is my daily motivation. I undoubtedly could not have done this without you. I would like to thank my parents, Mahmoud and Zohreh, and my sisters, Mohaddaseh and Maryam whose love and support are with me in whatever I pursue.

To

My wonderful husband, Alireza

Abstract

Lipid droplets (LD) are intracellular organelles controlling neutral lipid metabolism and storage. One of the recently discovered functions of LDs is the essential role they play in aging process. Alterations in membrane lipid composition are one of the major changes that are shown to take place in many of the aging models. An increase in cholesterol to phospholipid ratio was reported in rat models of aging. A reduction in the level of polyunsaturated fatty acyl is the next important age related variable observed in these aging systems. However, there is no systematic report characterizing the lipid composition of lipid droplets in aging models including *Caenorhabditis elegans* and mouse liver tissue.

In this thesis, ultra-high performance liquid chromatography coupled to mass spectrometry techniques were used to characterize the composition of lipid droplets. The performances of two high resolution mass spectrometers were compared with regards to detection and identification of small hydrophobic molecules. Different software packages and bioinformatics tools were compared to discover possible variation of the extracted information. The selected mass spectrometry platform and optimized data analysis workflow were used to study lipid droplets and identify candidate biomarkers of aging.

Preliminary identifications made here could potentially be used as biomarkers in aging diseases and could ultimately lead to treatments for age-related disorders.

Table of Contents

List of Tables

List of Figures

List of Abbreviations

AGC: Automatic gain control

APCI: Atmospheric pressure chemical-ionization

APPI: Atmospheric pressure photo-ionization

BHT: Butylated hydroxytoluene

C.elegans: *Caenorhabditis elegans*

CE: Capillary electrophoresis

CL: Cardiolipin

CS: ChemSpider

CV: Coefficient of variation

CVD: Cardiovascular disease

D1: Day 1

D4: Day 4

D7: Day 7

DI: Deionized water

DMEM: Dulbecco's Modified Eagle Medium

EDTA: Ethylenediaminetetraacetic acid

ESI: Electrospray ionization

FA: Fatty Acid

FAB: Fast atom bombardment

FTICR: Fourier transform ion cyclotron resonance

GC: Gas chromatography

h: Hour

HDMS: High definition mass spectrometry

HEPES: 4-(2-hydroxyethyl)-1-piperazineethanesulfonic acid

IM: Ion mobility

IM/MS: Ion mobility combined with mass spectrometry

LC: Liquid chromatography

LD: Lipid droplets

MALDI: Matrix assisted laser desorption ionization

min: Minute

MRM: Multiple reaction monitoring

MS: Mass spectrometry

NL: Neutral loss scanning

NMR: Nuclear magnetic resonance spectroscopy

Oa- TOF: Orthogonal acceleration time of flight

PA: Phosphatidic acid

PBS: Phosphate buffered saline

PC: Phosphatidylcholine

PCA: Principle component analysis

PE: Phosphatidylethanolamine

PG: phosphatidylglycerol

PI: Phosphoinositide

PNF: Post nuclear fraction

ppm: Parts per million

PREC: Precursor ion scanning

PS: Phosphatidylserine

Q-TOF: Quadrupole time of flight

S/N: Signal to noise

s: Second

SPM: Sphingomyelin

SPV: Sulfo-phospho-vanillin

Std Dev: Standard deviation

TAG: Triacylglyceride

TIC: Total ion chromatogram

TLC: Thin-layer chromatography (TLC)

TOF: Time of flight

UPLC: Ultra performance liquid chromatography

UPLC/MS: Ultra performance liquid chromatography coupled to mass spectrometry

UV: Ultraviolet

XIC: Extracted ion chromatograms

Chapter 1: Introduction

With a progressively growing elderly population, aging-associated pathologies such as heart disease, cancer, Alzheimer's, and diabetes are imposing a burden on global health.[1,2] It is estimated that the number of people 65 years of age and older is growing significantly from 524 million in 2010 to 1.5 billion in 2050.[3] In less developed countries the number of older people is expected to increase more than 250% between 2010 and 2050. Therefore, the study of aging and age-related diseases is vital to accompany the aging population with better health and wellbeing. The progression of aging is well known to result in dramatically altering lipid metabolism including lipid accumulation in skeletal muscle of aging patients.[4,5]

Lipid droplets (LD), the energy-reserve organelles, are dynamic organelles controlling neutral lipid metabolism and storage and participate in many critical cellular pathways.[6-9] One of the recently discovered functions of LDs is the essential role they play in longevity regulation.[10] Although the role and biogenesis of lipid droplets are relatively well studied, little is known about their composition and structure in aging.[11,12] Further characterization of lipid droplets is necessary to understand how the dynamics of this organelle is affected during chronological aging process which could ultimately lead to treatments for age-related disorders and diseases.[13] The elucidation of the distribution of lipids in subcellular organelles is a major challenge. Lack of methodologies and proper tools to analyze and process the complex data generated by untargeted lipid analysis makes it further complicated.[14] To address this issue, several lipidomics workflows have been developed to make reliable identifications of individual lipid species.

The goal of this thesis was to investigate the composition of lipid droplets during aging. Mass spectrometry methods and bioinformatics tool were utilized to gain insights of the composition of enriched lipid droplets from the worm *Caenorhabditis elegans* (*C. elegans*) and mouse liver tissues. A non-targeted liquid chromatography coupled to mass spectrometry (LC/MS) method and bioinformatics were applied to make preliminary identifications of lipids with altered abundance in lipid droplets during aging.

Chapter 2 covers the background of this thesis to expand upon the key points related to biochemistry of lipids and their major tasks in energy storage, structural functions, and cellular signaling. This chapter introduces lipid droplets as the subcellular organelles that store neutral lipids, and their importance in maintaining the health of an organism. Several analytical techniques used widely in lipidomic studies of biological matrices are discussed. This chapter further summarizes the computational tools for successful functional interpretation of lipidomic experiments.

Chapter 3 describes a comparison of two high resolution mass spectrometry platforms for lipidomic analyses. The level of diversity and high degree of molecular heterogeneity of lipids generates a need in developing advanced analytical methodologies. The goal of this study was to evaluate the performances of the two mass analyzers in terms of number of detected features, ability to utilize enhanced resolution to better resolve analytes in complex matrices, metabolite identification, and detection of very low abundant compounds. This chapter describes several bioinformatic tools and software packages and

compares the main data processing steps used in metabolomics research. Synapt G2 Q-TOF mass spectrometer and XCMS software were chosen for further studies.

Chapter 4 covers the bioanalytical strategies used to identify small molecules and lipids that significantly change in abundance between different *C. elegans* age populations. This chapter describes *C. elegans* as a model organism that has contributed significantly to the understanding of the biology of aging of multicellular organisms, including humans. The goal of this chapter was to investigate and compare the age related changes to the composition of lipid droplets purified from Day 1, Day 4, and Day 7 worms utilizing LC/MS. Our analysis identified unique lipid profiles specific to the age of the worm. We observed that lipid droplets have increased triglyceride content and decreased phospholipid content with age.

Chapter 5 describes LC/MS analysis of lipids in lipid droplet fractions of young and geriatric mice liver tissue. The goal of this chapter was to characterize age specific distributions of lipids. Preliminary identifications show that enriched lipid droplet fractions have characteristic lipidomic profiles specific to their age including increased triglyceride and decreased phosphatidylcholine and phosphatidylethanolamine content with age. Preliminary identifications made here could be further validated and investigated for their specific role in aging.

Chapter 6 covers the conclusions and future work. We have characterized the lipidome of lipid droplets in two different model organisms under different age conditions. These preliminary identifications are valuable in understanding the composition of lipid

droplets and changes in their compositions in aging. This chapter also describes future improvements to the analytical techniques, including sample preparation, LC/MS analysis, validation of the preliminary identifications, and bioinformatics of lipidomic data.

Overall, the work described in this thesis contributes to our fundamental understanding of lipid droplets and how their lipidomic profile changes in aging. The findings in this thesis add significantly to the field of lipidomic analysis and may result in new studies to determine the role of aging in lipid droplet biology.

Chapter 2: Background

2.1. Metabolomics

Metabolomics employs analytical instrumentation to comprehensively identify and analyze hundreds of small molecules (metabolites) in a given biological sample (biofluid, tissue, cells, etc.).[15] Metabolomics play a major role in early detection and diagnosis of variety of diseases that are known to alter cellular metabolism.[16] Recent advances in analytical instrumentation including mass spectrometry and statistical tools have provided metabolomics the ability to probe much further into disease biomarker discovery.[17] The search for metabolites as biomarkers has been particularly common in the area of neurodegenerative disease. Metabolomic studies of aging have sought potential biomarkers of age-related diseases.[18] Comparing quantifications of individual metabolites between diseased and control individuals allows researchers to determine if specific molecules are significantly different between the two groups. Modern metabolomics depends almost entirely on analysis by mass spectrometry and chromatography techniques which have greatly promoted the field.[19] There are two main subtypes: targeted metabolomics, which measures a selected set of metabolites[20] and untargeted metabolomics, which assesses metabolites in an unbiased manner.[21,22] In both targeted and untargeted metabolomics, quantification is performed by comparing signal intensities across different sample groups.

2.1.1. Lipidomics

Lipids are ubiquitous group of compounds exhibiting enormous structural diversity and are grouped under the following eight categories: Fatty acids, Glycerolipids, Glycerophospholipids, Sphingolipids, Sterols, Prenols, Saccharolipids, and Polyketides.[23]

Representative structures of lipid classes are summarized in Figure 2.1. Each category contains distinct classes, subclasses, subgroups, and subsets of lipid molecules with different physiochemical properties.[24] Polar lipids including glycerophospholipids, sphingolipids, and sterol lipids are classified based upon their headgroup moieties and interact with membrane proteins via hydrogen bonding. Neutral or non-polar lipids including sterol esters and glycerolipids participate in non-covalent interactions through their hydrocarbon chains with other lipids and hydrophobic regions of proteins.[25] These interactions have important consequences for the mechanisms of lipid functions.

The large number of categories and the extremely complex structures of lipids lead to a formidable challenge to comprehensively analyze lipids in biological matrices. The large-scale analysis of lipids in cells and tissues was made possible by a newly emerged discipline known as lipidomics.[26,27] Lipidomics studies lipids on a large scale utilizing analytical chemistry principles and technological tools, particularly mass spectrometry.

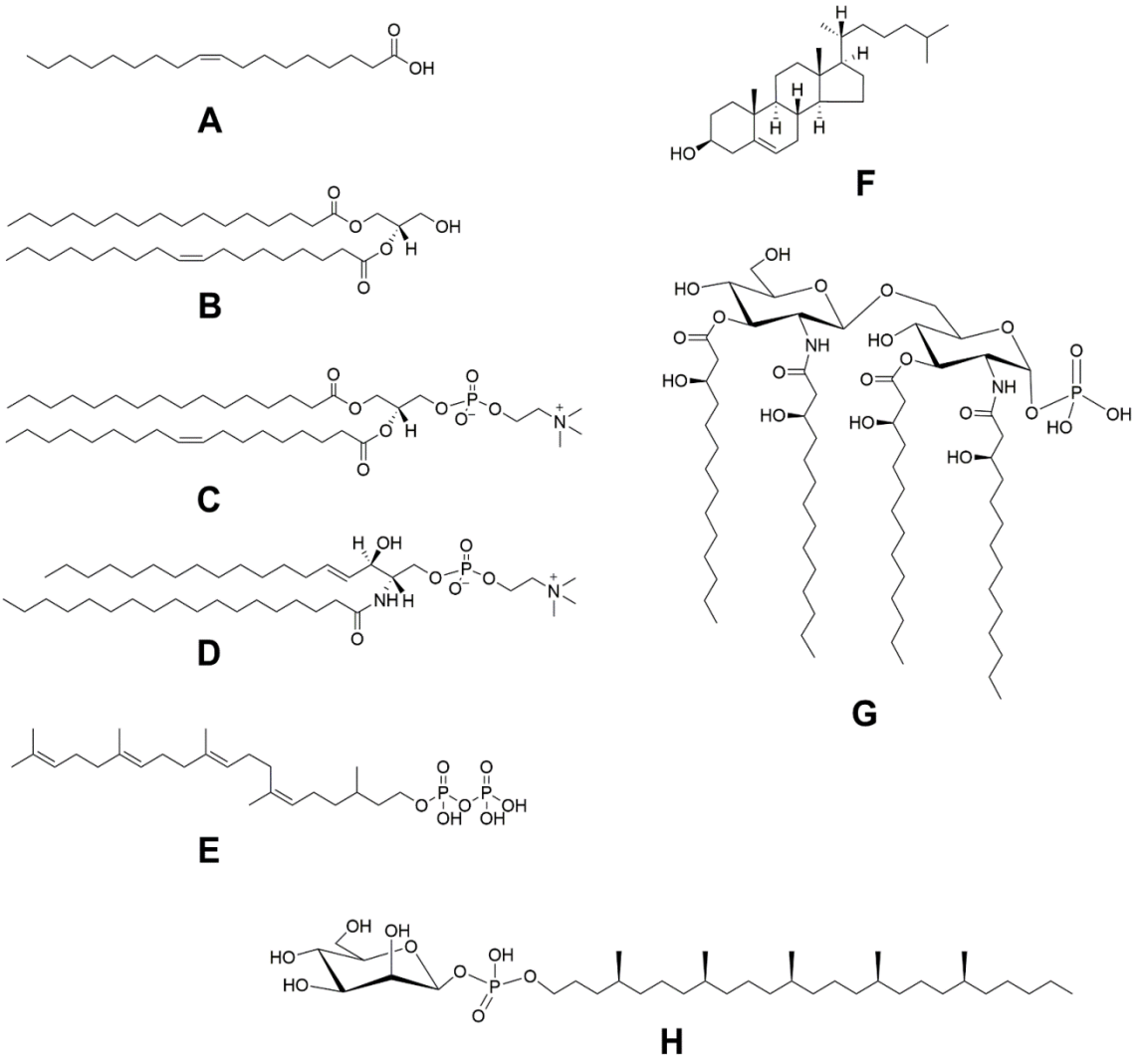

Figure 2.1. Representative structures of lipid classes. (A) Fatty Acyls, (B) Glycerolipids, (C) Glycerophospholipids, (D) Sphingolipids, (E) Prenol lipids, (F) Sterol lipids, (G) Saccharolipids, (H) Polyketides.

2.1.2. Cellular Functions of Lipids

Lipids play fundamental roles in maintaining cell membranes, participating in cell signaling pathways, serving as energy storage, and regulating cellular function and

disease.[28] Dysfunction in the lipid homeostasis has shown to be a risk factor for cancer, obesity, aging, and the many types of neurodegenerative disorders, including Alzheimer's disease, Huntington's disease, and Parkinson's disease.[29,30] Recent lipidomic studies have identified characteristic lipid signatures that have potential as diagnostic tools.[31] A summary of selected applications of lipidomics in biological and biomedical research is provided in Table 2.1.

The work described in this thesis investigates the changes to the lipid droplet lipidomic profiles with regards to aging. Aging is driven by lifelong accumulation of unrepaired cellular and molecular damage and is generally recognized as a process that results in the progressive decline of an organism over time.[2] It is predicted that by 2050 almost 25% of the world's population will be over 60 years of age.[3] Much data have been gathered on age dependent alterations in membrane lipid composition of different organs and tissues of mammals. One of the major compositional changes that is shown to take place in many of the aging systems is an increase in cholesterol to phospholipid ratio.[32] A reduction in the level of polyunsaturated fatty acyl is the next important age related variable observed in these systems.[33] Another commonly cited change is an increase in the ratio of sphingomyelin (SPM) to phosphatidylchofine (PC).[34-36] Altered lipid compositions seem to affect many membrane associated activities. Among these are the activity of various enzymes, signal transduction, the interaction of the receptors with the membrane bilayer, membrane permeability and potential, and transport of small molecules. So, it is important to gain a mechanistic understanding of the impact of aging on the dynamics of lipid metabolism in the biological systems.

Application	Type	Technique	Source of lipids	Findings and implications
Metabolic syndrome	Cardiovascular disease (CVD)	LC-based; shotgun; liquid extraction surface analysis; GC-MS	Plasma and tissue (e.g., plaque)	New insights into the association of molecular lipids with CVD; unraveling the lipid heterogeneity within atherosclerotic lesions; revealing biomarkers of atherosclerosis;
				understanding obesity risk factor of CVD; identifying lipidomic and metabolomics risk markers of vascular diseases
	Diabetes and obesity	LC-MS/MS; flow injection MS; shotgun; GC	Plasma	Positive association of plasma lipids with obesity; association of plasma lipidome with type 2 diabetes and similar association present in prediabetes; exploring the role of metabolomics analysis in diabetes research relating to the development of diabetes in children and changes in obese children with weight loss
Neurological disorders	Alzheimer's disease; Huntington disease; multiple sclerosis	LC-MS and MS/MS; shotgun	CSF; brain tissue; plasma; serum	Alterations in phospholipids; increased levels of diglycerides and others; reduced cholesteryl esters; changed lipid mediators; platelet activating factors as potential biomarkers in inflammation and neurodegeneration
Cancer	Breast; prostate; lung; ovary; esophagus; kidney; skin	LC-MS and MS/MS; shotgun; MALDI imaging; DESI-MS imaging	Plasma; tumor tissue; human and mouse squamous cell carcinoma	A panel of lipids as biomarkers; accumulation of cholesteryl esters; acyl chain elongation; high lysoPC and lower PC and TG; changed phospholipids; increased content if species containing PUFA; the role of cycloxyenase-2 in tumorigenesis

Table 2.1. Selected Applications of Lipidomics for Biological and Biomedical Research.[37]

2.2. Lipid Droplets and Their Role in Disease

Lipid droplets (LDs) are the major cellular organelles to store neutral lipids, such as triglycerides and sterol esters, in their core (Figure 2.2).[38] The surrounding phospholipid

monolayer is composed of over a hundred of different phospholipid molecular species protecting the neutral lipids from the hydrophilic environment of the cell. The variety of the different phospholipids in this monolayer fulfills important tasks in regulating the structure and function of this cellular organelle.[39] LDs function as building blocks for membrane synthesis and energy reservoirs that can be released when food is scarce. They also function in multiple other cellular processes, such as protein storage, autophagy, lipid transport and metabolism.[40,41]

Alterations in LD lipid profiles are associated with many diseases including obesity, cancer, liver disease, and cardiovascular disease.[42] Recently there has been remarkable advancement in understanding of LD biology and the role they play in health and disease. These LDs related studies usually only focus on analyzing the composition or changes of the LDs associated proteins which are embedded in the phospholipid monolayer.[43] However, the association between the changes of the LDs lipidome and regulation of cellular signal pathways is usually neglected. The lack of data about lipidomic composition of LDs hampers a detailed understanding of how they response to changes during different biological conditions. To address this issue, the work described in Chapter 3 and Chapter 4 investigates the age related differences in lipid composition of lipid droplets in two different model organisms.

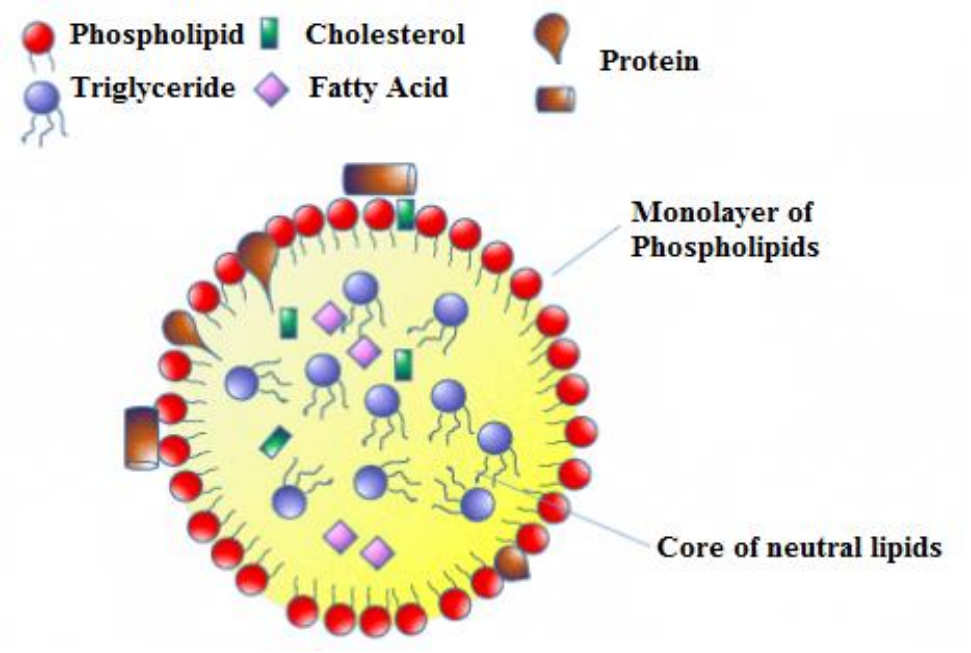

Figure 2.2. Schematic of lipid droplet composition.[44,45]

2.3. Methods to Analyze Lipids

2.3.1. Sample Preparation

Characterization and identification of lipids in biological membranes is highly dependent upon the preparation of high purity, morphologically distinct membranes or subcellular fractions.[23] Sample preparation should be quick and performed at controlled temperatures in the presence of antioxidants and inhibitors of hydrolytic enzymes and proteases to prevent lipid degradation and oxidation. To achieve optimal isolation extra care should be taken for the following steps: homogenization, membrane fractionation, and lipid extraction.[46]

Homogenization steps can dramatically impact the yield and purity of the specific organelles and affect the chemical integrity of extracted lipids.[47] Liquid homogenization was used in the work described in this thesis utilizing a Dounce homogenizer. The Dounce Homogenizer, also known as a tissue grinder, works by manually disrupting cells. This type of homogenizer is ideal for preparation of cell lysates or other tissues, and allows for maximum friction and cell disruption.

A variety of fractionation methods has been employed based on density gradient centrifugation, affinity chromatography, and immunoaffinity purification using antibodies specific for markers enriched in these fractions.[48,49] Density gradient centrifugation was used to isolate lipid droplets in this work. With a density less than water (specific gravity 0.92 g/cm3), lipid droplets float easily in aqueous solutions such as sucrose buffer.

The effectiveness of lipid extraction procedures highly depends on the chemical nature of the lipid components. Typically, a phase separation is created between immiscible solvents, with the lipids partitioning into the hydrophobic phase. Here, several methods were tested and a chloroform:methanol (1:2) based extraction was chosen to extract total lipids from lipid droplet samples. This method by Bligh and Dyer is regarded as the most reliable method for complete recovery of total lipids. A description of lipid extraction protocols and a comprehensive comparison of solvents used for lipid extraction are outlined on the Cyberlipid website (www.cyberlipid.org).[23]

2.3.2. Non Mass Spectrometry Based Approaches

The separation techniques that have been traditionally carried out for lipid analysis include thin-layer chromatography (TLC), gas chromatography (GC), capillary electrophoresis (CE), high performance liquid chromatography (HPLC), nuclear magnetic resonance (NMR) spectroscopy, and mass spectrometry (MS).[50] (Figure 2.3)

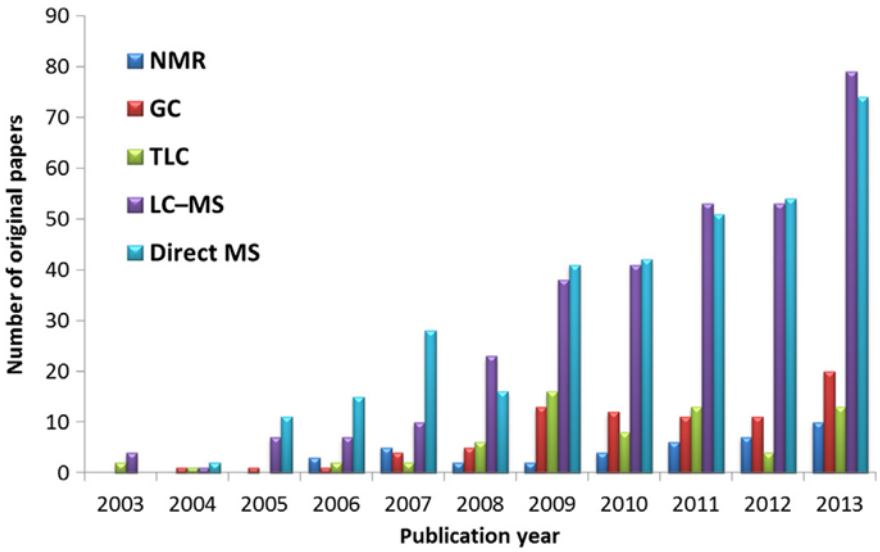

Figure 2.3. Number of original papers published over 11 years dedicated to lipidomics and different instrumental platforms.[51]

TLC is a simple chromatographic technique that allows the separation in a single run of a mixture of lipids with widely different polarities.[52,53] This method is easy to carry out and does not require complicated instrumentation and allows rapid screening of lipid extracts. Detection in TLC is generally based on the UV or visible absorption of the solutes or on the use of various detection reagents such as iodine vapor and class specific

dyes/radioactivity.[54] However, TLC based experiments are time consuming and lack resolution power, reproducibility, and specificity.

The advent of gas chromatography with MS based detection techniques has led to the analysis and identification of individual fatty acid molecular species, TAGs and sterols.[55] GC analysis is conducted at high temperatures that may result in lipid isomerization or decomposition. Multiple derivatization steps needed to improve volatility can be an issue for the analysis of low abundance lipid species. These steps are time consuming, and a major drawback of these methods is the large amount of starting material required for the derivatization.[56]

Nuclear magnetic resonance (NMR) has also been commonly used for the structural analyses and quantification of lipid species. Proton NMR, 31P-NMR, and 13C-NMR have been utilized to analyze lipid profiles of human erythrocytes[57] and the phospholipid composition of tissues and body fluids.[58] Two dimensional NMR was recently reported for the untargeted analysis of mycobacteria lipid compositions.[59] NMR spectra are dominated by very abundant lipids such as phosphocholine and cholesterol.[54] NMR suffers from low sensitivity which compromises the ability of this technique to resolve low abundance lipids.

Capillary Electrophoresis (CE) is a high-resolution technique for the separation of a wide range of lipids.[50] The most common capillary electrophoresis modes used in the context of lipid analysis include capillary zone electrophoresis, micellar electrokinetic chromatography, and microchip capillary electrophoresis. Lipid aggregation especially at concentrations above their critical micellar point is among the difficulties encountered with

the use of capillary electrophoresis for lipid separation. The other disadvantage of CE in lipid determination is the inability to resolve extremely hydrophobic lipids that are difficult to dissolve in aqueous electrolyte buffers. In addition, many solvents, buffer additives, and other analytes absorb in the region of 190–220 nm which pose a major challenge for the determination and quantitation of lipids by ultraviolet (UV) detection.[23]

High performance liquid chromatography (HPLC) is an easily automated method for separation and quantification of lipids.[54,60] HPLC has been applied for determining the lipid profiles of lipid mixtures using ultraviolet, fluorescence, flame ionization, refractive index or mass spectrometric detection methods. LC has become increasingly popular for obtaining maximum possible coverage since the majority of the metabolites in biological samples are non-volatile. Another advantage of LC over GC is due to the large diversity of separation mechanisms including normal phase (silica), reverse phase (C18, C8, C4, and phenyl), and hydrophilic interaction chromatography (HILIC).[61] Normal-phase HPLC generally separates phospholipids based on the polarity of their head groups, whereas the mechanism of action in reversed-phase chromatography is based on the lipophilicity of lipids, which is governed by the carbon chain length and the number of double bonds. HILIC is considered a variant of normal-phase chromatography and could be used to separate lipids according to their polarity.[62,63] Recently, decreased particle sizes of columns have allowed for improved resolution, sensitivity, decreased run time, and provides much higher separation power and peak capacity compared to conventional HPLC columns. This has been coined as ultra-performance liquid chromatography (UPLC).[64] UPLC has increased pressure and decreased particle size packed in the column to improve resolution

of adjacent chromatographic peaks allowing improved detection compared to conventional HPLC. Using UPLC leads either to better separation of narrower chromatographic peaks or to faster analysis without the loss of resolution.

2.3.3. Mass Spectrometry in Lipidomic Research

New mass spectrometry-based tools are advancing the number and types of lipids that can be identified and quantified.[27,65,66] A mass spectrometer has three essential components: (i) an ion source that converts the sample molecules into charged ions in the gas phase; (ii) a mass analyzer employs electric and/or magnetic fields to sort ions according to their *m/z* values; and (iii) a detector that measures the signal of each *m/z*-resolved ion.

The ionization source in modern mass spectrometers include electrospray (ESI), atmospheric pressure chemical-ionization (APCI), atmospheric pressure photo-ionization (APPI), and matrix assisted laser desorption ionization (MALDI). Choosing a particular mass spectrometry ionization technique strongly depends on the lipid class to be analyzed.[67,68] It is generally accepted that ESI is best suited for studying complex biological samples as minimal daughter ions are produced (soft technique) which allows compounds to be studied in the mass spectrometer. By employing both positive and negative ESI modes, as well as adjusting the pH of the lipid extract, it is possible to preferentially ionize various lipid classes under different experimental conditions (Table 2.2). APCI is usually used to analyze relatively nonpolar molecules with lower molecular weight like Sterols. APPI provides the highest S/N ratio in analyzing lipid molecular species separated by

normal-phase liquid chromatography.[62] MALDI is another soft ionization technique commonly used for lipid analysis.[69] Unlike ESI, MALDI can ionize the analyte directly from the solid phase. MALDI is mostly used in imaging mass spectrometry for investigating the distribution of lipids through the direct analysis of thin solid phase tissue sections.[70-72]

Subclass	**Polarity**	**Mass-to-charge ratio (*m/z*)**
Glycerophosphocholine	Positive	184
	Negative	168
Glycerophosphoethanolamine	Positive	141
	Negative	195
Glycerophosphoserine	Positive	185
	Negative	87
Glycerophosphoinositol	Positive	277
	Negative	241
Glycerophosphoglycerol	Positive	189
Glycerophosphate	Positive	115
Ceramide	Positive	264
Hexosylceramide	Positive	264
	Positive	180
Lactosylceramide	Positive	264
	Positive	180
Sphingomyelin	Positive	184
	Negative	168
Cholesterol ester	Positive	369
Cholesterol (as acetate)	Positive	77

Table 2.2. Examples of scanning modes in lipidomics.[73]

The mass analyzers frequently employed in lipidomics are Time-of-Flight, Ion Trap, Triple-Quadrupole, and Fourier Transform Ion Cyclotron Resonance.[74] Proper selection of the mass analyzer depends on the resolution, mass range, scan rate, and detection limit required for an application.

Triple-Quadrupole mass spectrometers provide quantitative analyses of high precision and accuracy using the multiple reaction monitoring (MRM) mode.[75] The main drawback of all quadrupole instruments is their low resolving power and limited mass precision and accuracy in *m/z* measurement for global identification of lipids. Some of these disadvantages are overcome by various hybrid instruments. The so-called Qq-TOF instruments, in which Q3 is replaced by a TOF, have been employed to improve resolving power for product ions in MS/MS mode and allows more precise *m/z* determinations for lipids.[76]

Fourier transform mass spectrometers are the highest resolution and mass accuracy for lipids have been obtained using FT-ICR mass spectrometers and hybrid instruments that use them as product analyzer (e.g., LIT-FT).[77] The further coupling of these instruments to HPLC-ESI makes possible the analysis of complex lipid mixtures.[78,79] FT-ICR instruments, however, are expensive and quite laborious when it comes to operation and maintenance. [50,51]

Hybrid mass spectrometers combining different types of mass analyzers (e.g., quadrupole linear ion trap, quadrupole TOF and linear ion trap-orbitrap), are regularly used in lipid identification and quantification.[80,81]

Hybrid TOF instruments have been extensively used for lipidomic analysis.[80] The main advantages of hybrid TOF instruments include duty-cycle related sensitivity, high speed which facilitates tandem mass with liquid chromatography, and excellent mass accuracy. This is essentially important when speed and sensitivity are simultaneously necessary, such as in tandem mass spectrometry.

Ion Trap mass spectrometers offer good sensitivity and high throughput. However, these instruments suffer from low dynamic range, and space-charge effects that limit the number of ions that can be stored at any one time.[82] Recent developments in the ion-trap family of mass analyzers, have made higher resolution and expanded dynamic range possible.[83] The Orbitrap mass spectrometer is a newer member of the ion trap type instruments which have been largely employed for high-quality lipidome identification and quantification with high mass accuracy and resolving power.[77]

The work described in Chapter 3 evaluates the performances of high resolution quadrupole time of flight (Q-TOF) and Orbitrap (Velos) mass spectrometers for untargeted lipidomic analysis. The schematic of these instruments are depicted in Figure 2.4.

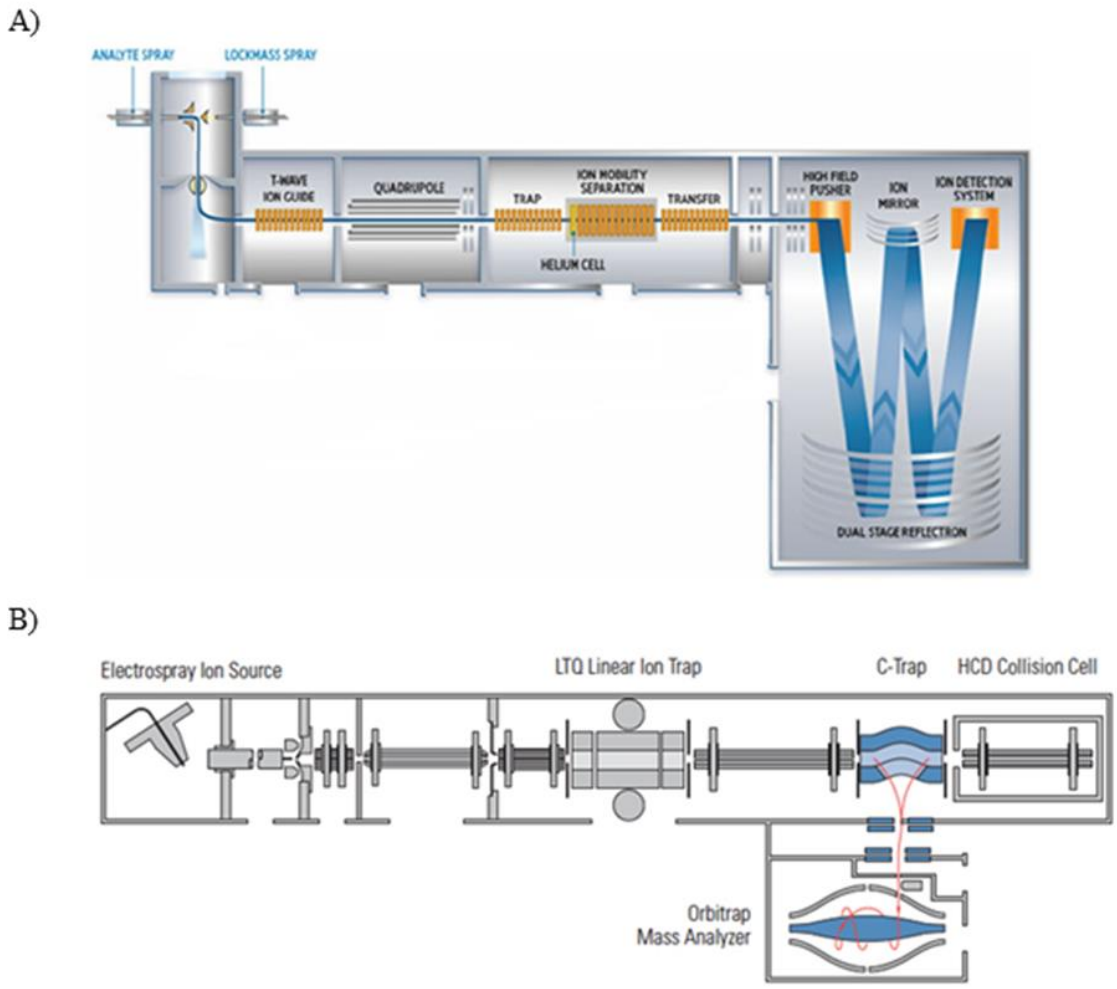

Figure 2.4. Schematic diagram of the Synapt[84] (A) and Orbitrap[85] (B) instruments.

2.4. Data Processing for Mass Spectrometry Based Lipidomics

The handling, processing, analysis and integration of massive data generated by LC/MS require specialized mathematical, statistical and bioinformatics tools.[86] One of the ongoing challenges of LC/MS metabolomics is the development of better data processing

methods.[87] Typical data processing workflow for the data generated by LC/MS approaches usually proceeds through multiple universal stages, including filtering, feature detection, alignment and normalization (Figure 2.5).

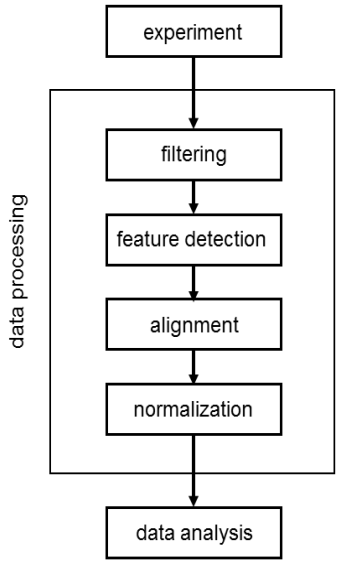

Figure 2.5. Summary of metabolomic data processing workflow.[88]

Filtering methods process the raw signal with aim of removing both chemical and random noise. Feature detection is an important step used to measure all signals caused by true ions and avoid detection of false positives. Alignment is needed for correcting retention time differences between multiple runs and combining data across different samples. Normalization steps remove the unwanted systematic variation in ion intensities between measurements, while retaining the interesting biological variation.[89]

Due to its complex nature, non-targeted lipidomics data processing has to be linked to advanced chemometric techniques, to reduce the data complexity into a smaller set of

manageable signals.[90] A major challenge lies in removing artifacts otherwise mistakenly interpreted as real lipids from large mass spectrometry data files. In addition, interpretation and translation of results into a biologically-useful meaning make identification and quantification imperative. Despite the improvements, several caveats still remain and a single workflow does not provide a perfect solution in terms of robust cleanup of all lipidomic datasets. Figure 2.6 shows a data processing workflow developed and utilized in the Arriaga group to automate data cleanup and peak finding and to putatively identify the resulting genuine ions. The developed workflow is comprised of the following: (1) untargeted UPLC/MS analysis of the biological systems of interest; (2) application of bioinformatics tools to identify candidate features characteristic of these systems; (3) confirmation of candidate features via evaluation of extracted ion chromatograms (XICs); (4) identification using online database searching; (5) mass accuracy confirmation and evaluation of fragmentation patterns. Application of this workflow results in more reliable, higher confidence preliminary identifications over a wide range of biological systems.

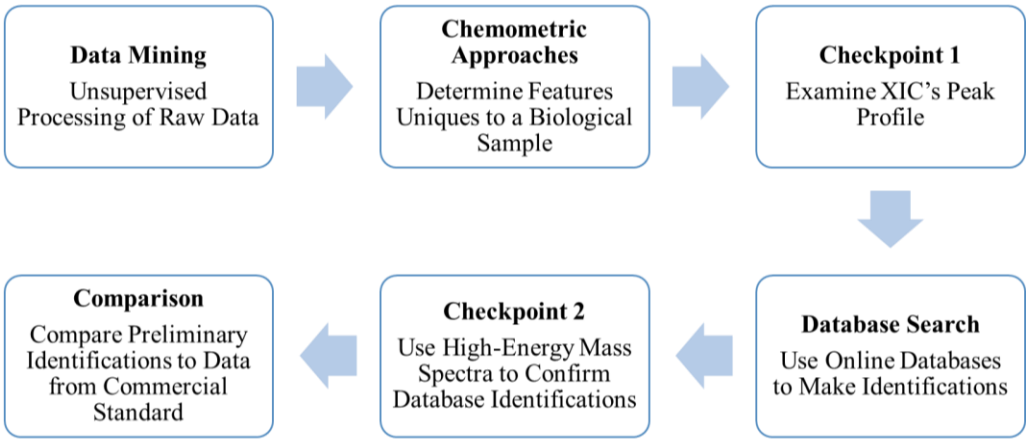

Figure 2.6. Workflow for preliminary identification of lipids from LC/MS.[91]

A number of software packages have been recently developed to meet the challenges of metabolomics data processing. Each program uses different algorithm, however they all aim to limit the number of false-positive peaks, while retaining true lipids. Available software tools are divided into two commercial and freely available categories which use various statistical tools to interpret a matrix containing peak intensities. Table 2.3 includes a list of the most commonly used tools for LC/MS metabolomics data analysis. In the work described in Chapter 3, five different software programs were compared to determine their effectiveness at analyzing untargeted datasets for lipidomics. These include the two vendor softwares (MassLynx and Xcalibur) as well as XCMS, Progenesis, and LipidSearch. Some aspects to consider in choosing the software for metabolomic data processing are quality of processing, ease of use, performance and overall cost of the software.[92]

Tool	Type	Reference
MetaboAnalyst	Web	Xia et al, 2012
XCMS	R	Smith et al, 2006
MetSign	MatLab	Lommen and Kools, 2012
MAVEN	Application	Melamud et al, 2010
mzMine	Application	Pluskal et al, 2010
MetDAT	Web	Xia et al, 2009
MetAlign	Web	Lommen and Kools, 2012
mzMatch	R	Scheltema et al, 2011
OpenMS	Web	Bertsch et al, 2010

Table 2.3. Common tools available for LC/MS metabolomics data processing.

Chapter 3: Comparison of High Resolution Quadrupole-Time-of-Flight and LTQ-Orbitrap Mass Spectrometers for Lipidomic Analyses

Lipidomic studies have increased exponentially over the last decade owing to the vital roles that lipids play in human physiological and pathological processes. However, because of the diversity and complexity of lipids, lipid analysis is still full of challenges. The recent developments of mass spectrometry technology methods greatly push forward the study of lipids in biological matrices. The benefits of high resolution mass spectrometry are well known and widely realized in various lipidomics applications.[93] However, comparisons between high resolution mass spectrometers for a comprehensive analyze lipids is not common place. Here, several analytical figures of merit are calculated to compare the performance of high resolution quadrupole time of flight (Q-TOF) and linear trap quadrupole-Orbitrap (LTQ-Orbitrap) mass spectrometers for untargeted lipidomic analysis of the post nuclear fractions (PNFs) of a mouse myoblast cell line. Both mass spectrometers are compared in terms of number of identifications, accuracy, resolution, reproducibility and signal-to-noise ratio. The output data are analyzed using XCMS, Progenesis[94], LipidSearch[95], Xcalibur[96], and MassLynx[89] to determine the software that provides the highest number of hits from the data analysis workflow.

Overall, both instruments show adequate mass accuracies (< 3ppm) allowing high confidence identifications of metabolites. The Q-TOF (Synapt G2) shows higher signal to noise ratio leading to enhanced sensitivity than the LTQ-Orbitrap (Velos) in positive ionization mode. The LTQ-Orbitrap has better mass resolution below 700 *m/z*, while the Q-TOF has better resolution above 700 *m/z*. Reproducibility of the peak intensities was better on the Synapt in both positive and negative electrospray mode. Our results support the use of the Q-TOF when lipids of interest are in low abundance and the use of the LTQ-

Orbitrap when detecting lipids with higher molecular mass. Overall, the use of Synapt G2 Q-TOF is recommended here for unbiased lipidomics and metabolomics analyses.

3.1. Introduction

Untargeted metabolomics is an emerging approach for the simultaneous analysis of intracellular metabolites in complex systems.[73] Metabolomics holds the promise to extensively contribute to the discovery of biomarkers of diseases in medical diagnostics, or evaluation of the alterations caused by environmental stressors or pharmacological influences.[97] Liquid chromatography coupled to mass spectrometry (LC/MS) have allowed metabolomics to become a fast growing field and is often the method of choice for global analysis of compounds in biological systems.[98] The comprehensive investigation of the metabolome is challenging due to its enormous complexity and dynamics.[99] Particularly because of a wide range of metabolite concentrations in biological fluids, different physiochemical properties, and the diversity of molecular species including small molecules, lipids, vitamins, simple amino acids and peptides.[100] Employing high resolution mass analyzers with high sensitivity, selectivity, and mass accuracy is necessary to determine the abundance and characterize the structure of metabolites in complex mixtures.[101]

The role of MS in metabolic profiling is evolving constantly, as both instrumentation and software becomes more sophisticated and researchers realize current technological capabilities. Development and improvement of mass analyzers, including the hybrid Quadrupole-time of flight (Q-TOF), Fourier transform ion cyclotron resonance

(FTICR), and Orbitrap has provided the ability to acquire more accurate and specific biological information in relatively high-throughput experiments.[102] Despite recent technological advancements in all mass spectrometry techniques, no single analytical platform or approach exists for untargeted metabolomics, all having advantages and limitations. The advantages and limitations of the different mass spectrometry platforms have been extensively reviewed elsewhere.[103,104] It is known that time of flight instruments often yield different mass spectrometry results from ion trap mass spectrometers due to their different design and operation modes. The hybrid Orbitrap and TOF instruments are the most widely used mass spectrometry platforms in metabolomics. Features of these instruments at their present stage of development include high mass resolution, high sensitivity, as well as high mass accuracy in regards to obtaining molecular and product ion spectra.

It is important to highlight that the challenge of metabolite identification is still a significant bottleneck in untargeted mass spectrometry analysis.[87] The massive amounts of information generated by LC/MS based experiments require specific data analysis strategies. Over the past decade significant innovations were observed and several software tools were successfully developed to facilitate MS based metabolomic data processing.[86,87] These programs operate differently due to differences in the algorithms used to identify and align peaks.

Herein, we conducted a comparison of a Synapt G2 quadrupole-TOF mass spectrometer (Q-TOF) and an LTQ-Orbitrap Velos (LTQ-Orbitrap) (see Chapter 2), both

coupled to LC systems. Metabolites from a post nuclear fraction of mouse myoblast cell line were extracted using sample preparation protocols that preferentially extracts lipids. Following reverse-phase LC/MS, the data derived from the two mass spectrometers were thoroughly examined with Masslynx 4.1 and Xcalibur 2.2 software as well as with XCMS[105] open source software. Performances of Q-TOF and Orbitrap mass analyzers have been previously compared for plant metabolomic analyses[106] and targeted drug discovery metabolite screening,[107] but not in the context of lipidomics. In present study, we compared mass accuracy, mass resolution, signal to noise ratio, and sensitivity of a Q-TOF (Synapt G2) and an LTQ-Orbitrap (Velos) in the analysis of complex biological samples enriched in lipids. Overall, both instruments showed adequate mass accuracies (< 3 ppm for all measured compounds), however mass accuracy values were statistically higher for most of the lipid standards on the Synapt. Signal to noise were higher on the Synapt, which is an advantage in detecting the low abundance metabolites in biological matrices. Reproducibility associated with the peak intensities was better on the Synapt, with 79% of metabolites exhibiting a median CV of < 30% in positive ESI mode compared to 55% on the Orbitrap. The overall sensitivity was similar for both mass spectrometers using XCMS platform, though the LTQ-Orbitrap proved slightly more sensitive for certain compounds in negative ESI mode. Resolution on the Q-TOF was better for $m/z > 700$, while the LTQ-Orbitrap had better resolution for $m/z < 700$.

3.2. Materials and Methods

3.2.1. Reagents

The solvents used for extraction were HPLC grade chloroform and methanol from Fisher Scientific (Fairlawn, NJ). Dubelco's Modified Eagle Medium (DMEM) high glucose cell medium, and fetal bovine serum were from Thermo Scientific (Waltham, MA). Phosphate buffered saline (PBS, 10× concentration, 1.37 M NaCl, 27 mM KCl, 80 mM Na_2HPO_4, and 20 mM KH_2PO_4, pH 7.4) was obtained from Bio-Rad (Hercules, CA). 0.5% trypsin-EDTA (10× concentration, no phenol red) was obtained from Life Technologies (Grand Island, NY). Sucrose, 4-(2-hydroxyethyl)-1-piperazineethanesulfonic acid (HEPES), mannitol, ethaminetetraacetic acid (EDTA) were obtained from Sigma-Aldrich (St. Louis, MO). Cell homogenization buffer consisted of 70 mM sucrose, 215 mM mannitol, 4.31 mM HEPES, and 4.94 mM EDTA, pH 7.4. Water was purified with a Millipore Synergy UV system (18.2mΩ/cm, Bedford, MA). Ultra LC/MS-grade methanol, acetonitrile, and water were from Formic acid was from EMD (Darmstadt, Germany). Standards including: 1,2-distearoyl-*sn*-Glycero-3-Phosphoethanolamine, 1-palmitoyl-2-oleoyl-*sn*-glycero-3-phosphocholine, 1-stearoyl-2-hydroxy-*sn*-glycero-3-phosphocholine, 1-palmitoyl-2-oleoyl-*sn*-glycero-3-phosphate, 1-palmitoyl-2-oleoyl-*sn*-glycerol, D-erythro-sphingosine-1-phosphate, 1-palmitoyl-2-oleoyl-*sn*-glycero-3-phosphoinositol, and 1',3'-bis[1,2-dimyristoyl-*sn*-glycero-3-phospho]-*sn*-glycerol, were purchased from Avanti Polar Lipids (Alabaster, AL). Cholesterol, L-α-phosphatidylcholine, C18:1 ceramide (d18:1/18:1(9Z)), and L-α-phosphatidyserine were purchased from Sigma Aldrich (St. Louis, Mo).

3.2.2. Sample Preparation and Extraction

C2C12 cells (mouse myoblast cell line) were cultured in a T75 flask for 48 hours at 37 °C, 5% CO_2 in DMEM supplemented with 10% fetal bovine serum containing 110 µg/mL gentamycin. Cells were lifted with trypsin in PBS (0.5% v/v) after 90% confluency was reached and then split 1:20 (v/v) into new flasks. Cells were harvested by differential centrifugation at 600*g* for 10 minutes at 4 °C and then washed once by suspending in homogenization buffer and differential centrifugation at 1,000*g* for 10 minutes. Cell disruption was done in an ice-cooled cell disruption bomb (Parr Instrument Co., Moline, IL) charged to 500–600 psi with nitrogen gas for a minimum of 15 min prior to pressure release. The lysate was collected in a 50-mL falcon tube and then centrifuged at 1,000*g* for 10 min to pellet unbroken cells and nuclei. The post nuclear fraction (the supernatant) was removed and collected to a clean microcentrifuge tube. All steps were performed on ice or at 4 °C.

To extract the lipids, a previously published protocol was used.[108] Briefly, 3.75 ml of ice cold chloroform: methanol 1:2 v/v was added to 1 ml of the collected fraction and vortexed for 2 min. Sample was treated with 1.25 ml of chloroform and vortexed for 1 min. Subsequently, 1.25 ml of water was added to the sample and vortexed for 1 min. Sample was centrifuged in glass tubes at 13,000*g* for 10 min to pellet any non-extracted materials. The upper phase containing salts and other water soluble metabolites were removed and protein phase was pierced with a pipette tip and discarded. The organic phase (lower phase) was collected and transferred to a new siliconized 0.6 ml Eppendorf tube and evaporated

overnight at room temperature under vacuum to remove extraction solvents. Tubes were filled with nitrogen to remove any air and stored dry at -80 °C prior to analysis.

3.2.3. LC/MS Conditions

The pellet recovered from the Bligh and Dyer extraction was resuspended in 200 µL 1:1:1 HPLC-grade MeOH : $CHCl_3$: H_2O with a syringe, vortexed for 30 s, and incubated for 5 min. The samples were centrifuged at 16,100*g* for 5 min to remove any non-resuspended materials.

Twelve pure lipid standards were purchased and stock solutions were prepared in HPLC-grade MeOH : $CHCl_3$ 1 : 1 v/v at a final concentration of 1 mg/mL. Standards were mixed from their stocks to a final concentration of 50 µg/mL and vortexed for 1 minute. Standards samples were added to mass spectrometry sample tubes from Microsolv Technology Corporation (Leland, NC) for analysis on both MS platforms. Standard mixture was then spiked from the stock into post-nuclear fraction of C2C12 cells at two different stages, to the fraction prepared with nitrogen cavitation prior to Bligh and Dyer lipid extraction, and to the reconstituted pellet right before the LC/MS analysis.[91] Standards were spiked at a final concentration of 50 µg/mL.

The two mass spectrometers were coupled to different LC systems operated at different flow rates, while still using the same mobile phase composition and gradient conditions. The Synapt G2 HDMS Q-TOF was coupled to Waters Acquity UPLC™ system and the reversed-phase column used was a Waters HSS T3 C18, 2.1 mm × 100 mm column (1.7 µm diameter particles). The Orbitrap Velos was paired with Thermo Scientific UHPLC pump and a Dionex

UHPLC C18, 0.5 mm × 100mm (1.8 µm diameter particles) was used at a temperature of 45 °C. The following 16 min linear gradient separations were employed at a flow rate of 400 µL/min on the Q-TOF and 10 µL/min on the Orbitrap using a binary mobile phase system where A: Methanol:Water, 60:40 v/v, 10mM ammonium acetate, containing 0.1% formic acid and B: Methanol:Isopropanol 10:90 v/v, 10mM ammonium acetate, containing 0.1% formic acid. The gradient profile was: 40% B, 0 min to 5 min; 40% B to 100% B, 5 min to 13 min; 100% B, 13 min to 16 min.

The Synapt G2 instrument was calibrated with 2 µg/µl Sodium iodide solution in 50/50 2-propanol/Water. Simultaneous low- and high-collision energy (CE) mass spectra were collected in centroid mode over the range *m*/*z* 50–1200 every 0.2 s during the chromatographic separation. Samples were analyzed in high-definition MS^e mode ($HDMS^e$) and the TOF analyzer was operated in the *V* resolution mode. MS^e parameters in positive electrospray ionization mode were as follows: capillary, 0.3 kV; sampling cone, 35.0 V; extraction cone, 5.0 V; desolvation gas flow, 800 L/h; source temperature, 100 °C; desolvation temperature, 20 °C; cone gas flow, 20 L/h; trap CE, off (low CE collection), trap CE ramp 15–65 V (high CE collection); lockspray configuration used the average of three *m*/*z* measurements (0.2 s scan, *m*/*z* 100–1200, every 10 s) of protonated leucine-enkephalin (*m*/*z* 556.2771) formed from infusion of a 5 µg mL^{-1} solution. All MS^e parameters were identical in negative ionization mode except the following: capillary, 2.5 kV; sampling cone, 30.0 V; extraction cone, 4.0 V.

The LTQ-Orbitrap Velos instrument was calibrated with Polysiloxane solution and mass accuracy was calculated based on the background ions including 371.10124 *m/z*. Mass spectra were recorded from *m/z* 200-2000 with a spray voltage of 3.5 kV and 3.10 kV in

positive and negative ion mode respectively. The sheath and auxiliary gas flows (both nitrogen) were optimized at 50 and 0 arbitrary units (a.u.), respectively. Capillary temperature was set to 300 °C. Automatic gain control (AGC) target value was set at 1×10^6 charges and maximum injection time was set to 100 ms, and the gate lens offset to 90 V and -90 V in positive and negative electrospray. The mass spectra were acquired in the profile mode and external calibration was applied. MS^2 fragmentation with no precursor ion selection was performed with normalized collision energy set to 35% with a ramp of 50% and nitrogen was used as collision gas. The resolution was set at 70,000 at $m/z = 200$.

3.2.4. Data Treatment

Raw data files collected on the Q-TOF (Synapt G2) and LTQ-Orbitrap (Velos) were initially processed by the individual manufacturer software including MassLynx 4.1 (Waters) and Xcalibur 2.2 (Thermo Fisher Scientific) for mining chromatographic and mass spectrometric data. Additional software packages used for data processing include: Progenesis QI, LipidSearch, and XCMS Online.[109] These software packages have been effective for feature detection and perform pre-processing steps, such as data reduction, noise filtering, background subtraction, mass calibration and retention time alignment.[110]

Relative mass accuracies were calculated by dividing the mass error by the theoretical *m/z* values for the standard samples that were commonly detected on both platforms and are expressed in parts per million (ppm). Resolution was calculated by taking the ratio of peak mass to the peak width at half maximum intensity. Signal to noise values

were calculated by dividing the peak signal intensities by an estimated noise level. Noise was calculated as the standard deviation of the baseline over a selected window before the peak. Reproducibility in signal intensity was measured as the average relative standard deviation (n=3) for the intensities of all the peaks observed in the MS spectra.

The raw mass spectrometric file types from both instruments were processed by XCMS online software (xcmsonline.scripps.edu). Raw data acquired by two platforms were converted to .mzXml common data format using Proteowizard File converter (proteowizard.sourceforge.net) and the following parameters used in this analysis: (i) Feature detection: centWave method, min. and max. peak width = 5 and 20, S/N threshold = 6, mzdiff = 0.01, integration method = 1, prefilter peaks = 3, prefilter intensity = 100, Noise filter = 0; (ii) Retention time correction: Obiwarp method, profStep = 1; (iii) Alignment: mzwid = 0.015, bw = 5, minfrac = 0.5, max = 100, minsamp = 1. The data were processed for peak detection, retention time correction, chromatographic alignment, statistical analysis, and identification through METLIN database. The identifications include possible adducts, fragments and isotopes. The results output includes XICs, boxplots, cloud plots, and principal component analysis (PCA) for sample discrimination.

Preliminary identification of features by XCMS was based on a previous workflow,[105,109] consisting of 5 steps: (1) LC/MS profiling of the biological systems of interest; (2) chemometric analysis to determine characteristic/unique hits of different biological groups; (3) manual evaluation of extracted ion chromatograms (XICs) referred

to as Checkpoint 1; (4) structural database searching; (5) mass accuracy confirmation and evaluation of fragmentation patterns from tandem mass spectra referred to as Checkpoint 2. Extracted ion chromatograms (XICs), were manually examined to confirm identified features by having a true chromatographic peak profile, referred to as Checkpoint 1 in the workflow (see Chapter 2). Fragmentation patterns of each feature were evaluated by comparison of high-collision energy (MS2) mass spectra with simulated fragmentation patterns calculated *in silico* using METLIN software, referred to as Checkpoint 2 (see Chapter 2).

In addition to XCMS, Progenesis QI (Nonlinear Dynamics, Newcastle, UK) was used to search for compounds in ChemSpider and Progenesis MetaScope databases.[94] Default parameters included m/z hits within a 5 ppm tolerance and a score value above 30.[111,112] The statistical output of univariate (cloud plots) and multivariate (PCA plots) data analysis were generated by adjusting the threshold and range of the parameters mentioned elsewhere.[113] Identifications for each database were combined and counted after elimination of redundancies.

In addition to XCMS, LipidSearch[60] (version 4.1, Thermo Fisher Scientific) was used for lipid identification of the data collected on the Orbitrap. This software uses a database search of precursor accurate masses and their predicted fragment ions. The following parameters were used in this analysis: precursor mass tolerance = 5 ppm, product mass tolerance = 5 ppm, relative product intensity threshold = 1, m-score threshold = 2, retention time tolerance = 0.2 min, retention time range = 0-20 min.

3.3. Results

This study compared the analytical performance of a Q-TOF and an LTQ-Orbitrap by analyzing lipid standards and metabolites in a post nuclear fraction (PNF) of a mouse myoblast cell line. Mobile phase compositions and gradient profiles were identical to minimize the effect of chromatographic differences on the data. Raw data from the Q-TOF and the LTQ-Orbitrap were (1) low- and high-collision energy mass spectra (MS^e) and (2) MS1 and MS2 spectra, respectively.

The initial comparison used twelve lipid standards. Lipid standards were run on both MS platforms and typical extracted ion chromatograms and MS profiles are shown in Figure 3.1. The results are obtained using positive ESI, for 1-palmitoyl-2-oleoyl-*sn*-glycero-3-phosphocholine with *m/z* 759.5780. Although the chromatographic conditions were matched, columns were different which resulted in expected differences in chromatographic retention times (Figure 3.1 A and B). The exact mass and fragment ions demonstrate differences resulting from using different types of mass spectrometers. MS/MS fragmentation using the LTQ-Orbitrap gives a fragment at *m/z* 672 which corresponds to the loss of ethyltrimethylammonium ($C_5H_{14}N^+$) with a molecular weight of 88 g/mol. In contrast, high energy MS on the Q-TOF gives a unique fragment at *m/z* 184 which corresponds to the loss of the protonated phosphatidylcholine head group.

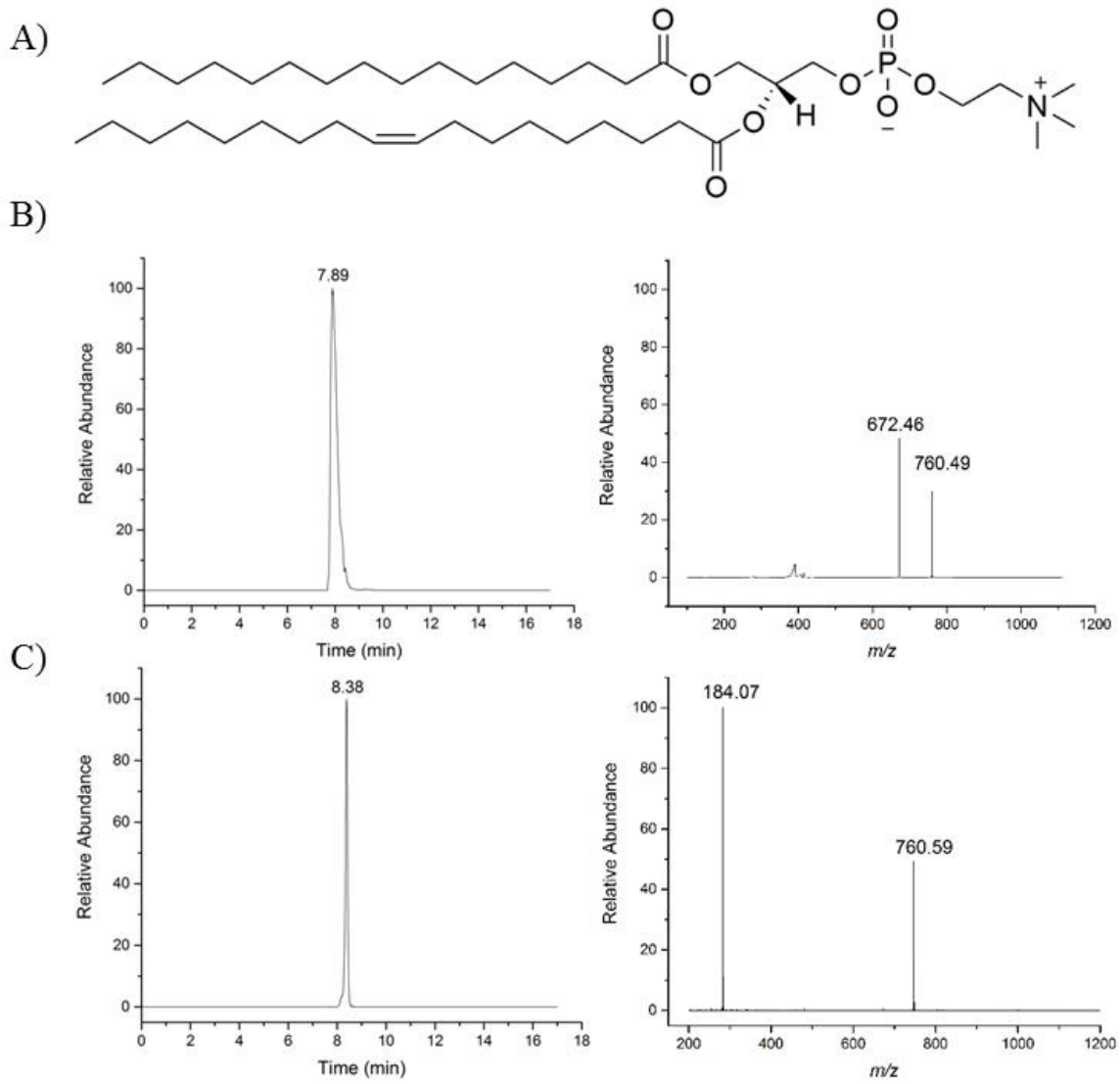

Figure 3.7. Representative data for *m/z* 759.5780. Structure of standard 1-palmitoyl-2-oleoyl-*sn*-glycero-3-phosphocholine (A); Extracted ion chromatogram and mass spectrum obtained on the LTQ-Orbitrap (B); and on the Q-TOF instruments (C).

The second comparison was based on analysis of post nuclear fractions (PNFs) of a mouse myoblast cell line, which displays the expected complexity of a biological sample. This comparison included reproducibility in signal intensity, mass resolution, and signal-to-noise ratio detected peaks that pass Checkpoint 1 (See Section 3.2.4).

3.3.1. Reproducibility

Reproducibility of ion intensity was based on the analysis of technical replicates, after Checkpoint 1. For Synapt in positive ion mode, the range for the coefficients of variation (CV) was between 0.1 – 76 %, (average = 23, std. dev = 13, N = 3 technical replicates for all CV values included here). For Synapt in negative ion mode, the range for CV was between 11 – 95 %, (average = 30, std. dev = 11, N = 3 technical replicates for all CV values included here). For any of the two electrospray ionization polarities, CVs were not correlated with signal-to-noise ratio (Figure 3.2). For the LTQ-Orbitrap in positive ion mode, the coefficients of variation (CV) was between 1.1 - 149 %, (average = 53, std. dev = 42, N = 3 for all CV values included here). For the LTQ-Orbitrap in negative ion mode CV range was between 0.4 - 104 %, (average = 27, std. dev = 22, N = 3 for all CV values included here). For any of the two electrospray ionization polarities, CVs were not correlated with signal-to-noise ratio (Figure 3.3).

Overall, when comparing the mean CV values in positive ESI, 79% and 55% of the metabolites showed a mean CV of <30% (a level generally considered acceptable with respect to laboratory error) on the Synapt and Orbitrap respectively.[114] In negative ESI, 73% and 58% of the metabolites showed a mean CV of <30% on the Synapt and Orbitrap respectively..

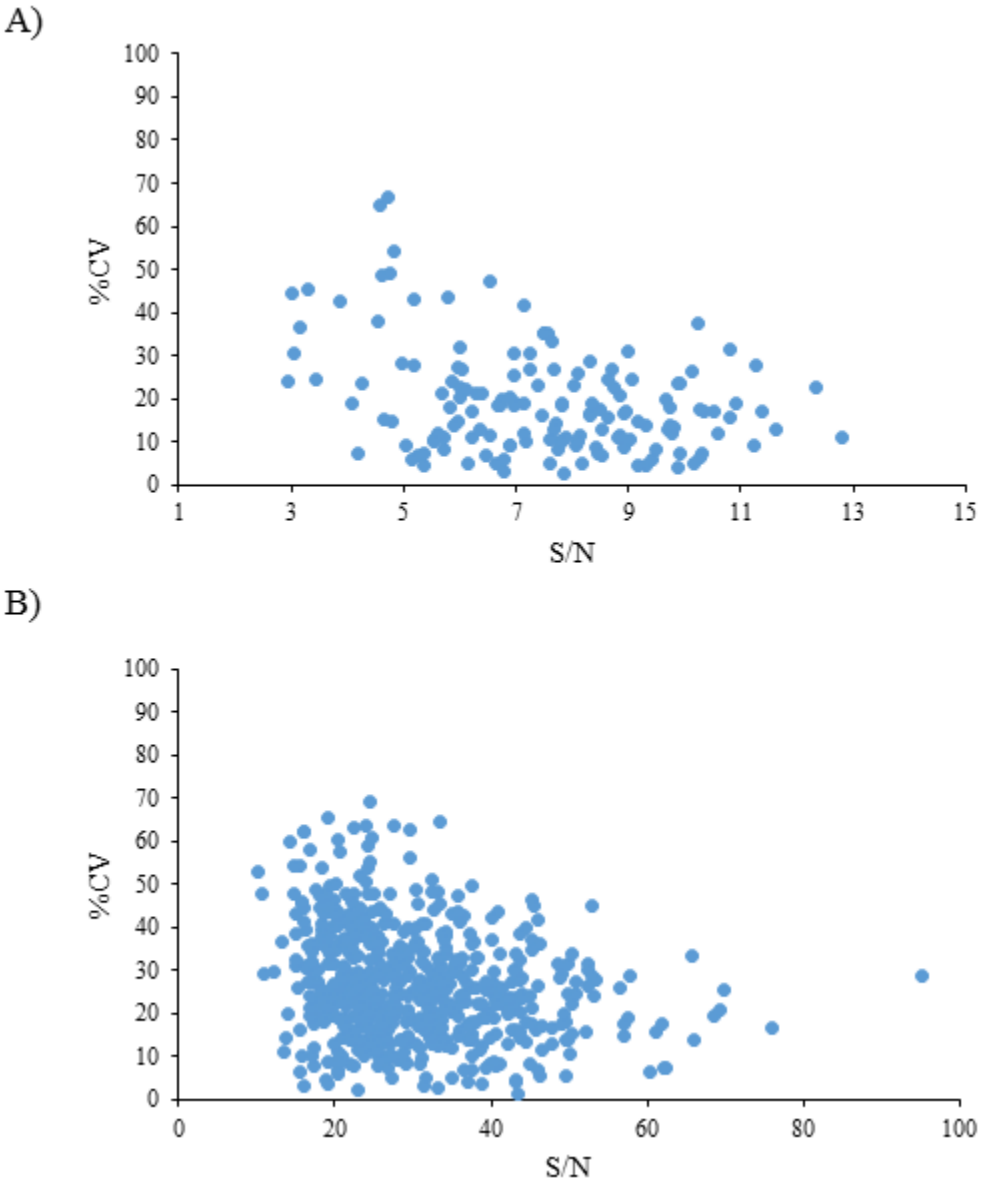

Figure 3.8. Reproducibility in technical replicates analyzed on the Q-TOF instrument. Positive ionization mode (A); Negative ionization mode (B).

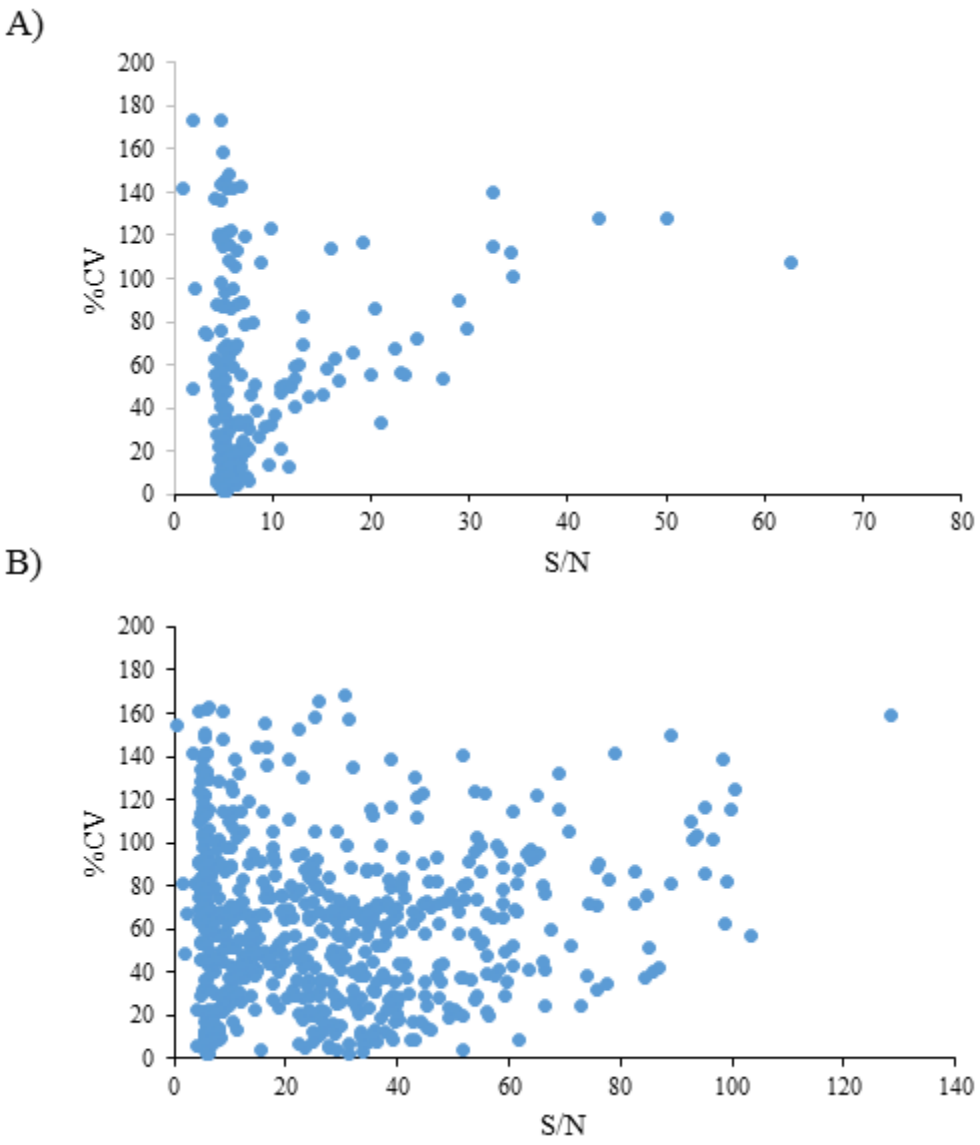

Figure 3.9. Reproducibility in technical replicates analyzed on the LTQ-Orbitrap instrument. Positive ionization mode (A); Negative ionization mode (B).

3.3.2. Mass Accuracy

High mass accuracy is needed for identification and structural characterization of unknown compounds.[115] Twelve lipid standards were used to determine mass accuracy of each instrument, but not all were detected (Figure 3.4). In positive ion mode, 1-stearoyl-2-

hydroxy-*sn*-glycero-3-phosphoethanolamine, 1-palmitoyl-2-oleoyl-*sn*-glycero-3-phosphocholine, and 1-stearoyl-2-hydroxy-*sn*-glycero-3-phosphocholine were detected by both instruments (Table 3.1.A). In negative ionization mode, seven compounds were detected on both the Q-TOF and LTQ-Orbitrap instruments and four standards were not detected at all (Table 3.1.B). The standard 1',3'-bis[1,2-dimyristoyl-*sn*-glycero-3-phospho]-*sn*-glycerol was never detected on any of the two mass spectrometers in positive or negative ion mode. A summary of the mass accuracies calculated in positive and negative ESI is shown in Table 3.1.

In general, the overall measured masses differed from the calculated monoisotopic masses by less than 3 ppm on both instruments. Mass accuracy was 0.6 ± 0.5 ppm (average ± SD, n=3 technical replicates) ppm and 1.7 ± 0.3 ppm (average ± SD, n=3 technical replicates) for species detected under positive ion mode in the Q-TOF and the LTQ-Orbitrap, respectively. Similarly, mass accuracy was 1.3 ± 0.5 ppm (average ± SD, n=3 technical replicates) ppm and 1.8 ± 0.5 ppm (average ± SD, n=3 technical replicates) for species detected under negative ion mode in the Q-TOF and the LTQ-Orbitrap, respectively. A t-test was performed on the individual mass accuracies of individual *m/z* values in positive and negative ESI. Results show that the differences are statistically significant ($p = 0.02$, $p = 0.04$) for compound 1-palmitoyl-2-oleoyl-*sn*-glycero-3-phosphocholine (Compound C, Figure 3.4) and 1-stearoyl-2-hydroxy-*sn*-glycero-3-phosphoethanolamine (Compound F, Figure 3.4) in positive ESI data (Table 3.1 A). Similarly, a t-test results show a significant difference ($p < 0.05$) in negative ESI data for C18:1 Ceramide (d18:118:1(9Z)) (Compound B, Figure 3.4), 1-palmitoyl-2-oleoyl-*sn*-

glycero-3-phosphocholine (Compound C, Figure 3.4), 1-stearoyl-2-hydroxy-*sn*-glycero-3-phosphocholine (Compound D, Figure 3.4), and 1-palmitoyl-2-oleoyl-*sn*-glycerol, (Compound G, Figure 3.4). The rest of the comparisons are not significantly different (Table 3.1 B).

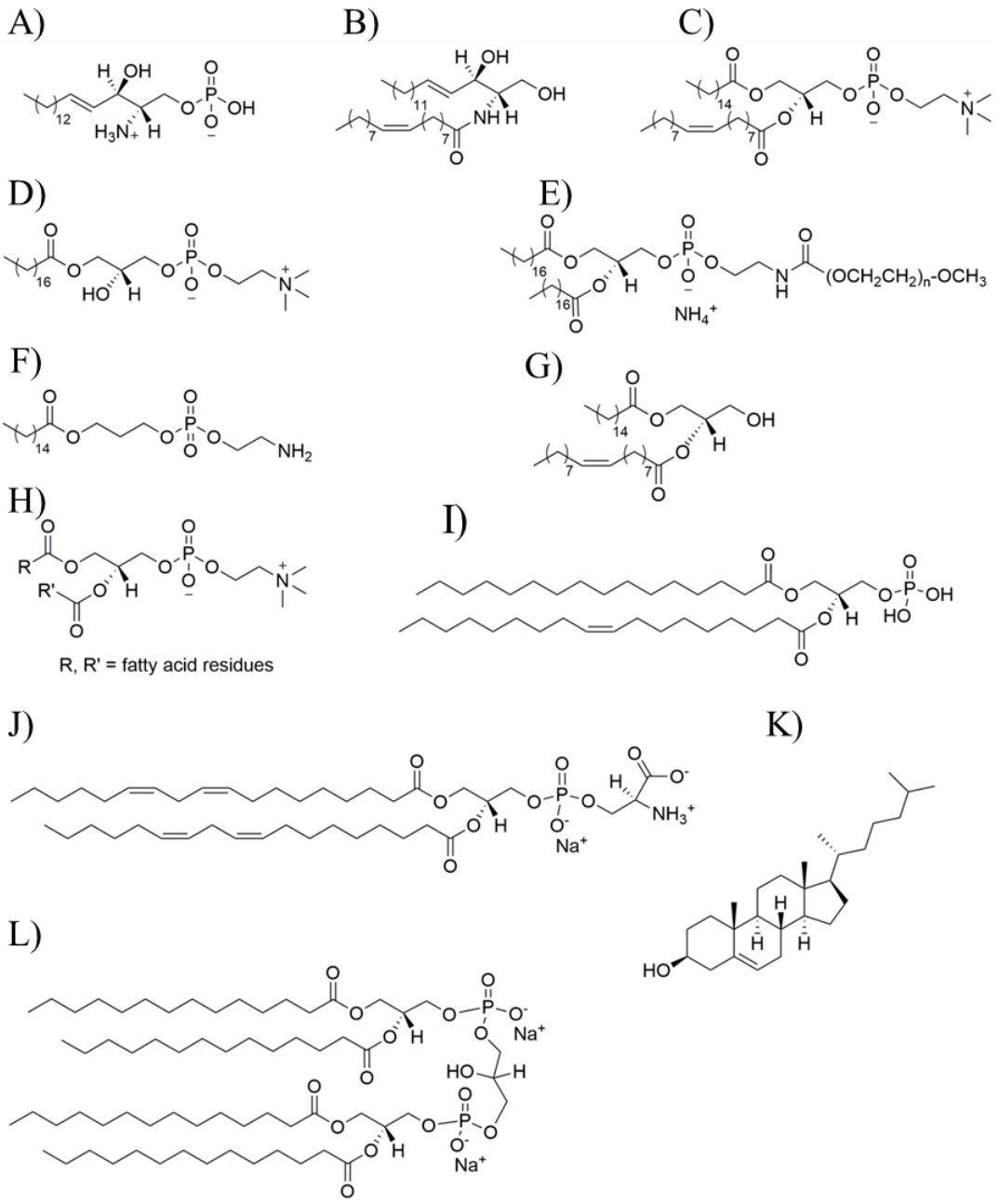

Figure 3.10. Lipid standards used to compare performance of Q-TOF and LTQ-Orbitrap. (A) D-erythro-sphingosine-1-phosphate, (B) C18:1 Ceramide (d18:118:1(9Z)), (C) 1-palmitoyl-2-oleoyl-*sn*-glycero-3-phosphocholine, (D) 1-stearoyl-2-hydroxy-*sn*-glycero-3-phosphocholine, (E) 1-palmitoyl-2-oleoyl-*sn*-glycero-3-phosphoinositol (ammonium salt), (F) 1-stearoyl-2-hydroxy-*sn*-glycero-3-phosphoethanolamine, (G) 1-palmitoyl-2-oleoyl-*sn*-glycerol, (H) L-α-Phosphatidylcholine, (I) 1-palmitoyl-2-oleoyl-*sn*-glycero-3-phosphate, (J) L-α-phosphatidylserine (sodium salt), (K) Cholesterol, (L) 1',3'-bis[1,2-dimyristoyl-*sn*-glycero-3-phospho]-glycerol (sodium salt).

(A). Positive ESI	Accuracy, ppm (±SD)	
	Q-TOF	LTQ-Orbitrap
1-stearoyl-2-hydroxy-*sn*-glycero-3-phosphoethanolamine (*m/z* 747.5780)*	0.29 (0.13)	1.83 (0.21)
1-palmitoyl-2-oleoyl-*sn*-glycero-3-phosphocholine (*m/z* 759.5780)*	0.41 (0.02)	2.17 (0.25)
1-stearoyl-2-hydroxy-*sn*-glycero-3-phosphocholine (*m/z* 523.3640)	0.96 (0.90)	0.95 (0.49)

(B). Negative ESI	Accuracy, ppm (±SD)	
	Q-TOF	LTQ-Orbitrap
1-stearoyl-2-hydroxy-*sn*-glycero-3-phosphoethanolamine (*m/z* 747.5780)	0.76 (0.64)	0.89 (0.38)
1-palmitoyl-2-oleoyl-*sn*-glycero-3-phosphocholine (*m/z* 759.5780)*	0.61 (0.21)	2.36 (0.24)
1-stearoyl-2-hydroxy-*sn*-glycero-3-phosphocholine (*m/z* 523.3640)*	1.37 (0.56)	1.75 (0.41)
1-palmitoyl-2-oleoyl-*sn*-glycerol (*m/z* 620.5380)*	1.22 (0.46)	2.10 (0.38)
D-erythro-sphingosine-1-phosphate (*m/z* 379.2490)	1.21 (0.16)	1.45 (0.25)
C18:1 Ceramide (d18:1/18:1(9Z)) (*m/z* 563.5280)*	1.49 (0.76)	1.81 (0.76)
L-α-Phosphatidylcholine (*m/z* 767.9999)	2.42 (0.51)	2.62 (0.67)

Table 3.4. Mass accuracies of lipid standards analyzed using the Q-TOF and the LTQ-Orbitrap instruments. (A) Positive ionization mode. (B) Negative ionization mode. Reported values (ppm) are mean of 3 replicates (±SD). Only standards that detected commonly on both instruments are shown here. Compounds with statistically different accuracies ($p < 0.05$) are marked with an asterisk.

3.3.3. Mass Resolution

High mass resolution is essential to distinguish among compounds with similar molecular masses, which are common place in complex biological mixtures. Including the mass resolution of all peaks detected in the analysis of PNF, the LTQ-Orbitrap had an average resolution of 7.4×10^4 and 6.3×10^4 in positive and negative ionization modes,

respectively. The Q-TOF had an average resolution of 4.3×10^4 and 4.2×10^4 in positive and negative ionization modes, respectively. Further examination of resolution as a function of *m/z* revealed opposite trends in resolution as a function of *m/z* (Figure 3.5). For the Q-TOF resolution increased when *m/z* increases. For the LTQ-Orbitrap resolution decreased when *m/z* increases. In summary, the LTQ-Orbitrap had higher mass resolution from 200 to 700 *m/z*, while the Q-TOF had higher mass resolution from 700 to 1200 *m/z*.

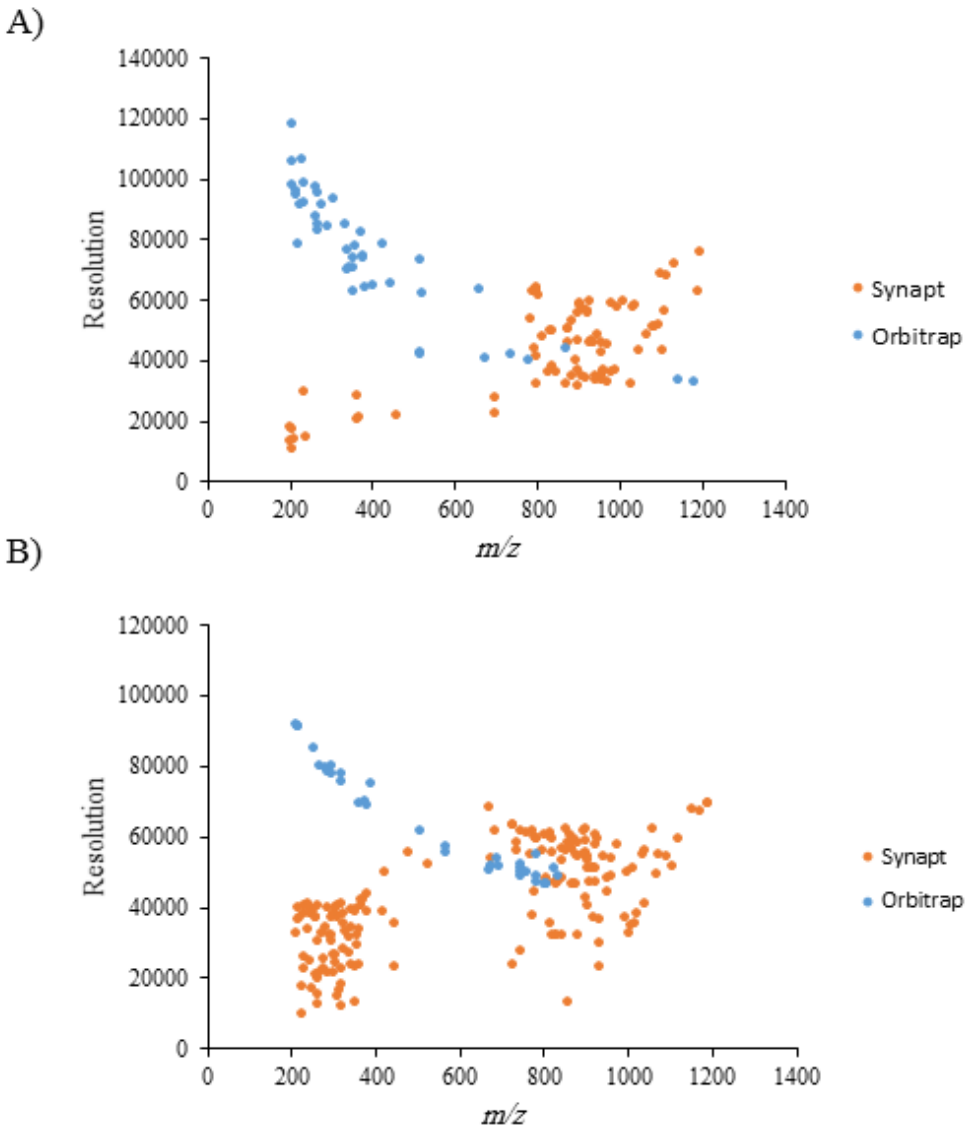

Figure 3.11. Mass resolution comparison. (A) Positive ionization mode. (B) Negative ionization mode. Using the LTQ-Orbitrap, n = 44 and 36 for positive and negative ionization modes, respectively. Using the Q-TOF, n = 81 and 182 for positive and negative ionization modes, respectively.

3.3.4 Signal to Noise Ratio

The signal-to-noise ratio (S/N) of a mass spectrometer defines the ability to detect low abundance species, which are present in complex biological samples. The comparison

of S/N values of species detected in both LTQ-Orbitrap and Q-TOF was based on (1) the analysis of twelve lipid standards (Table 3.2, Figure 3.4) spiked into PNFs and (2) comparisons between peaks detected in both the LTQ-Orbitrap and Q-TOF when analyzing the same PNF. A summary of the signal to noise values calculated in positive and negative ESI is shown in Table 3.2.

As an example, the S/N for 1-palmitoyl-2-oleoyl-*sn*-glycero-3-phosphocholine standard (*m/z* 759.5780) spiked into PNF in positive ionization mode was 6.8 ± 0.3 and 4.9 ± 0.2 (average ± SD, n = 3 technical replicates) for analysis done on the Q-TOF and LTQ-Orbitrap, respectively. The S/N for the same compound in negative ionization mode was 29.0 ± 0.5 and 99.0 ± 0.5 (average ± SD, n = 3 technical replicates) for analysis done on the Q-TOF and LTQ-Orbitrap, respectively.

Another example shows the S/N for 1,2-distearoyl-*sn*-glycero-3-phosphoethanolamine standard (*m/z* 747.5780) in positive ionization mode was 8.0 ± 0.3 and 9.0 ± 0.7 (average ± SD, n = 3 technical replicates) on Q-TOF and LTQ-Orbitrap, respectively. The S/N for the same compound in negative ionization mode was 18.0 ± 0.3 and 21.0 ± 0.5 (average ± SD, n = 3 technical replicates) for analysis done on the Q-TOF and LTQ-Orbitrap, respectively.

(A). Positive ESI	Signal to Noise, ppm (±SD)	
	Q-TOF	LTQ-Orbitrap
1-stearoyl-2-hydroxy-*sn*-glycero-3-phosphoethanolamine (*m/z* 747.5780)*	8.02 (0.32)	9.43 (0.73)
1-palmitoyl-2-oleoyl-*sn*-glycero-3-phosphocholine (*m/z* 759.5780)	6.88 (0.31)	4.96 (0.21)
1-stearoyl-2-hydroxy-*sn*-glycero-3-phosphocholine (*m/z* 523.3640)	6.12 (0.43)	5.41 (0.91)

(B). Negative ESI	Signal to Noise, ppm (±SD)	
	Q-TOF	LTQ-Orbitrap
1-stearoyl-2-hydroxy-*sn*-glycero-3-phosphoethanolamine (*m/z* 747.5780)	18.62 (0.33)	21.18 (0.53)
1-palmitoyl-2-oleoyl-*sn*-glycero-3-phosphocholine (*m/z* 759.5780)*	29.28 (0.54)	99.25 (0.52)
1-stearoyl-2-hydroxy-*sn*-glycero-3-phosphocholine (*m/z* 523.3640)	32.73 (0.71)	39.64 (0.11)
1-palmitoyl-2-oleoyl-*sn*-glycerol (*m/z* 620.5380)*	27.96 (0.37)	18.02 (0.23)
D-erythro-sphingosine-1-phosphate (*m/z* 379.2490)	49.06 (0.35)	40.24 (0.83)
C18:1 Ceramide (d18:1/18:1(9Z)) (*m/z* 563.5280)*	31.08 (0.65)	47.53 (0.74)
L-α-Phosphatidylcholine (*m/z* 767.9999)*	19.83 (0.45)	47.27 (0.14)

Table 3.5. Signal to noise values of lipid standards analyzed using the Q-TOF and the LTQ-Orbitrap. (A) Positive ionization mode. (B) Negative ionization mode. Reported values (ppm) are mean of 3 replicates (±SD). Only standards that detected commonly on both instruments are shown here. Compounds with statistically different S/N ($p < 0.05$) are marked with an asterisk.

To compare the S/N values of peaks detected at the same *m/z* in both instruments, S/N values at each *m/z* were reported as a ratio of the value obtained with the Q-TOF over that obtained with LTQ-Orbitrap (Figure 3.6). Out of 528 features in positive ESI mode, 344 features (65% of the features) had a relative S/N value higher than 1,177 features (34% of the features) had a S/N value lower than 1, and 7 features (1% of the features) had

relative S/N value of 1 (corresponding to zero in the log graph in Figure 3.6). Out of 89 features in negative ESI mode, 67 features (75% of the features) had a relative S/N value higher than 1, 13 features (15% of the features) had a S/N value lower than 1, and 9 features (10% of the features) had relative S/N value of 1. These values show that signal to noise values were higher for the data collected on the Q-TOF, overall. Furthermore, a t-test was performed on the average signal to noise values in positive and negative ESI using both instruments. Compounds with statistically different S/N ($p < 0.05$) are marked with an asterisk in Table 3.2.

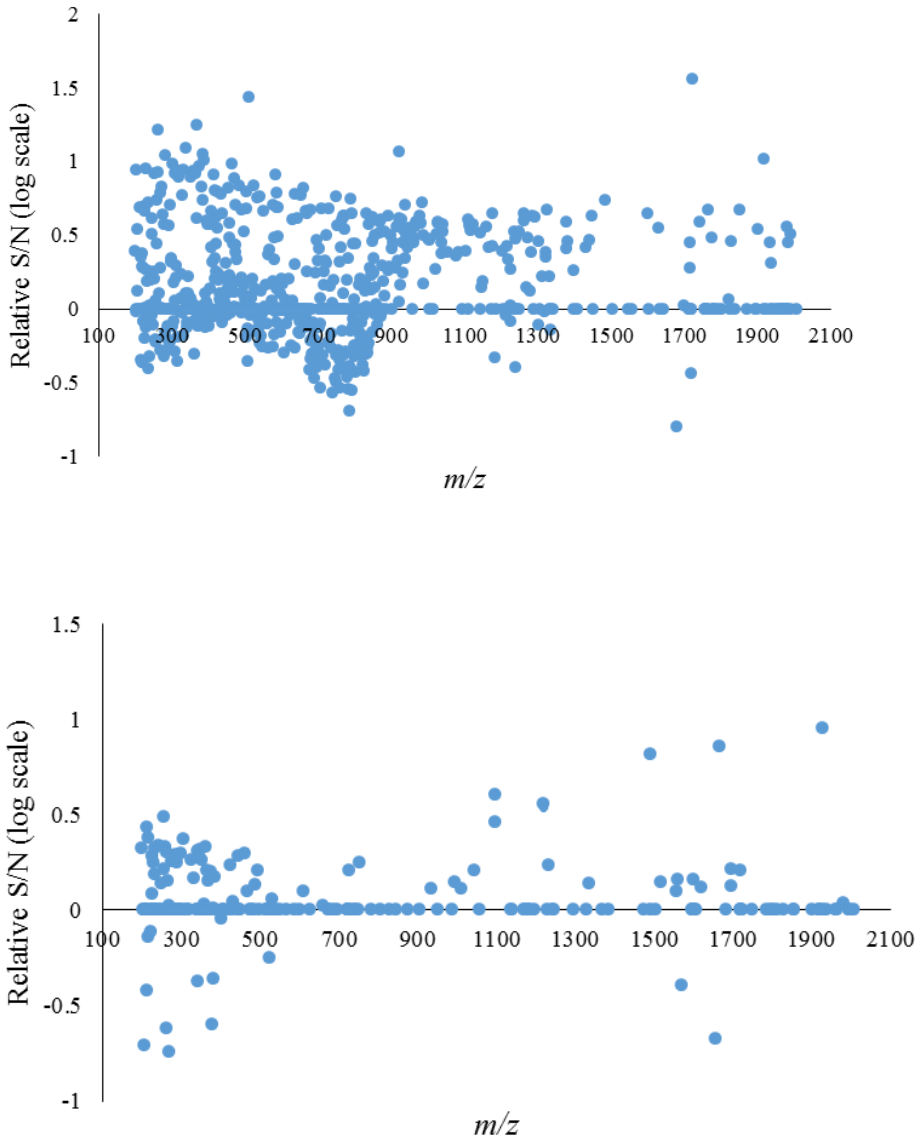

Figure 3.12. Relative signal to noise values. The S/N of peaks at a given *m/z* that were detected on both instruments and passed Checkpoint 1 (see Section 3.2.4) is plotted as their ratio (Q-TOF/LTQ-Orbitrap) on a log scale (y-axis). (A) Positive ionization mode (n= 528). (B) Negative ionization mode (n= 89).

3.3.5. Data Analysis

Data processing and interpretation represent the most challenging and time-consuming steps in high-throughput metabolomic experiments, regardless of the analytical platforms used for data acquisition.[116] The software used for data analysis and search in databases influence the data outcomes, particularly in terms of discrimination between true and false positives. This study compared five commonly used programs in metabolite analysis: XCMS, Progenesis, LipidSearch, Xcalibur, and MassLynx[117] in their ability to assign maximum number of potential molecular identities in databases based on the mass spectra of peaks that were selected through the workflow described in Section 3.2.4.

Xcalibur and Masslynx were limited in platform versatility as they are only compatible with data analysis collected with the LTQ-Orbitrap (Velos) and the Q-TOF (Synapt G2), respectively (Figure 3.7). Xcalibur assigned 210 and 612 peaks to potential molecular identities in positive and negative ionization mode, respectively. Masslynx assigned 980 and 689 peaks to potential molecular identities in positive and negative ionization mode, respectively.

Progenesis and XCMS were capable of analyzing data collected with both the LTQ-Orbitrap (Velos) and the Q-TOF (Synapt G2) (Figure 3.7). Progenesis found 184 and 680 potential molecular identities, under positive ionization mode, with the LTQ-Orbitrap (Velos) and the Q-TOF (Synapt G2), respectively. Under negative ionization mode, these two platforms showed 38 and 86 potential molecular identities, respectively. XCMS

assigned 68 and 664 peaks to potential molecular identities to data collected, under positive ionization mode, with the LTQ-Orbitrap (Velos) and the Q-TOF (Synapt G2), respectively. Under negative ionization mode, these two platforms assigned 335 and 32 peaks to potential molecular identities, respectively. The compatibility of XCMS with different analytical platforms and its ability to assign higher numbers of peaks to potential molecular identities are clear advantages to process data with either one of the instruments that were compared in this study.

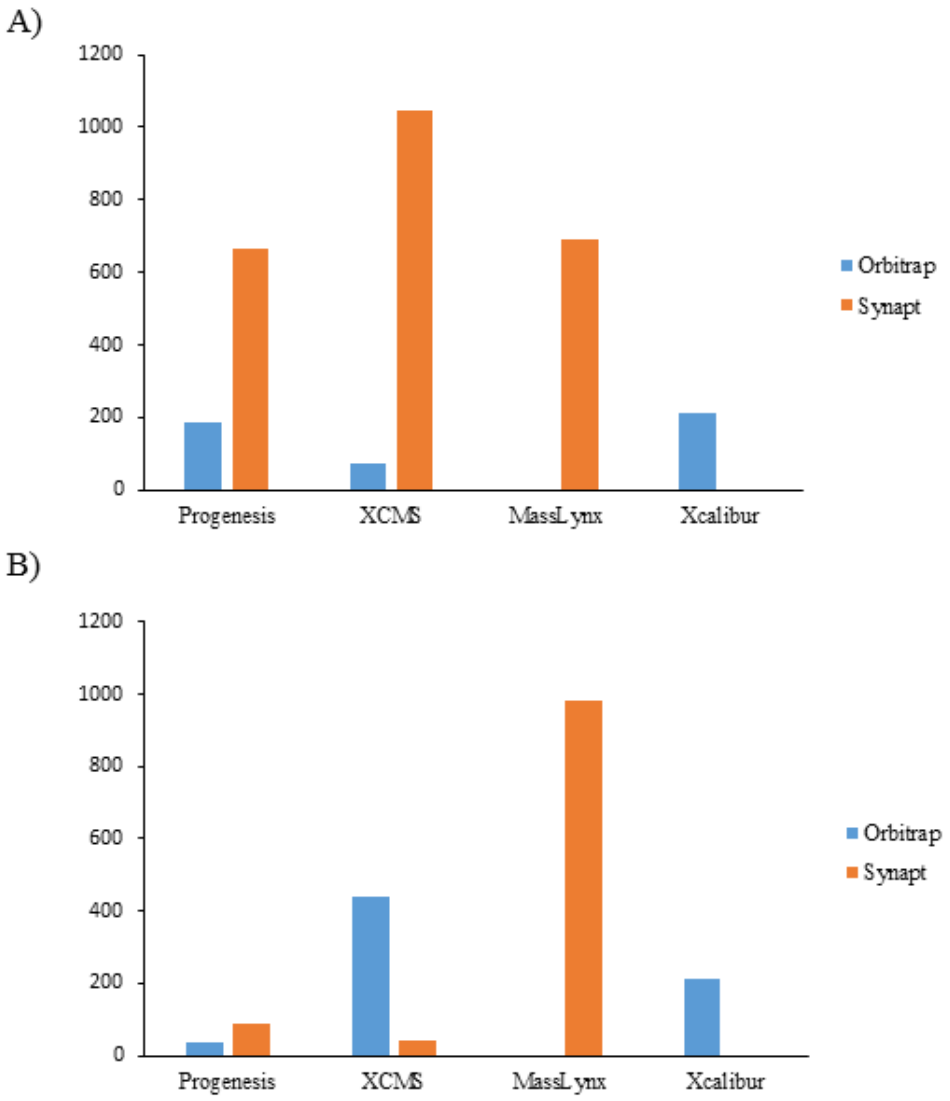

Figure 3.13. Number of potential assignments to molecular identities using different software platforms. (A) Positive ionization mode. (B) Negative ionization mode. The number of potential assignments required processing of the raw data using the workflow described in Section 3.2.4.

3.4. Discussion

The goal of thisstudy was to compare two mass spectrometry platforms, LTQ-Orbitrap and Q-TOF, to determine their suitability for unbiased analysis of compounds from lipid extracts of PNFs of a mouse myoblast cell line.

Analysis of lipid standards was key to the comparison of the two platforms. As expected, not all the lipids were detected equally under positive and negative ion mode (Figure 3.4, Table 3.1).

In positive ion mode, phosphatidylcholines (1-palmitoyl-2-oleoyl-*sn*-glycero-3-phosphocholine, 1-palmitoyl-2-oleoyl-*sn*-glycero-3-phosphocholine) and phosphatidylethanolamine (1-stearoyl-2-hydroxy-*sn*-glycero-3-phosphoethanolamine) were detected, as expected from their positive polar head group. Adducts of ceramides (C18:1 Ceramide (d18:118:1(9Z)), and neutral lipids (1-palmitoyl-2-oleoyl-*sn*-glycero-3-phosphoinositol, 1-palmitoyl-2-oleoyl-*sn*-glycerol, 1',3'-bis[1,2-dimyristoyl-*sn*-glycero-3-phospho]-glycerol) might be detected as sodium and ammonium ions in positive ion mode, as reported previously in the literature.[118,119] In our study, these species were not detected on either the Q-TOF or Orbitrap platforms. Lipids that were detected under negative ion mode included phosphatidylcholines (1-palmitoyl-2-oleoyl-*sn*-glycero-3-phosphocholine, 1-palmitoyl-2-oleoyl-*sn*-glycero-3-phosphocholine), phosphatidylethanolamine (1-stearoyl-2-hydroxy-*sn*-glycero-3-phosphoethanolamine), phosphatidylinositol (1-palmitoyl-2-oleoyl-*sn*-glycero-3-phosphoinositol), phosphatidylserine (L-α-

phosphatidylserine), phosphatidylglycerol (1-palmitoyl-2-oleoyl-*sn*-glycerol), phosphatidic acid (1-palmitoyl-2-oleoyl-*sn*-glycero-3-phosphate), ceramide (C18:1 Ceramide (d18:1/18:1(9Z)), and sphingolipids (D-erythro-sphingosine-1-phosphate).

As described in the results section, mass accuracy for 6 out of 10 lipid standards the Synapt had better mass accuracy than the LTQ-Orbitrap in both negative and positive ionization modes. The other four lipid standards were had statistically similar mass accuracy when compared across instruments. This observation is in agreement with previous reports.[106] These findings are not surprising as mass accuracy is dependent on the design and operation modes unique to each instrument design. The narrow spread of the initial velocity in a TOF decreases uncertainty in the time-of-flight which results in accurate masses. In the Orbitrap, the frequencies of axial oscillation of each ion cause an image current with the same frequency that are transformed into *m/z* values.[120] Error in the current image centroids, which is more prominent at low signal intensities, tends to introduce more error in mass accuracy that observed in TOF configurations.[85,121]

It is worth noticing that our study used external mass calibration for both the Q-TOF and the LTQ-Orbitrap. Further improvements in mass accuracy (< 1 ppm for Q-TOF and ~ 2 ppm for LTQ-Orbitrap) might be obtained with the use of internal calibration for each of these instruments, as reported elsewhere.[122] Lastly, other hybrid Orbitraps (Exactive Plus) have been compared with the Q-TOF (Synapt G2) in terms of mass accuracy in a plant metabolomics study.[106] The authors claimed that both instruments showed an average mass accuracy of < 2.5 ppm (*m/z* range= 100-1200) using external

calibration for all measured compounds. This is not surprising as it has been shown that the Q Exactive outperforms the LTQ-Orbitrap Velos in metabolome and proteome analyses.[123]

There are currently no prospective studies comparing the reproducibility of peak intensities of TOF and Orbitrap based instruments. In this study, reproducibility of the peak intensities was calculated to establish the level of variation among technical replicates using two different mass spectrometers. Our data showed that Synapt outperformed the Orbitrap in reproducibility in both positive and negative ESI. Previous studies on the comparison between LTQ and high resolution Orbitraps showed that Orbitraps can produce more reproducible identifications than LTQs for analyzing lipids and proteins; however, the difference is not large.[124]

Mass resolution was *m/z* dependent and better for the LTQ-Orbitrap below 700 *m/z*, while better for the Q-TOF above 700 *m/z*. These observations are consistent with the design of these mass analyzers. In Orbitrap mass analyzers, the axial frequency used to derive the *m/z* ratio is inversely proportional to the square root of *m/z*.[85,125,126] Because axial frequency is independent of the initial properties of the ions, including kinetic energy or ion velocity, Orbitrap mass analyzers tend to have excellent mass resolution in the low *m/z* range.[127] In TOF mass analyzers, mass resolution is related to differences in time of flight of ions with similar *m/z* and is directly proportional to the square root of *m/z*. At low *m/z* values the broadening in the time-of-flight dominates, compromising mass resolution.[128] At large *m/z* values, TOF mass analyzers tend to have superior resolution.

Detection and identification of low-abundance metabolites in complex biological samples presents major challenges in metabolomics studies. Signal to noise ratio is a key parameter to assess the detection capabilities of mass spectrometers which depends on the instrumentation design and performance. Our results indicated that higher values of the signal to noise ratio can be obtained on the Synapt G2. Previous studies reported *m/z* dependent and compound specific differences comparing the performances of Orbitrap and QTOF instruments.[106]

Background ions originating from solvent clusters generated by the electrospray ionization are considered a factor limiting the detection threshold (and noise) in TOF instruments.[126] The effect of background ions on instrument noise is less relevant in Orbitrap instruments as Fourier transform-based filtering is used to remove the chemical background.[129] On the other hand, overloading of the C-trap in Orbitrap instruments can cause ion suppression decreasing signal intensity, thereby decreasing the signal-to-noise ratio.[130,131]

Existing computational tools are essential to assign molecular structures found in databases to experimental mass spectral data.[132] Oftentimes the selection of such tool is defined by the analytical platform used to collect the data (e.g. Masslynx for Synapt and Xcalibur for Velos). Other computational resources are compatible with multiple platforms, such as Progenesis and XCMS used in this study. Overall XCMS provided more potential molecular identities assignments for both the Q-TOF (Synapt) and the LTQ-Orbitrap (Velos) (Figure 3.7). Using XCMS to analyze the data resulted in different number of identifications from these two instruments. Different number of features detected by

XCMS online (set under equal parameters) for both systems suggests dissimilar sensitivity for the vast majority of compounds. We presume the differences in the number of preliminary identification are likely due to databases used in each program. METLIN database within XCMS, includes 961,829 molecules (as of 2018) ranging from lipids, steroids, small peptides, carbohydrates, exogenous drugs/metabolites, central carbon metabolites and toxicants. The results from this comparison is in agreement with a previous report[86] that there is only a partial overlap in the results obtained with different software programs of LC-MS metabolomic analysis. Even within the same software, the use of different parameters and thresholds strongly affects peak detection performance.[105]

3.5. Conclusions

This study evaluated reproducibility, mass accuracy, resolution, signal to noise ratio in a comparative analysis of small molecules in lipid-enriched extracts that used both a Q-TOF (Synapt) and LTQ-Orbitrap (Velos) instruments. Overall, both Synapt and Orbitrap mass spectrometers showed adequate mass accuracies. However, the accuracy was better using the Synapt for multiple lipid standards in both positive and negative ESI. The LTQ-Orbitrap had higher mass resolution from 200 to 700 *m/z*, while the Synapt had higher mass resolution from 700 to 1200 *m/z* values. Reproducibility associated with the metabolite peak intensities was better using the Synapt in both positive and negative ESI. Synapt data showed significantly higher signal to noise values (65% and 75% of the detected features on both instruments have relative S/N greater than 1 in positive and negative ESI respectively), which is an advantage in omics studies of biological matrices.

Differences in signal to noise ratios obtained on the two instruments were not statistically significant in the negative ESI data. XCMS was preferred as automated software for processing the metabolomics data while assigning more peak IDs in a shorter time. Taken together, our results suggest that, as used in this study, Q-TOF is better suited for untargeted metabolomics and lipidomics studies.

Chapter 4: Comparative Lipidomic Analysis of lipid droplets from *C. elegans* at Different Ages

Lipid droplets are cytoplasmic organelles that store neutral lipids for membrane synthesis and function as cellular energy reserves.[39] The lipid droplets are composed primarily of triacylglycerols, surrounded by a phospholipid monolayer composed mainly of phosphatidylcholine and phosphatidylethanolamine. The significance of lipid droplets in regulation of various cellular processes, lipid homeostasis, transport, and metabolism is increasingly recognized, yet the unique lipid composition and properties of lipid droplets remains poorly understood.[133] Here, an LC/MS method was employed to investigate the composition of purified *Caenorhabditis elegans (C. elegans)* lipid droplets to characterize their lipid profiles in an aging study. Comparison of the lipid droplet profiles of nematodes at Day 1 (D1), Day 4 (D4), and Day 7 (D7) of the adult stage showed alterations in the lipidome over different stages of adulthood. Untargeted LC/MS analysis resulted in 82 metabolite features with significantly changed abundance in all the biological replicates in D1 compared to D4 samples, 95 metabolite features with statistically changed abundance in D1 compared to D7 samples and 16 metabolite features with statistically changed abundance in D4 compared to D7 samples. From the 65 potential identifications of triglycerides detected in both day 1 and day 7 samples, 90.7% increased in abundance with age. From the 59 potential identifications of triglycerides detected in both day 1 and day 4 samples, 94.5% increased in abundance with age. From the 12 potential identifications of triglycerides in both day 4 and day 7 samples, 83.3% increased in abundance with age. Overall, this lipidomics survey provides further incentive to systematically study lipid droplets, so that a better understanding of aging related lipid dysfunction can be achieved.

4.1. Introduction

Over the past decades, a large body of work has led to the identification of genes and proteins that affect longevity in different model organisms. Recently, it was discovered that lipids play vital roles in human physiological and pathological processes.[134,135] However, the role of lipids in aging remains poorly understood. The nematode *Caenorhabditis elegans (C.elegans)* is being used extensively as a model organism for understanding the molecular mechanisms of aging.[136,137] The popularity of *C. elegans* as an aging model is largely due to its short life span (~ three weeks), and the ability to knock down genes that affect worm function and behavior. The nematode can easily be maintained under laboratory conditions and is used in high-throughput automated experiments.

C. elegans store neutral lipids in cytosolic lipid droplets (LDs). Lipid droplets are fat-storing organelles consisting of a hydrophobic core of triacylglycerol (TAG) and cholesterol ester surrounded by a phospholipid monolayer containing various proteins (see Chapter 2).[8,138] Lipid droplets are involved in membrane synthesis and are energy reserves.[8,39,139] In addition to energy storage and membrane synthesis, lipid droplets play important roles in the regulation of various cellular processes, including lipid transport and cellular metabolism.[140,141] Prior work showed that lipid composition of this model organism may change during aging, since the pathways that influence aging also regulate lipid metabolism pathways.[142,143] Previous aging related studies exhibited several differences in the composition of lipid droplets isolated from wild type *C. elegans* and

longer lived *daf-2* mutants.[144] Some studies describe an increase in the abundance of TAGs sequestered within LDs in the long lived *daf-2* mutants.[136,145]

Comprehensive measurement of lipids is challenging due to their diverse structures. Liquid chromatography coupled to mass spectrometry (LC/MS) is the most broadly applicable technology in the field of metabolomics and lipidomics, which allows relative and/or absolute quantification.[146] Use of LC/MS techniques give the possibility to separate and quantitate different classes of compounds according to their physicochemical properties. Due to their high sensitivity, selectivity, and mass accuracy, high resolution mass analyzers are often the method of choice for providing global metabolite analysis.[147]

Data processing and compound identification is still the bottleneck in LC/MS based metabolomics.[146] The data-processing pipeline usually proceeds through multiple stages (see Chapter 2). Computational tools and online databases have been developed for mass spectral lipid analysis including METLIN, MassBank, and LipidMaps.[100,112] In a former study comparing multiple data processing software (the work described in Chapter 3), we indicated that XCMS allows for data processing tasks to be programmed and performed automatically. In addition, XCMS shows significant advantages over other data processing methods. These include the ease of peak integration and detection, automated statistical analysis, and multiple visualization tools of raw data for validation purposes.[105,148]

Here we used an optimized mass spectrometry and data analysis method (see Chapter 3) to profile the composition of purified lipid droplets in adult *C. elegans* of

different ages. Our findings show that the dynamics of LD metabolome are influenced by *C. elegans* aging, in particular, that aging affect lipid storage in lipid droplets.

4.2. Materials and Methods

4.2.1. Reagents

Buffers used for lipid droplet isolation were as follows: Buffer A is composed of 20 mM tricine and 250 mM sucrose by dissolving 1.79 g of tricine in 400 ml of deionized (DI) water and 50 ml of 2.5 M sucrose in 500 ml of DI water. The pH was adjusted to 7.8 with KOH. Buffer B is composed of 20 mM 4-(2-hydroxyethyl)-1-piperazineethanesulfonic acid (HEPES), 100 mM KCl and 2 mM $MgCl_2$ (pH 7.4) by dissolving 0.95 g of HEPES, 1.49 g of KCl and 0.038 g of MgCl2 in 180 ml of deionized water. The pH was adjusted to 7.4 with KOH and the volume was brought up to 200 ml. Collagenase 3 buffer used for worm homogenization included 100 mM Tris-HCl, and 1 mM $CaCl_2$, with or without Collagenase 3 enzyme (collagenase 3). The solvents used for extraction were HPLC grade chloroform and methanol from Fisher Scientific (Fairlawn, NJ). Butylated hydroxytoluene (BHT) was made by dissolving 100 mg of 2,6 Di-tert-butyl-methyl phenol (Sigma Aldrich) in chloroform. M9 buffer (42 mM Na_2HPO_4, 22 mM KH_2PO_4, 86 mM NaCl, and 1 mM $MgSO_4.7H_2O$) was used for washing worms off the plate (200 µl for Day 1 to 400 µl for Day 4 and Day 7). Protease Inhibitor cocktail (AEBSF, aprotinin, bestatin, E-64, leupeptin and pepstatin A, Thermo Fisher, Waltham, MA) were added to all buffers in accordance with manufacturer's instructions. Canola Oil (15 mg/ml) in chloroform (Sigma Aldrich) was used as the standard for lipid quantification. Vanillin

(Sigma Aldrich), o-phosphoric acid (85%), and sulfuric acid (95-98%, Sigma Aldrich) were used for lipid quantification.

4.2.2. Lipid Droplet (LD) Isolation

This part was performed by Joseph Renner Daniele and Gilbert Garcia, who were in Andrew Dillin's laboratory, Department of Molecular and Cell Biology, University of California, Berkley. *C. elegans* cultures (~200,000 worms from 200 plates at 1000 worms per plate) were collected from day 1, day 4, and day 7 adult stage into a large beaker by washing them off plates with M9 + 0.1% Tween. Worms were transferred to 50 ml tubes and sedimented at 200 g at 4 °C for 5 minutes to reduce volume. The pellet was collected and transferred to 15 ml tube and washed once with 10 ml of M9 + 0.1% Tween and then with 10 ml of M9. Sedimented pellet was treated with collagenase buffer (at 1 mg/ml concentration) and the tube was incubated at 20 ºC with end over end agitation for 30 minutes. Worms were sedimented at 2,000 g for 5 minutes and the collagenase buffer was aspirated. Worms were washed 5 times with M9 at room temperature and washed twice with cold Buffer.

The pellet was moved on ice to a metal Dounce homogenizer with a glass pipette. The pellet was resuspended in Buffer A and protease inhibitor to a final volume of 7 ml of worms/buffer and was homogenized with 20 strokes (on ice). Worm lysate was transferred into 15 ml conical tubes on ice and the homogenizer was washed with ~3.5 ml Buffer A (with protease inhibitor) to collect all the lysate. The lysate (500 µl) was saved on ice and frozen with liquid nitrogen; the remaining 10 ml of lysate was spun at 1,500 g for 11

minutes at 4 ºC to pellet nuclei/debris. The nuclear pellet was resuspended in 1.5 ml of Buffer B (with protease inhibitor) and frozen in a tube with liquid N2. Homogenized *C. elegans* fraction was transferred into a 12 ml Ultra Centrifuge SW41 tube and Buffer B (with protease inhibitor) was carefully layered on top and the tube spun at 11,000 rpm (15,000 g) for 70 min at 4 ºC. LD fraction (white, cloudy) was collected from the top of the tube and was transferred via a glass pipet to a siliconized microcentrifuge tube. Collected fraction was spun at 18,000 g for 10 minutes and the bottom, aqueous layer was removed. Isolated lipid droplets were shipped to University of Minnesota (UMN) in chloroform on dry ice. Samples were stored at -80 ºC under nitrogen until LC/MS analysis.

4.2.3. Metabolite (Lipid) Extraction

Ice cold methanol and chloroform (1:1) were added to the collected lipid droplet samples and vortexed for 30 seconds at 4 ºC. Samples were shaken for 20 minutes with a tube shaker set to 1400 rpm and vortexed for additional 30 seconds. Sample tubes were centrifuged at 20,000 *g* for 10 minutes at 4 ºC. Polar phase was collected and stored at -80 ºC. Protein interphase between the aqueous and organic phase was removed and 200 µL of nonpolar phase was collected by tilting tube 45 ºC and transferred to ice cold glass vials. Chloroform (2 ml) was added to each sample vial followed by an addition of 5 µl of 10 mg/ml BHT/chloroform and stored at -80 ºC.

Ice cold methanol (1 ml) was added to the interphase protein fraction and spun at 20,000 *g* for 10 minutes at 4 ºC. Methanol was then removed from protein pellet and the organic phase was dried under vacuum and was centrifuged at 30 ºC for 15 minutes. Pellets

were resuspended in 2x Laemmli buffer (200 µl for Day 1 to 400 µl for Day 4 and Day 7). Samples were pipetted up and down and stored at -80 ºC.

4.2.4. Lipid Quantification

A modified colorimetric method was used for quantitative analysis of total lipids. The sulfo-phospho-vanillin (SPV) assay[149] possesses many advantages including small amount sample volume, less time and less labor, and more consistent color development. Canola oil used as a generic triglyceride standard was loaded into 96 well plate in a range of 0 mg to 3.6 mg of lipids in chloroform. Purified lipid droplet samples were added (10 µl) into empty wells, in triplicate. The solvent was evaporated under chemical fume hood and 100 µl of sulfuric acid was added to all wells and incubated at 90 °C for 10 min. Vanillin/H_2O (6.4 ml of 1mg/ml) mixture, 8 ml o-phosphoric acid, and 25.6 ml hot water was freshly made and used to make the final vanillin reagent. The plate was cooled on ice to room temp (~2 min) and 100 µl of vanillin-phosphoric acid reagent was added to all wells. After ~5 min the color was developed and absorbance was measured at 540 nm on a UV spectrophotometer.[150] Samples were normalized to the total lipid content (100 µg/ml) upon injection to the LC/MS.

4.2.5 LC/MS Conditions

Samples were resuspended in 200 ml 1:1 v/v methanol:chloroform to a final concentration of 50 µg/ml and were vortexed for 30 s to resuspend the pellet. A Waters Acquity UPLC coupled to a Waters Synapt G2 HDMS quadrupole orthogonal acceleration time of fight mass

spectrometer was used for UPLC/MS analysis. The reversed-phase column used was a Waters HSS T3 C18, 2.1 mm × 100 mm (1.7 µm diameter particles) operating at a temperature of 45 °C. The following gradient separation was employed at a flow rate of 400 µL/min using a binary solvent manager system (Waters). Mobile phase A included Methanol:Water, 60:40 v/v, with 10mM ammonium acetate, containing 0.1% formic acid. Mobile phase B was Methanol:Isopropanol 10:90 v/v with 10mM ammonium acetate, containing 0.1% formic acid. The gradient profile was: 40% B, 0 min to 5 min; 40% B to 100% B, 5 min to 13 min; 100% B, 13 min to 16 min.

The Waters Synapt instrument was tuned with the tuning solution containing sodium iodide in 50:50 2-propanol:water. Simultaneous low- and high-collision energy (CE) mass spectra were collected in centroid mode over the range *m/z* 50–1200 every 0.2 s during the chromatographic separation. Samples were analyzed in high-definition mode (HDMS) and the TOF analyzer was operated in the *V* resolution mode. MS parameters in positive electrospray ionization mode were as follows: capillary, 0.3 kV; sampling cone, 35.0 V; extraction cone, 5.0 V; desolvation gas flow, 800 L/h ; source temperature, 100 °C; desolvation temperature, 20 °C; cone gas flow, 20 L/h; trap CE, off (low CE collection), trap CE ramp 15–65 V (high CE collection); lockspray configuration used the average of three *m/z* measurements (0.2 s scan, *m/z* 100–1200, every 10 s) of protonated leucine-enkephalin (*m/z* 556.2771) formed from infusion of a 5 µg/ ml solution. All MS parameters were identical in negative ionization mode except the following: capillary, 2.5 kV; sampling cone, 30.0 V; extraction cone, 4.0 V.

4.2.6. Data Processing

For each age (D1, D4, D7), there were three biological replicates. Each one of three biological replicates were analyzed three times. Data collected on the Synapt G2 Q-TOF were processed by XCMS online software.[105] Raw data acquired were converted to mzXml common data format using Proteowizard file converter (proteowizard.sourceforge.net) and the following parameters were used in this analysis: (i) Feature detection: centWave method, minimum peak width = 5 and maximum peak width = 20, S/N threshold = 6, mzdiff = 0.01, integration method = 1, prefilter peaks = 3, prefilter intensity = 100, noise filter = 0; (ii) Retention time correction: Obiwarp method, profStep = 1; (iii) Alignment: mzwid = 0.015, bw = 5, minfrac = 0.5, max = 100, minsamp = 1. Principle component analysis (PCA) was used for selecting the metabolite features that are significantly different among the sample groups (see Chapter 2). The three biological replicates of each age were combined and then all features, regardless of whether they were detected once, twice, or three times in the replicates, were used for comparison with other age groups. The data were processed for peak detection, retention time correction, chromatographic alignment, and identification through METLIN database. A workflow (See Chapter 2) was used to evaluate and confirm preliminary identification of features by XCMS.[91]

Extracted ion chromatograms (XICs), were manually examined to select those features that have a true chromatographic peak profile, referred to as Checkpoint 1 in the workflow (see Chapter 2). Retention time correction was applied to the raw data to generate an extracted ion chromatogram for each technical replicate. Fragmentation patterns of

features with matches in the databases were evaluated to provide preliminary identifications, referred to as Checkpoint 2 (see Chapter 2). The top features with the highest significant difference (p-value > 0.05) and the greatest fold change (fold change > 2) were selected from each LC/MS dataset. P-values were calculated in XCMS by performing a Welch's t-test for unequal variances. Identifications were based on a METLIN search of the accurate masses. Multiple adducts were used for the database search. In silico fragmentation data were generated at collision energies of 10, 20, and 40 eV.

Cloud plots and Volcano plots were used in this study for visualization of metabolites that show a combination of fold change and statistical significance (p-value).[151] The three pairwise files that were generated by XCMS were imported into meta-XCMS and filtered by fold change (≥ 2) and p-value (≤ 0.05). Meta-XCMS is a software for performing second-order ("meta") analysis of untargeted metabolomics data from multiple sample groups. Performing second-order (meta-analysis), facilitates the integration and identification of shared patterns of metabolic variation across the results of multiple biologically relevant samples.[113]

4.3. Results

Ultra-high performance liquid chromatography (UPLC) coupled to acquisition of low- and high-collision energy mass spectra analysis was carried out to investigate the composition of enriched lipid droplet fractions from *C. elegans*. For this analysis, we compared the profiles of lipid droplets isolated from nematodes of different ages. For

investigating metabolite changes, we chose to compare lipid profiles of *C. elegans* at their reproductive stages of adulthood (D1 to D4) and middle-aged adults (D7) to describe changes of lipid droplet composition with aging. The link to a full list of identifications is provided in Appendix A.

4.3.1. The Composition of Lipid Droplets isolated from *C. elegans* Differs with Age

The goal of this experiment was to determine metabolite features whose abundance were significantly different between two ages (D1 versus D4, D1 versus D7, D4 versus D7). These are referred as D1D4, D1D7, and D4D7, respectively, in the rest of this chapter. Metabolite profiling from D1, D4, and D7 *C. elegans* lipid droplet fractions was performed by LC/MS. The XCMS online platform was used to visualize and interpret the data. A workflow was utilized to make preliminary identifications from each of the two-group comparisons (see Chapter 2).

Comparison of D1 and D4 samples sets, using LC/MS in the negative ionization mode, resulted in 127 data features. Checking for statistical significance of each feature, 25 hits had a p-value ≤ 0.05, 5 hits had a fold change ≥ 2 and 4 hits were selected that had both p-value ≤ 0.05 and fold change of ≥ 2. At a mass window of 5 ppm, none of these four compounds pass the XIC inspection in either samples D1, D4 or both (see Chapter 2). Based on the results, negative ionization mode was not used for the rest of the experiments.

Using LC/MS in the positive ionization mode enabled multiple comparisons. Tables 4.1, 4.2, and 4.3 show the number of mass features that are statistically different (fold change (≥ 2) and p-value (≤ 0.05)) in D1D4, D1D7, and D4D7 comparisons.

	Replicate 1	Replicate 2	Replicate 3
Raw Data	1078	993	1041
P-value < 0.05	297	485	452
Fold Change > 2	439	673	587
P-val < 0.05 and FC > 2	254	453	397
XIC checkpoint	73	423	389

Table 4.6. Summary of hits resulting from the comparative analysis of lipid droplets isolated from *C. elegans at* Day 1 and Day 4 of adulthood. Data are from three independent biological replicates, each analyzed once. Lipid extractions included both polar and non-polar extractions (see Materials and Methods). ESI analysis was performed in positive (+) ionization mode.

	Replicate 1	Replicate 2	Replicate 3
Raw Data	1095	993	1091
P-value < 0.05	311	485	534
Fold Change > 2	471	673	703
P-val < 0.05 and FC > 2	271	453	500
XIC checkpoint	235	445	481

Table 4.7. Summary of hits resulting from the comparative analysis of lipid droplets isolated from *C. elegans at* Day 1 and Day 7 of adulthood. Other conditions are as described in Table 4.1.

	Replicate 1	Replicate 2	Replicate 3
Raw Data	1124	1087	1118
P-value < 0.05	140	317	319
Fold Change > 2	177	258	341
P-val < 0.05 and FC >2	79	178	202
XIC checkpoint	54	70	235

Table 4.8. Summary of hits resulting from the comparative analysis of lipid droplets isolated from *C. elegans at* Day 7 and Day 7 of adulthood. Other conditions are as described in Table 4.1.

Figures 4.1, 4.2, and 4.3 illustrate data supporting the identification of features that passed the XIC checkpoint in D1D4, D1D7, and D4D7 comparisons.

Reproducibility of the mass spectral intensities of a given feature that appeared at least in one of the biological replicates was calculated after checkpoint 2. The values included in these comparisons varied widely. Coefficient of variations (CVs) for D1, D4 and D7 had ranges of 3-156 % (average = 29 ± 18, n = 368), 1-116 % (average = 201 ± 15, n = 199), and 2 -79 % (average = 18 ± 14, n = 408) respectively. While it is usually recommended to remove individual features with CV > 30% when comparing technical replicates,[152] we anticipated larger variations among these biological replicates, therefore, features with large CVs were not removed.

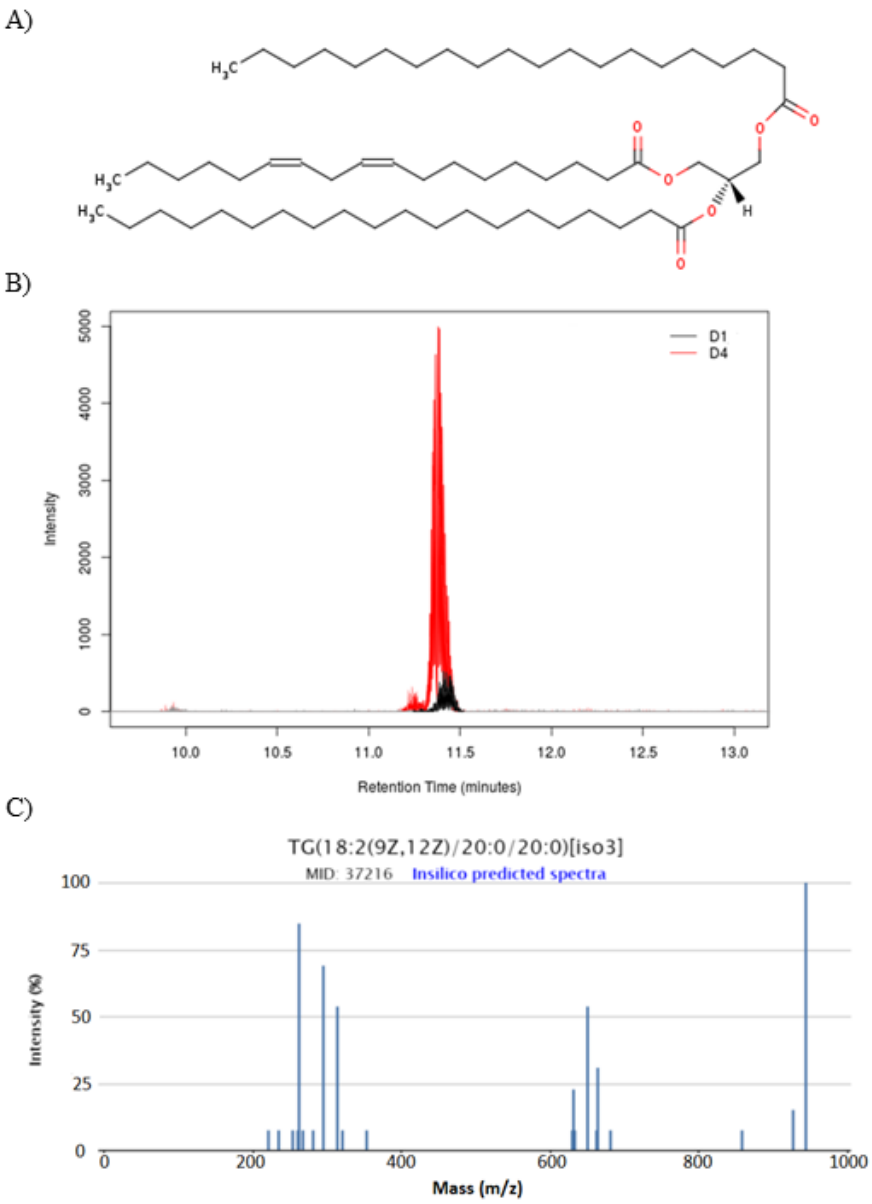

Figure 4.14. Preliminary identification of *m/z* 942.8615 in lipid droplet enriched fractions of Day 1 and Day 4 samples. (A) Structure of 1-(9Z,12Z-octadecadienoyl)-2,3-dieicosanoyl-sn-glycerol, (B) Extracted ion chromatogram of Day 1 (black) and Day 4 (red) samples collected in positive ESI, (C) Matching in silico predicted MS spectra by METLIN. (TR = 10.23 min, p-value = 2.67 x 10^{-4}).

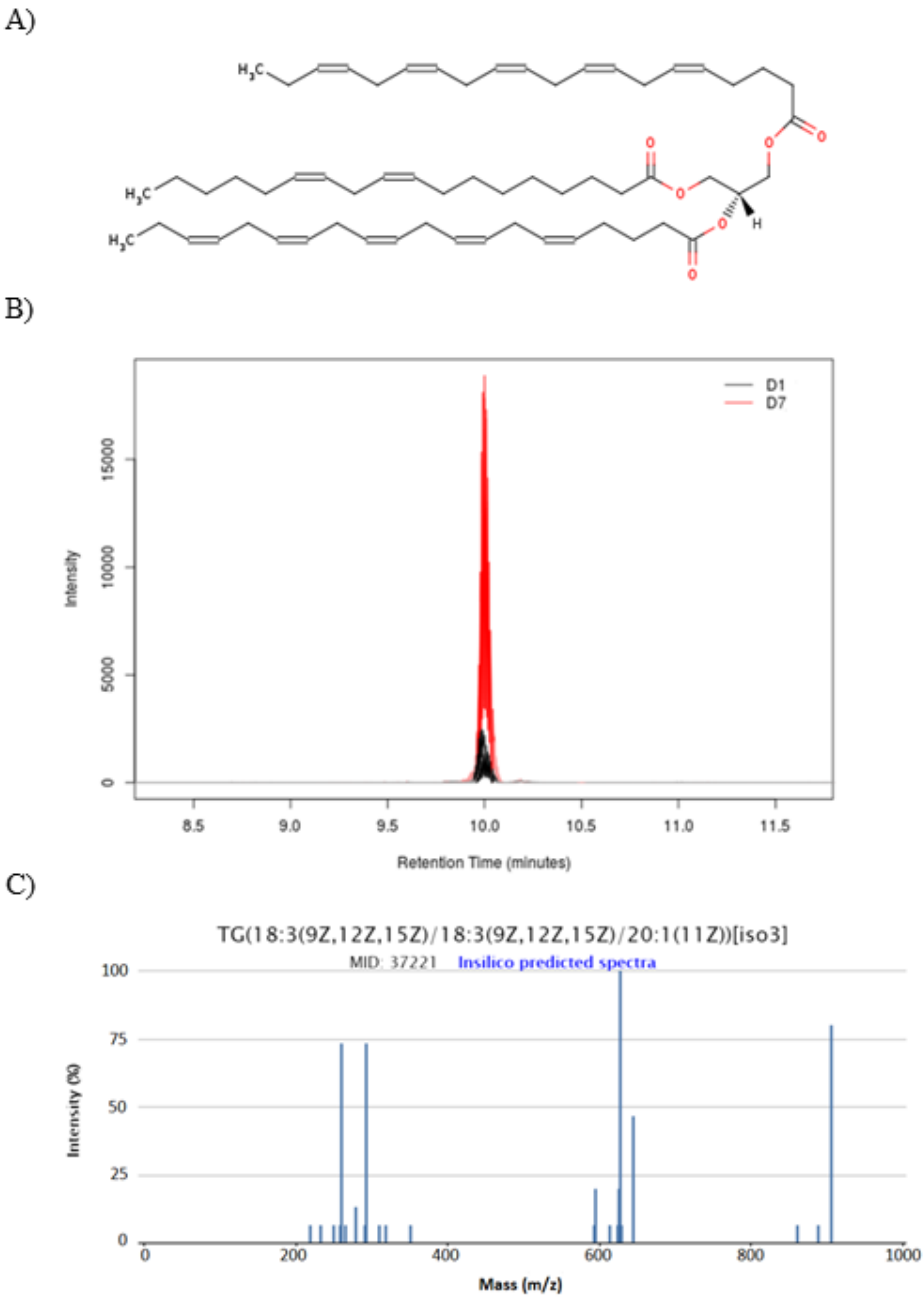

Figure 4.15. Preliminary identification of *m/z* 922.7050 in lipid droplet enriched fractions of Day 1 and Day 7 samples. (A) Structure of (1-(9Z,12Z-octadecadienoyl)-2,3-di-(5Z,8Z,11Z,14Z,17Z-eicosapentaenoyl)-sn-glycerol), (B) Extracted ion chromatogram of Day 1 (black) and Day 7 (red) samples collected in positive ESI, (C) Matching in silico predicted MS spectra by METLIN. (TR = 14.55 min, p-value = 4.91 x 10^{-6}).

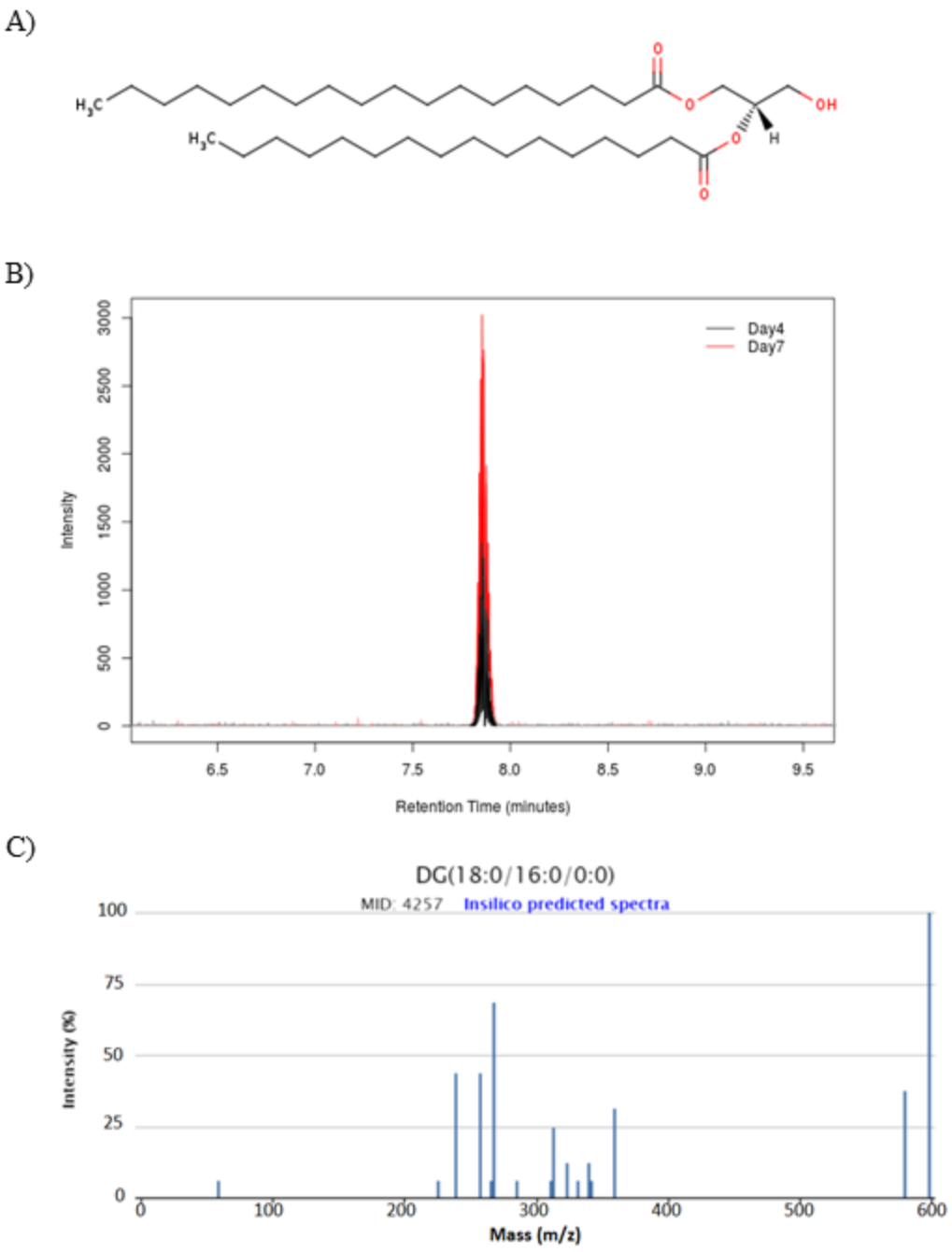

Figure 4.16. Preliminary identification of *m/z* 596.5379 in lipid droplet enriched fractions of Day 4 and Day 7 samples. (A) Structure of 1-octadecanoyl-2-hexadecanoyl-sn-glycerol, DG (18:0/16:0/0:0), (B) Extracted ion chromatogram of Day 4 (black) and Day 7 (red) samples collected in positive ESI, (C) Matching in silico predicted MS spectra by METLIN. (TR = 7.86 min, p-value = 2.99×10^{-3}).

Visualization of comparisons of features that passed the XIC checkpoint (Tables 4.1, 4.2, and 4.3) is key to identify metabolites of potential biochemical interest. [113] The results of using three visualization tools are shown in Figures 4.4, 4.5, and 4.6.

Common and distinct features are visualized by traditional Venn diagram (Figures 4.4A, 4.5A, and 4.6A). The numbers of shared metabolite features that are significantly altered in each of the three biological replicates are displayed at the center of each Venn diagram.

The interactive cloud plot of XCMS online was used to facilitate the comparison and characterization of metabolite features in this untargeted analysis (Figures 4.4B, 4.5B, and 4.6B). The interactive cloud plots have improved interpretation capabilities over the Volcano plots, which use only p-value and fold-change in intensity to identify features of interest (Figures 4.4C, 4.5C, and 4.6C). To use of interactive cloud plots made possible improve the power of comparisons because it provides information about *m*/*z*, retention time, p-value, fold change, and potential identification.

Using the interactive cloud plots, among the 82 features common in the comparison of D1 versus D4 (Figure 4.4A), 72 had METLIN identifications. Similarly, for the comparison of D1 versus D7 (Figure 4.5A), 77 out of the 95 common features had METLIN identifications. Lastly, the comparison of D4 versus D7 samples (Figure 4.6A), 14 out of 16 common features had METLIN identifications. These identifications are documented in Appendix A.

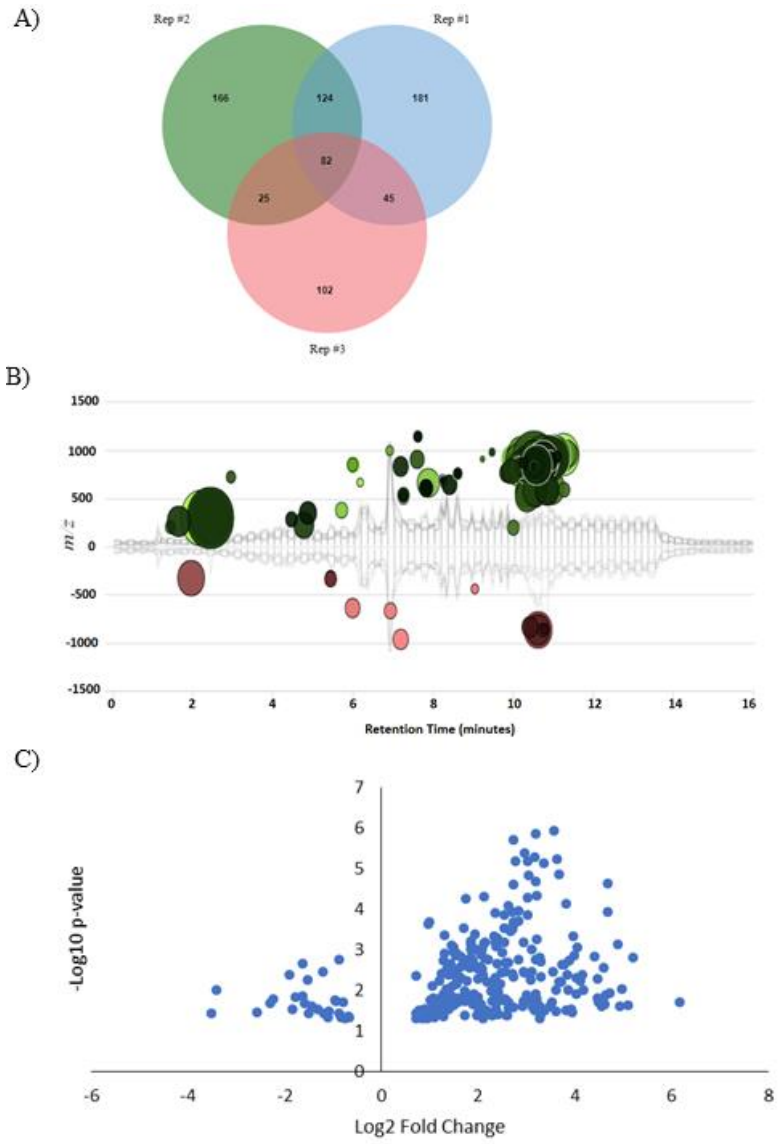

Figure 4.17. Comparative visualization of Day 1 versus Day 4 data. (A) Venn diagram illustrate the overlap of shared changed preliminary identifications between the three biological replicates. (B) Cloud plots indicating the metabolite features whose level varies significantly across the two age groups. Each metabolite feature is represented by a bubble. Statistical significance (p-value) is represented by the bubble's color intensity. The size of the bubble denotes feature fold change. Features surrounded by a black line have database hits in METLIN, (C) Volcano plots displaying the metabolites that are statistically and biologically significant (p-value below a 5% significance level based on a t-test and an average fold change larger than 2). Metabolites with a relatively low fold-change between the two groups appear near the center and metabolites that have significant p-values are found in the upper-right or upper-left regions.[153]

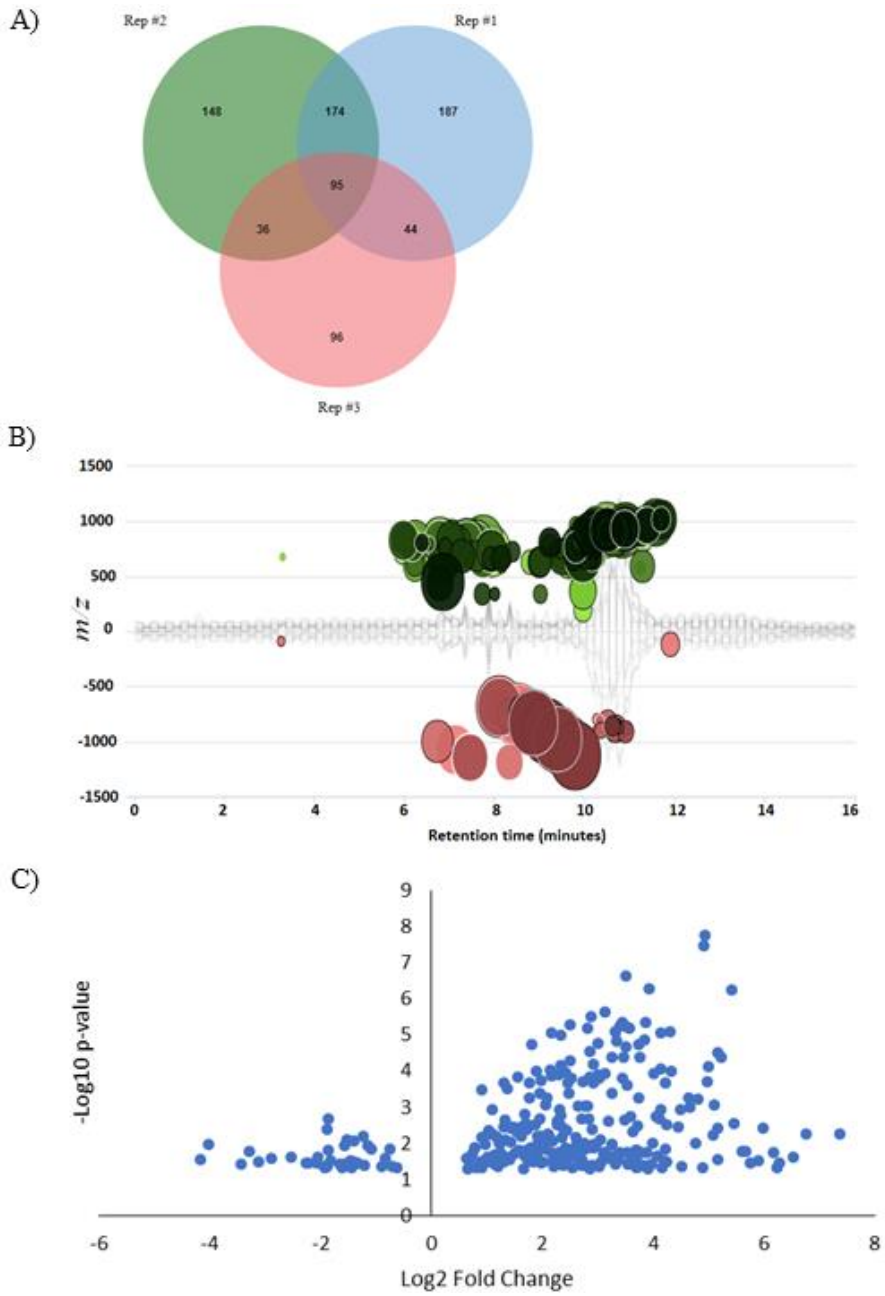

Figure 4.18. Comparative visualization of Day 1 versus Day 7 data. Other details are as described in Figure 4.4.

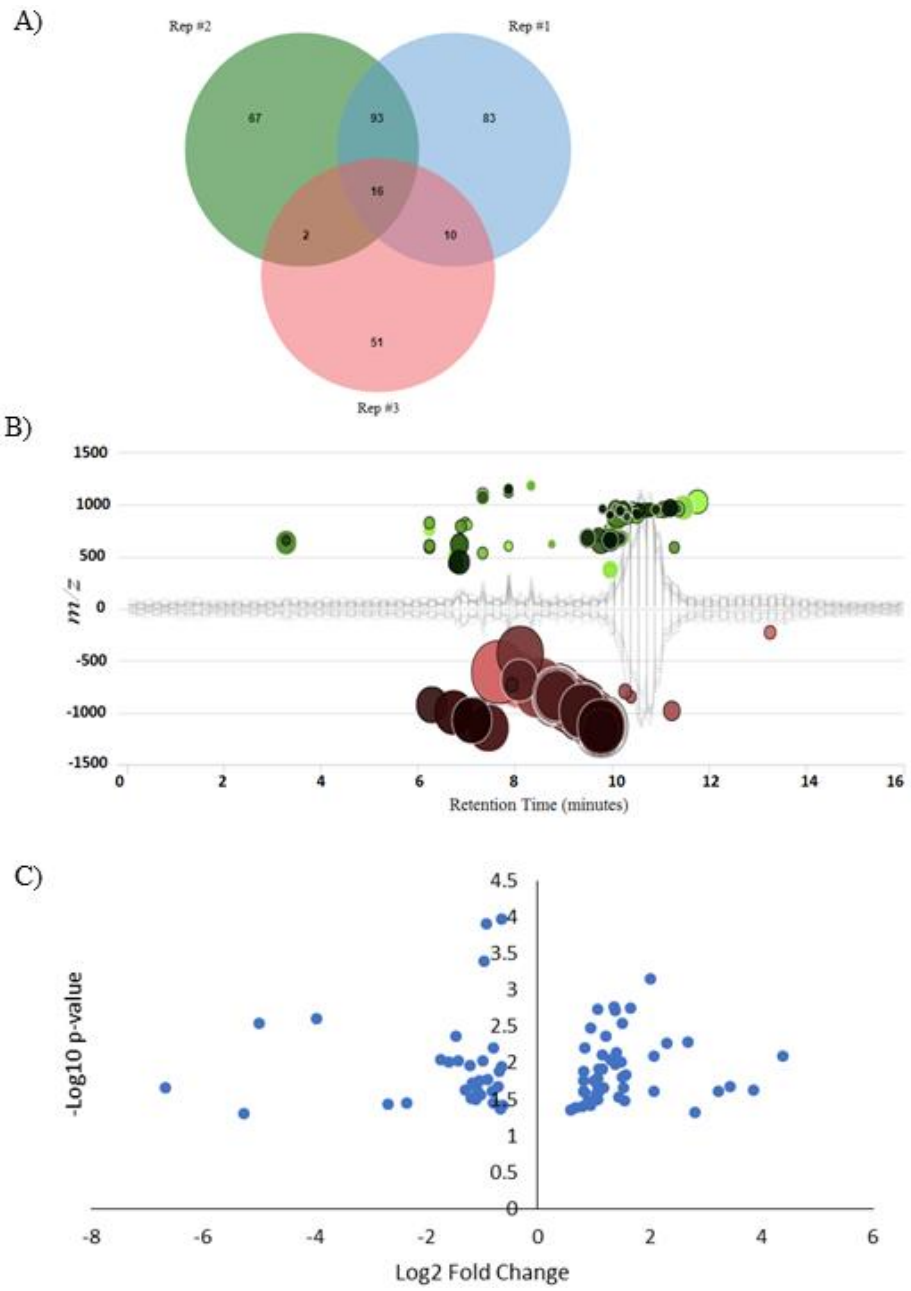

Figure 4.19. Comparative visualization of Day 4 versus Day 7 data. Other details are as described in Figure 4.4.

There were 13 features that were detected in each of the biological replicates of D1, D4, and D7 samples. The comparison of the average abundance of these features among D1, D4 and D7 was used to build a heat map (Figure 4.7). The heat map analysis displays the relative increase or decrease of each one of these features, identified by its *m/z* value, relative to D1. All features show statistically significant (p-value < 0.05, fold change (FC) ≥ 2) changes in abundance. The heat map shows four hits (*m/z* 845.77, 911.79, 943.81, and 955.19) whose abundance is different between D1, D4 and D7. The respective preliminary identifications in METLIN are: 1-hexadecanoyl-2,3-di-(9Z,12Z-heptadecadienoyl)-sn-glycerol, 1-(9Z,12Z-heptadecadienoyl)-2-(9Z,12Z,15Z-octadecatrienoyl)-3-(11Z-eicosenoyl)-sn-glycerol, 1-(9Z,12Z-heptadecadienoyl)-2,3-di-(11Z-eicosenoyl)-sn-glycerol, and 1-(9Z-octadecenoyl)-2,3-di-(11Z,14Z-eicosadienoyl)-sn-glycerol.

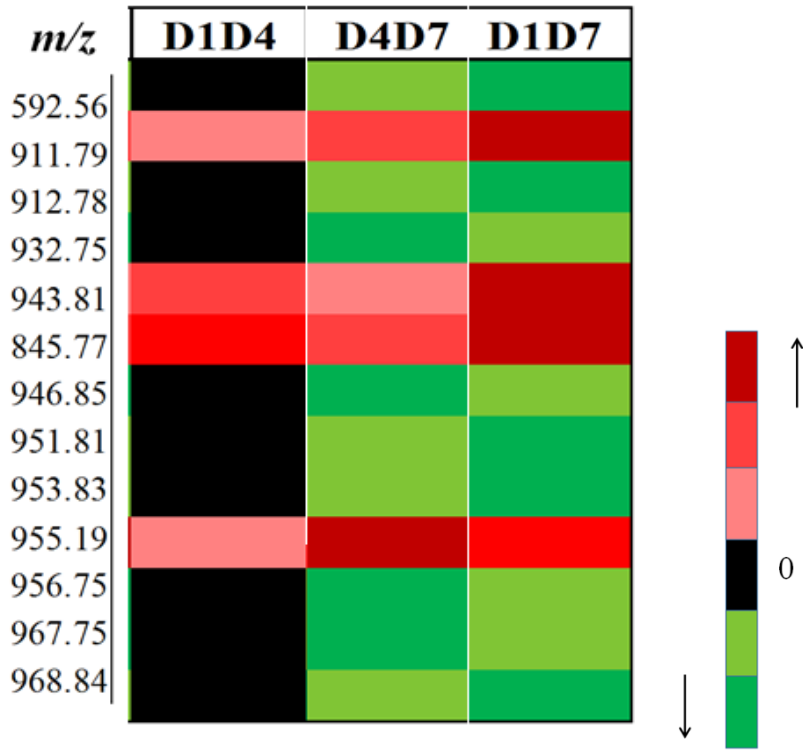

Figure 4.20. Heat map of relative abundance of features commonly detected in D1, D4, and D7 samples. Columns represent pairwise comparisons and rows refer to *m/z* values. Shades of red represent elevation of a metabolite and shades of green represent a decrease of a metabolite relative to the median metabolite levels in the early age group (see scale).

4.3.2. Most Significant Lipids Changed in Lipid Droplets with Aging

The comparative analysis of three independent lipid droplet preparations for each D1, D4, and D7 nematodes pointed to multiple compounds that showed differences in abundance (Figures 4.4, 4.5, and 4.6). Lipids categorized as triglycerides (TG) were among the top compounds to significantly increase in abundance in D7 vs D1 lipid droplets (fold change ranging from 3.22 to 44.7). From the 65 potential identifications of triglycerides detected in both day 1 and day 7 samples, 90.7% increased in abundance with age. From

the 59 potential identifications of triglycerides detected in both day 1 and day 4 samples, 94.5% increased in abundance with age. From the 12 potential identifications of triglycerides in both day 4 and day 7 samples, 83.3% increased in abundance with age.

Other lipid species to show an increase in abundance in D7 samples relative to D1 age group were phospholipids. As an example, compound with *m/z* 806.5699 preliminary identified as 1-hexadecanoyl-2-(4E,7E,10E,13E,16E,19E-docosahexaenoyl)-sn-glycero-3-phosphocholine increased in D7 samples by a fold change of 30.6 compared to D1 (p-value = 0.007). The lipid with *m/z* 663.4966, preliminary identified as 1-dodecanoyl-2-heneicosanoyl-glycero-3-phosphate, increased by 31.5-fold in D7 samples relative to D1 age group (p-value = 0.0001).

Lipids categorized as phosphatidylglycerols (PG) were among compounds to significantly (p-value < 0.05, fold change (FC) > 2) decrease in D7 vs D1 lipid droplets. Examples include: the lipid *m/z* 740.5824, had a 16 fold decrease in abundance in D7 samples and was identified as 1-octadecyl-2-pentadecanoyl-glycero-3-phospho-(1'-sn-glycerol). Another lipid (*m/z* 745.5374), that significantly decreased by 10.7 fold in D7 samples compared to D1 was preliminary identified as 1-(1Z-octadecenyl)-2-(9Z,12Z-heptadecadienoyl)-glycero-3-phospho-(1'-sn-glycerol). Compound with *m/z* 881.7444 preliminary identified as 1-eicosyl-2-docosanoyl-glycero-3-phospho-(1'-sn-glycerol), decreased by 16.2 fold in D7 samples compared to D1.

4.4. Discussion

The goal of this study was to investigate the age-related changes of the composition of lipid droplets purified from nematodes at D1, D4, and D7 of adulthood. LC/MS analysis followed by XCMS analysis of data lead to selection of features that display differences in abundance between ages. Older nematodes displayed an increase in the abundance of TGs and a decrease in the abundance of PGs in lipid droplets (See the link to preliminary identifications in Appendix).

This is in agreement with previous reports that several long-lived *C. elegans* strains have enlarged LDs with increased PC and LysoPC contents compared to wild type.[154] This is also consistent with prior work that found an aging-related decline in the *C. elegans* homolog of phospholipase D3, an ER membrane protein that hydrolyzes PC into choline and phosphatidic acid.[155]

Other reports showed several phospholipids including PCs and PEs were abundant during the larval stage and early adulthood (Day 1) and lowered during the remainder of adult lifespan.[156] In the same study, other PLs such as PG and SM species presented an opposite pattern; they were less abundant during early adult stages and accumulated at later stages of life. Results for changes in PL abundance during aging are provocative and there is no clear correlation in the literature. This is not surprising since PL synthesis is derived from a series of processes that results in complex lipid compositions with different head groups and multiple acyl chains.

Furthermore, performing pairwise comparisons, we observed an increase in the abundance of TGs in lipid droplets with aging (90.7% from day 1 to day 7, 94.5% from day 1 to day 4, 83.3% from day 4 to day 7). Triacylglycerol is the major storage form of energy in animals and are crucial for normal cellular functioning such as maintenance of membrane composition.[6] The regulation of triacylglycerol plays a critical role in disorders such as aging, obesity, and diabetes.[42,157] Aging was previously shown to be associated with increased rates of FA uptake, and rates of FA uptake correlated with rates of TG synthesis. Studies on the effects of aging on FA metabolism are few and have focused on the basal state. However, in general, these studies have indicated that cellular FA disposal is altered with aging.[158]

It is assumed that TG accumulation with aging could be attributed to an increase in TG synthesis, a decrease in TG utilization, or both.[158] However, the metabolic factors responsible for the accumulation of TG with aging have not been determined.

4.5. Conclusions

The LC/MS based analysis and data analysis workflow employed here resulted in 193 preliminary identifications of enriched lipid droplets isolated from *C. elegans*. These represent compounds with changes in abundance as a function of the nematode's age. We observed that the lipid composition of lipid droplets is affected and altered by aging. These identifications require further exploration, which ultimately may provide a framework to elucidate the role of lipid droplets in the mechanisms of aging and age-related diseases.

Chapter 5: Lipidomic Analysis of Enriched Lipid Droplets from Young and Geriatric Mice Reveals Distinct Signatures of Aging

Aging is a progressive process that includes the loss or decline of tissue and organ function over time.[122] Changes in lipid storage and dysfunction in lipid droplet (LD) processes are commonly associated with several diseases including aging.[7,10,159] Characterizing LDs composition is important for investigating their role in altered lipid storage disorders. Ultra-high pressure liquid chromatography coupled to mass spectrometry[99] are used in this study to determine age associated changes in the lipid composition of lipid droplets isolated from mouse liver tissue. Mass spectrometry data reveals total 416 features that are significantly changed in young and old mice in positive electrospray ionization (ESI) mode (p-value ≤ 0.05 and fold change of ≥ 2). This number is 12 for negative ESI. Lipid droplets purified from livers of old mice are highly enriched in triacylglycerols. In addition, such lipid droplets have lower phospholipid (mainly phosphatidylcholine and phosphatidylethanolamine) content compared to young liver tissue. These preliminary identifications suggest future areas of focus on the analysis of lipid droplets lipidomes and investigation of LD roles in aging related disorders.

5.1. Introduction

Aging is defined as a decline in biological functions, and the progression of aging is well known to result in altering lipid metabolism.[160] Lipids are widely involved in a variety of biological functions and exhibit structural and chemical variety with diverse head groups and fatty acid chains.[161] The dysregulation of lipid metabolism due to aging impacts human health significantly.[29,122]

Within cells, lipids are stored in specialized organelles called lipid droplets (LDs).[133,141,162] Lipid droplets are intracellular structures, which serve as energy reservoirs. Lipid droplets are shielded by a phospholipid monolayer, mostly phosphatidylcholine with lesser amounts of phosphatidylethanolamine, phosphatidylinositol, lyso-phosphatidylcholine, and lyso-phosphatidylethanolamine.[41] The monolayer surrounds a hydrophobic oil core which mainly comprises triacylglycerols (TAG) and sterol esters.[163-165] Lipid droplets participate in many cellular processes in different organisms.[159,162] Abnormal lipid accumulation in lipid droplets in the liver has been reported in many metabolic diseases, including the metabolic syndrome and obesity.[159]

Ultra performance liquid chromatography coupled to mass spectrometry (UPLC/MS) based lipidomic approaches, are becoming specialized tools for better understanding of LDs and lipid metabolism at systems biology levels.[44,45] These "omics" approaches allow dissection of subcellular organelle lipidomes and identification of LD roles in lipid metabolism. In this work, we profiled the liver lipid droplet compositions of young (35 weeks), and geriatric (115 weeks) mice. LC/MS comparison resulted in more than 500 features for both the old and young LDs, of which 343 features changed significantly (p-value < 0.05, Fold Change > 2) during aging in positive ESI mode. Out of these, 199 compounds had assigned IDs and 145 compounds remained unidentified. In negative ESI mode, 12 features changed significantly from young to old mice. Out of these, 8 compounds were identified using online libraries and 4 remained unidentified. We found that compounds preliminary identified as triglycerides were more abundant in

LDs in old mice; however, compounds identified as phospholipids showed lower abundance in aged mice.

5.2. Materials and Methods

5.2.1. Reagents

Sucrose and ethaminetetraacetic acid (EDTA) were obtained from Sigma Aldrich (St. Louis, MO). Tris base was obtained from Thermo Fisher (Waltham, MA). Water was purified with a Millipore Synergy UV system (18.2 mΩ/cm, Bedford MA). Liver homogenization buffer (Buffer H) consisted of 250 mM sucrose, 10 mM Tris, pH 7.0. Buffer A consisted of 500 mM Sucrose, 2 mM EDTA, and 1.22 g Tris-base in 500 mL water, pH 7.8. Sucrose gradient step solutions were mixed with Millipore water to a final concentration of 1X Buffer A. Pierce Protease Inhibitor Mini Tablets (AEBSF, aprotinin, bestatin, E-64, leupeptin and pepstatin A, Thermo Fisher, Waltham MA) were added to all buffers in accordance with manufacturer's instructions (simply dissolve 1 tablet in 10 mL of buffer or lysate). The solvents used for extraction were HPLC grade chloroform and methanol from Fisher Scientific (Fairlawn, NJ). Canola Oil (15 mg/ml) in chloroform (Sigma Aldrich, 100ml) was used as the standard for lipid quantification. Vanillin (Sigma Aldrich), O-phosphoric acid (VWR, 85%), and Sulfuric Acid (95-98%, Sigma Aldrich, 100 ml) were used for lipid quantification.

5.2.2 Lipid Droplet Isolation from Mouse Liver Tissue

This part was done by Katherine A. Muratore at University of Minnesota. Lipid droplets were prepared from the liver tissues of C57BL6 female mice.[166] Mice in the adult group were ~35 weeks and mice in the geriatric group were ~115 weeks. All isolation steps were performed at 4 °C. Mice were euthanized by intraperintal injection of pentorbital (mg/g) and the liver was excised. The liver was weighed and minced in a petri dish using a flat razorblade into small (1 mm) pieces and resuspended in 3 ml of Buffer H. The liver was transferred into a nitrogen cavitation chamber and charged to 200 psi. After 15 minutes on ice, the cell lysate was released from the nitrogen cavitation chamber into a 50 ml conical tube and centrifuged at 1000 g for 10 minutes. The post nuclear supernatant was loaded onto a sucrose step gradient (4 mL 35% Sucrose Buffer A, 4 mL 25% Sucrose Buffer A) and centrifuged at 36,000 rpm in a Beckman SW 41 rotor for 4 hours. The lipid droplet fraction appeared as white film at the top of the tube, which was removed with a Pasteur pipette.[165] All mice were housed in a designated clean facility and treated in accordance with protocols approved by the University of Minnesota Insitutional Animal Care and Use Committee.

5.2.3. Metabolite (Lipid) Extraction

A previously published protocol was used to extract the lipids from purified lipid droplet fractions.[108] Briefly, 3.75 ml of ice cold chloroform : methanol 1:2 v/v was added to 1 ml of the collected fraction and vortexed for 2 min. Sample was treated with 1.25 ml of chloroform and vortexed for 1 min. Subsequently, 1.25 ml of water was added to the

sample and vortexed for 1 min. Sample was centrifuged in glass tubes at 13,000 g for 10 min to pellet any non-extracted materials. The upper phase containing salts and other water soluble metabolites were removed and protein phase was pierced and discarded. The organic phase (lower phase) was collected and transferred to a new sterile siliconized Eppendorf tube and evaporated overnight at room temperature under vacuum to remove extraction solvents. Tubes were filled with nitrogen to remove any air and stored dry at -80 °C prior to analysis.

5.2.4. Lipid Quantification

A modified colorimetric method was used for quantitative analysis of total lipids (See Materials and Methods in Chapter 3).[149,150] Lipid standards (canola oil) were loaded into 96 well plate in a range of 0 mg to 3.6 mg of lipids. Samples were added (10 µl), in triplicate, to each well. The solvent was evaporated in the hood and 100 µl of sulfuric acid was added to each well and incubated at 90 °C for 10 min. Vanillin (1 mg/ml), 8 ml o-phosphoric acid, and 25.6 ml hot water were used to make the final vanillin reagent. The plate was cooled on ice to room temp (~2 min) and 100 µl of vanillin reagent was added to each well. After ~5 min the color was developed and absorbance was measured at 540 nm.

5.2.5. UPLC/MS Conditions

Samples were resuspended in 200 ml 1:1 methanol:chloroform to a final concentration of 50 µg/ml and were vortexed for 30 s. A Waters Acquity UPLC coupled to a Waters Synapt G2 HDMS quadrupole orthogonal acceleration time of flight mass

spectrometer was used for UPLC/MS^e analysis. The reversed-phase column used was a Waters HSS T3 C18, 2.1 mm × 100 mm column (1.7 µm diameter particles) operating at a temperature of 45 °C. The following linear gradient separations were employed at a flow rate of 400 µL/min using a binary mobile phase system where A: Methanol: Water, 60:40 v/v, 5 mM ammonium formate, containing 0.1% formic acid and B: Methanol:Isopropanol 10:90 v/v, 5 mM ammonium acetate, containing 0.1% formic acid. The gradient profile was: 40% B, 0 min to 10 min; 40% B to 100% B, 10 min to 15 min; 40% B, 15 min to 20 min. The Waters Synapt G2 was calibrated for mass accuracy with 2 µg/µl sodium iodide solution in 50/50 2-propanol/Water. Simultaneous low- and high-collision energy (CE) mass spectra were collected in centroid mode over the range *m/z* 50–1200 every 0.2 s during the chromatographic separation. Samples were analyzed in high-definition MS^e mode (HDMS) and the TOF analyzer was operated in the V resolution mode. MS^e parameters in positive electrospray ionization mode were as follows: capillary, 0.3 kV; sampling cone, 35.0 V; extraction cone, 5.0 V; desolvation gas flow, 800 L/h; source temperature, 100 °C; desolvation temperature, 20 °C; cone gas flow, 20 L/h; trap CE, off (low CE collection), trap CE ramp 15–65 V (high CE collection); lockspray configuration consisted of infusion of a 5 µg/mL solution of leucine-enkephalin and acquisition of one mass spectrum (0.2 s scan, m/z 100-1200) every 10 s. Three lockspray *m/z* measurements of protonated leucine-enkephalin were averaged and used to apply corrections to measured *m/z* values during the course of the analysis. All MS^e parameters were identical in negative ionization mode except the following: capillary, 2.5 kV; sampling cone, 30.0 V; extraction cone, 4.0 V.

5.2.6. Data Treatment

Samples were categorized into two groups of young (n=4, biological replicates) and old (n=4, biological replicates). Each sample was analyzed separately using the the Synapt G2 Q-TOF instrument. Collected data were processed by XCMS online software (xcmsonline.scripps.edu). Raw data acquired were converted to .mzXml common data format using Proteowizard file converter (proteowizard.sourceforge.net) and the following parameters used in this analysis: (i) Feature detection: centWave method, min. and max. Peak width = 2 and 25, S/N threshold = 10, mzdiff = 0.01, integration method = 2, prefilter peaks = 3, prefilter intensity = 500, Noise filter = 0; (ii) Retention time correction: Obiwarp method, profStep = 1; (iii) Alignment: mzwid = 0.015, bw = 2, minfrac = 0.5, max = 1000, minsamp = 1. The data were processed for peak detection, retention time correction, chromatographic alignment, statistical analysis, and identification through METLIN database with 5 ppm tolerance. The identifications include possible adducts, fragments and isotopes. A workflow that has been previously developed in our lab was used to make preliminary identification of features by XCMS (See Chapter 2).[91] Extracted ion chromatograms (XICs), were manually examined to confirm that identified features have a true chromatographic peak profile, referred to as Checkpoint 1 in the workflow (see Chapter 2). Fragmentation patterns of each feature from low- and high- collision energy mass spectra were examined to provide preliminary identifications of features, referred to as Checkpoint 2 (see Chapter 2).

Each biological replicate was run three times and reproducibility of the peak intensities for each biological replicate was calculated after all checkpoints. This value was between 4 % and 107 % CV, (Average ± Standard deviation, 24 ± 16, N= 219) in young mouse liver in positive ion mode, and between 61 % and 106 % CV in negative ion mode (Average ± Standard deviation, 95 ± 26, N= 12). This value is between 1.4 % and 85 % in LDs isolated from old mouse liver (Average ± Standard deviation, 19 ± 9, N= 219) in positive ion mode, and between 11 % and 98 % in negative ion mode (Average ± Standard deviation, 79 ± 17, N= 12).

5.3. Results

We used UPLC/MS analysis to investigate the lipid composition of lipid droplets (LDs) in mouse liver tissue.[167,168] A chemometric approach known as principle component analysis (PCA) was used for processing the UPLC/MS data to expedite the classification of potential features into one of two comparative biological fractions (young and old). We found that triglycerides (TAG) showed higher abundance (defined by fold change) in lipid droplets isolated from old mouse compared to young. Also, compounds identified as PC and PE showed lower abundance in lipid droplets isolated from old mouse compared to young. The link to a full list of identifications is provided in Appendix B.

5.3.1. Preliminary Identifications from Mouse Liver

Using positive ESI, in total we found 1346 features that were detected at least once in both young and old groups, but had different signal intensities between the age groups.

Comparative analysis of the resulting total ion chromatograms was performed using XCMS software tool. Cloud plots of MS analysis revealed 343 hits (counting isotopes of each feature as one hit) with a p-value ≤ 0.05 and fold change of ≥ 2 (Figure 5.1.A). Complete lists of these features that change in abundance (p-value < 0.05 and FC > 2) are summarized in Table B.1 of Appendix B. Searching against the METLIN database resulted in 119 features with matching MS/MS spectra. The interactive volcano plot in Figure 5.1.B shows the relationship between statistical significance (often scaled logarithmically) and biological relevance (often presented in terms of fold change). Two regions of interest in the volcano plot include those points that are found towards the top of the plot that are far to either the left- or the right-hand side. These represent values that display large magnitude fold changes as well as high statistical significance (p-value). Yet, volcano plots do not provide information about feature intensity and retention time that are often important for the interpretation of metabolomics results. Results from volcano and cloud plots are complimentary (Figure 5.1 A and B).

In negative ESI mode, 12 features differed in signal intensities between the young and old age groups. A representation of the cloud plot and the volcano plot results is shown in Figure 5.2.

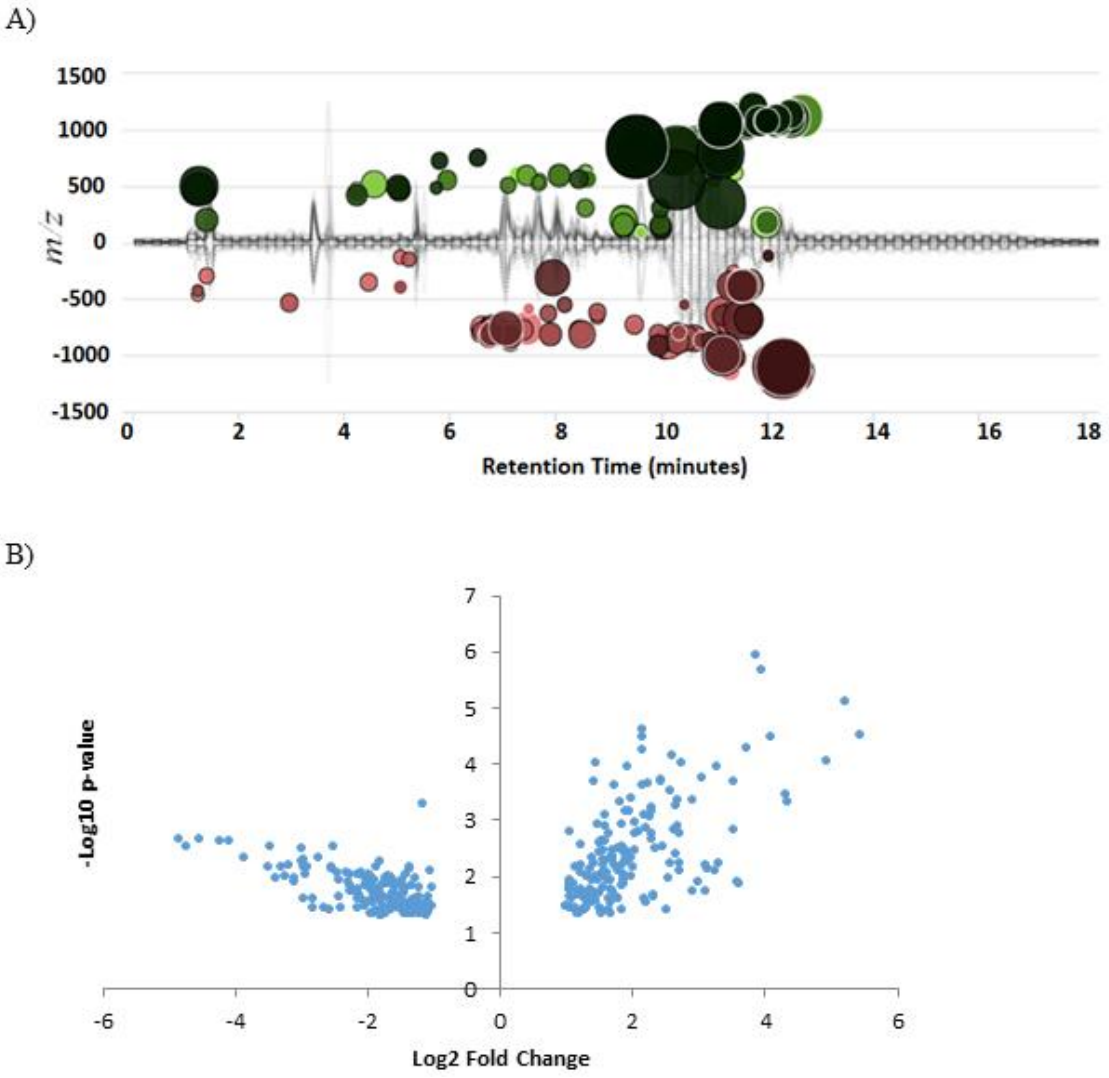

Figure 5.21. Mass spectrometry results of enriched lipid droplet fractions in young and old mouse liver samples in positive ESI. (A) Cloud plots indicating features whose level varies significantly in young and old lipid droplets. Each metabolite feature is represented by a bubble. Statistical significance (p-value) is represented by the bubble's color intensity. Features with low p-values are brighter compared to features with high p-values. The size of the bubble denotes feature fold change. Features surrounded by a black line have database hits in METLIN, (B) Volcano plots displaying features that are statistically and biologically significant (p-value below a 5% significance level based on Welch t-test with unequal variances and an average fold change larger than 2). Metabolites with a relatively low fold-change between the two groups appear near the center and metabolites that have significant p-values are found in the upper-right or upper-left.

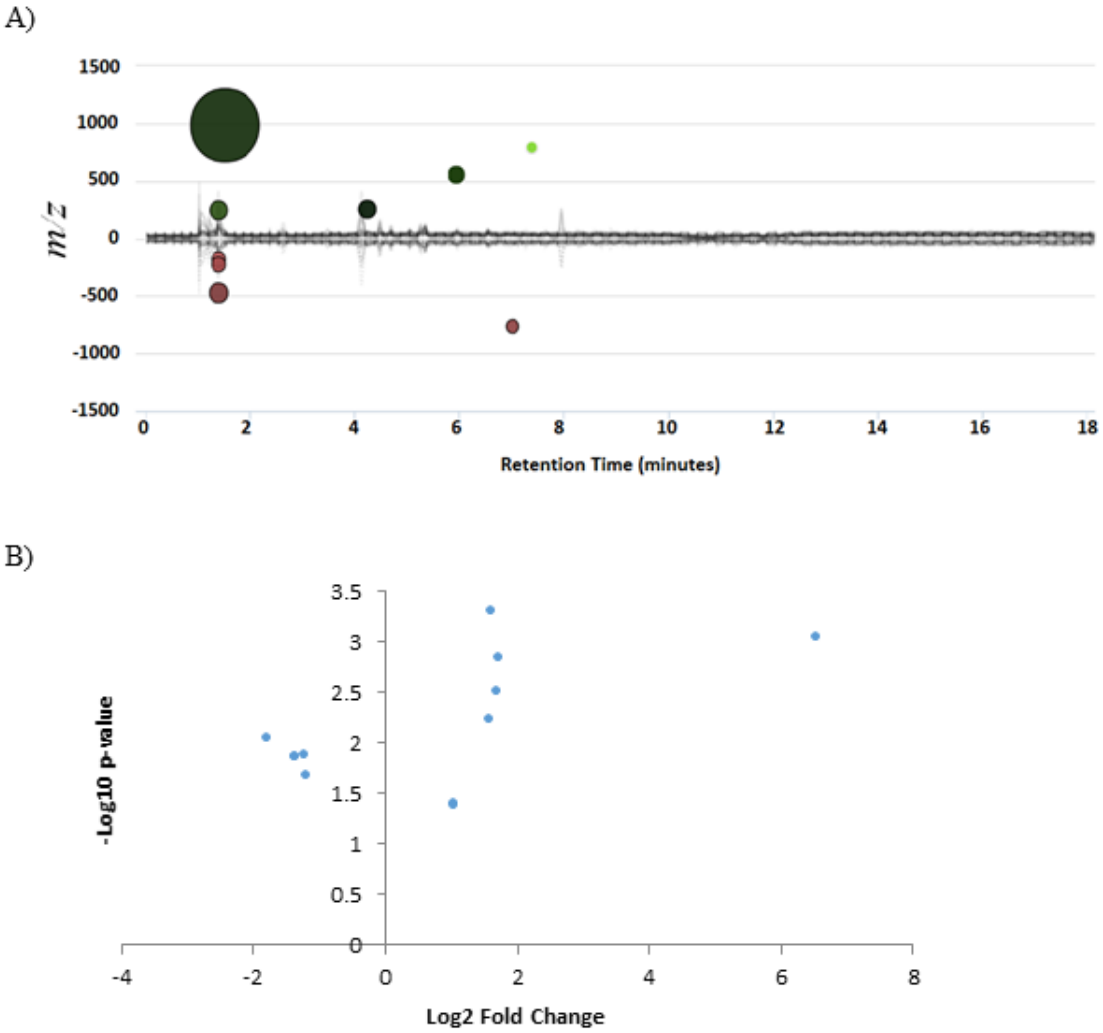

Figure 5.22. Mass spectrometry results of enriched lipid droplet fractions in young and old mouse liver samples in negative ESI. See Figure 5.1 for details.

5.3.2. Triglycerides Increase in Aged Liver Lipid Droplets

An increase in the abundance of triglycerides (TG) was observed in the aged liver lipid droplets. Three examples include: a protonated peak of a compound with *m/z*

929.7541, tentatively identified as 1,2-di-(9Z,12Z,15Z-octadecatrienoyl)-3-eicosanoyl-*sn*-glycerol, increased in abundance in the old liver lipid droplets by a fold change of 3.6 (p-value= 0.04). Figure 5.3 illustrates data supporting the identification of such compound. The structure (A), the aligned extracted ion chromatograms (B), and the mass spectrum at 10.45 min (C) of this compound are shown in this figure. Sodium adduct of a compound with *m/z* 753.4884, tentatively identified as 1-(7Z,10Z,13Z,16Z,19Z-docosapentaenoyl)-2-(4Z,7Z,10Z,13Z,16Z,19Z-docosahexaenoyl)-*sn*-glycerol, increased in abundance in the old mice by a fold change of 2.9 (p-value= 0.0001). Protonated mass of a compound with *m/z* 941.6986, tentatively identified as 1-hexadecanoyl-2,3-di-(5Z,8Z,11Z,14Z-eicosatetraenoyl)-*sn*-glycerol, increased in abundance in the old liver lipid droplets by a fold change of 2.9 (p-value= 0.02). See Appendix B.

No TGs were identified in negative ESI mode. Lists of 12 features that change in abundance (p-value < 0.05 and FC > 2) in negative ESI are summarized in Appendix Table B.2.

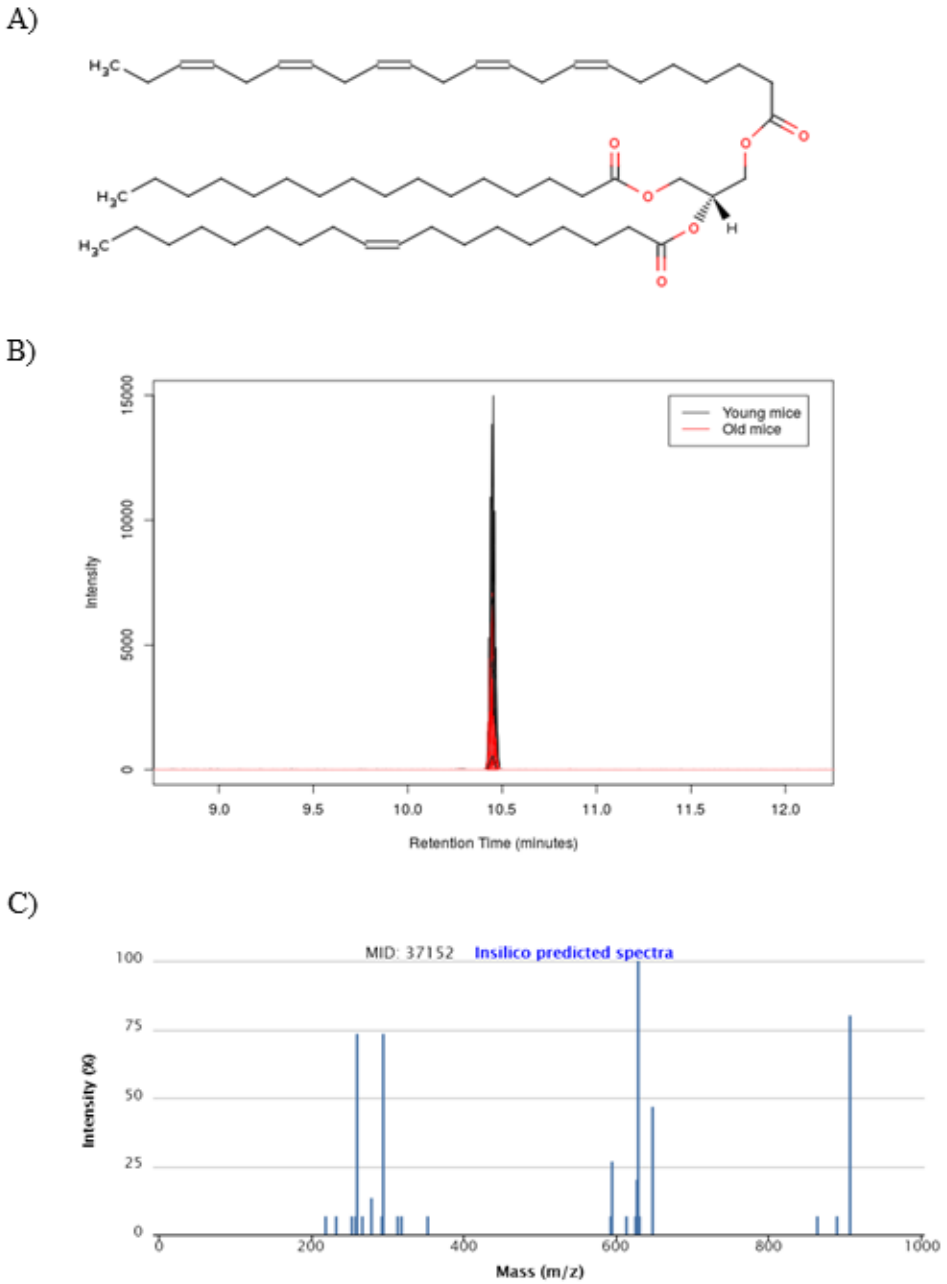

Figure 5.23. Preliminary Identification of *m/z* 929.7541. A) Structure of 1-hexadecanoyl-2-(9Z-octadecenoyl)-3-(7Z,10Z,13Z,16Z,19Z docosapentaenoyl)-*sn*-glycerol, found in lipid droplet enriched fractions; B) Extracted ion chromatogram for *m/z* 929.7541; C) Mass spectrum at TR: 10.45 min; (p-value: 0.04, fold change: 3.6).

5.3.3. Phospholipids Decrease in Aged Liver Lipid Droplets

There is a reduction in the abundance of phosphatidylcholines (PCs), phosphatidylethanolamines (PEs), phosphatidic acids (PAs), and phosphatidylinositols (PIs) in lipid droplets from liver of 115 weeks old mice compared to young (35 weeks) samples. Examples include: Compounds with *m/z* 832.5854 and 806.5697 preliminary identified as 1-(9Z-octadecenoyl)-2-(4Z,7Z,10Z,13Z,16Z,19Z-docosahexaenoyl)-sn-glycero-3-phosphocholine, and 1-hexadecanoyl-2-(3Z,6Z,9Z,12Z,15Z,18-docosahexaenoyl)-sn-glycero-3-phosphocholine, significantly decreased in abundance in lipid droplets of old mice liver by fold changes of 4 and 3.8, respectively (p-value < 0.01). PEs with *m/z* 766.5384 and 772.5848 preliminary identified as 1-palmitoyl-2-docosapentaenoyl-sn-glycero-3-phosphoethanolamine, and 2-octadecanoyl-3-(5Z,8Z-eicosadienoyl)-sn-glycero-1-phosphoethanolamine, considerably decreased in the old liver lipid droplets by fold changes of 3.8 and 3.2, respectively (p-value < 0.03). The sodium adduct of a feature tentatively identified as 1-docosanoyl-2-eicosanoyl-glycero-3-phosphate (PA(22:0/20:0)) with *m/z* 811.6196 decreased in lipid droplets of old mice liver by a fold change of 3.2. Another feature identified as 1-(1Z-hexadecenyl)-2-tridecanoyl-glycero-3-phospho-(1'-myo-inositol) with *m/z* 753.4884 significantly decreased in old groups compared to young lipid droplet samples by a fold change of 2.7. These examples were selected because of their highest significant difference (Wilcoxon rank test) and the greatest fold change (See Appendix B).

Top lipids that significantly decreased (p-value < 0.01) in lipid droplets of old mouse liver in negative ESI, were also tentatively identified as phospholipids. $[M-H]^-$ of a feature tentatively identified as 1-tridecanoyl-2-(4Z,7Z,10Z,13Z,16Z,19Z-docosahexaenoyl)-glycero-3-phosphocholine with *m/z* 764.5230 decreased in abundance in lipid droplets of old mice liver by a fold change of 2.3. Another lipid tentatively identified as 1-hexadecyl-2-(9Z-tetradecenoyl)-glycero-3-phosphate, with *m/z* 605.4539 decreased in lipid droplets of old mice liver by a fold change of 2. Another compound tentatively identified as 1-(5Z,8Z-eicosadienoyl)-2-octadecanoyl-sn-glycero-3-phosphoethanolamine with *m/z* 772.5848 decreased in abundance in lipid droplets of old mice liver by a fold change of 3.2. See Appendix B.

5.4. Discussion

In this study, we used UPLC/MS to investigate the lipidomic profile of lipid droplets in the liver of young and geriatric mice. Although the biogenesis of lipid droplets is relatively well documented, little is known about changes in their composition and structure as a function of aging. Currently there are no studies assessing age-related changes in the lipid composition of lipid droplets.

The variety of the different phospholipids in lipid droplet monolayer protecting the neutral lipids from the hydrophilic environment of the cell suggests that they play important tasks in regulating the structure and function of this cellular organelle.[169-171] In mammalian cells and yeast, phosphatidylcholine (PC) with 60% of the total lipid content is the most prominent phospholipid in the lipid droplet outer layer.[139,172] Phosphatidylethanolamine

(PE) and phosphatidylinositol (PI), ranging up to 24% and 8% are the second and third most abundant lipids in the outer layer.[172,173] Other phospholipids including PS and the lyso-forms of PC and PE are present in minor amounts.

PCs are crucial to stabilize growing LDs and they play key roles in maintaining the stability of LDs in cells.[12] In addition, the surface lipid monolayer could also be involved in the differential recruitment of lipid droplet proteins. This phospholipid class in general has been shown to decrease with age in mouse mitochondrial fractions of brain and liver tissues.[174] The same decreasing trend was observed in the results obtained on lipid droplets in our work. We observed that lipids preliminary identified as PCs are decreased in the lipid droplets isolated from old mouse liver compared to young. However, reports on age related changes on the composition of phospholipids have made contradictory observations. PCs were previously shown to either increase or decrease in aged mice, compared to young mice in targeted metabolomic analysis of serum metabolites.[170] A decrease in the abundances of phosphatidic acid (PA) was also observed with age in our work. As an example, compound preliminary identified as 1-docosanoyl-2-eicosanoyl-glycero-3-phosphate (22:0/20:0) decreased in abundance in old samples compared to young (p-value = 0.002, fold change = 4.3). In previous studies, PAs have not been found in considerable amount in lipid droplets lipid profiles.[7,175]

TGs are involved in normal cellular functioning such as energy storage and maintenance of membrane composition.[176] General accumulation of TGs is found in aging, obesity and type 2 diabetes.[177,178] TG content has previously shown to increase in

mitochondria-rich tissues including heart, liver, and skeletal muscle in rat models of aging.[179] Similar trend was observed in the abundances of TGs in lipid droplets isolated from old mouse liver. It has been proposed that a metabolic shift is in the conversion of diacylglycerol to triglycerides is caused by aging.[176]

Further biological insight could be gained through parallel lipidomics studies of aging related diseases in different model organisms. Overall, results obtained here are in agreement with our prior lipidomics findings in *C. elegans* described in Chapter 4; in which lipid droplets are enriched in TGs during aging and the surrounding phospholipid monolayer have lower levels of PC and PE.

5.5. Conclusion

Comparative lipidomic analyses of mouse lipid droplets were conducted in this study. We have demonstrated that enriched lipid droplet fractions have characteristic lipidomic profiles specific to their age. Preliminary identifications of the lipid components in lipid droplets isolated from mouse liver suggest an increased TG content and decreased PC and PE content during normal aging. These data suggest that changes in LD compositions impact lipid metabolism.

Chapter 6: Conclusions and Future Work

6.1. Conclusions

At the onset of this work, there were no reports of a systematic characterization and comparison of lipids found in lipid droplets from different aging populations. The work described in this thesis applied LC/MS strategies to investigate the compositions of lipid droplets and determine age associated changes in lipid profiles. Untargeted characterization of lipids in lipid droplets was performed by LC/MS on a Q-TOF mass spectrometer of *C. elegans* at different ages, and liver of young and geriatric mice. This resulted in preliminarily identifications of compounds that were significantly changed between aging groups. These preliminary results are important in understanding age associated changes of lipid droplet compositions.

The diversity of lipids makes it highly unlikely to have universal analysis procedures for this class of compounds.[180,181] A wide range of mass spectrometry instruments is currently being used for lipid analysis. However, none of these platforms have been comprehensively compared for their analytical capabilities in analyzing lipids. The work described in Chapter 3 provides a comparison of the performances of high resolution Q-TOF (Synapt G2) and Orbitrap (Velos) instruments for lipidomic analysis. The main analytical parameters that influence detection and identification of lipids specific to a biological sample were explored. Overall, the mass accuracy was better using the Synapt for multiple lipid standards in both positive and negative ESI. The LTQ-Orbitrap had higher mass resolution from 200 to 700 *m/z*, while the Synapt had higher mass resolution from 700 to 1200 *m/z* values. Reproducibility associated with the metabolite

peak intensities was better using the Synapt in both positive and negative ESI. Synapt data showed significantly higher signal to noise values (65% and 75% of the detected features on both instruments have relative S/N greater than 1 in positive and negative ESI respectively), which is an advantage in omics studies of biological matrices. Differences in signal to noise ratios obtained on the two instruments were not statistically significant in the negative ESI data. XCMS was preferred as automated software for processing the metabolomics data while assigning more peak IDs in a shorter time. Taken together, our results suggested that, as used in this study, Q-TOF is better suited for untargeted metabolomics and lipidomics studies.

Advances in the mass spectrometry field have enabled the large scale characterization of lipids in a variety of biological samples.[19] Yet, integration and visualization of metabolomics data is a formidable task that requires advanced computational framework.[182] Four different algorithms were used to analyze the mass spectrometry data from the Synapt G2 and Orbitrap Velos instruments and their ease of use and robustness were compared. XCMS software offered a powerful solution ranging from basic data structures to sophisticated algorithms for data analysis. Additionally, a rigorous data analysis workflow was used to both select features that had extracted ion chromatograms with acceptable chromatographic peak profiles and to ensure that the product ions from high collision energy mass spectra possessed matching XIC with its parent ion.[91]

The optimized mass spectrometry platform and data analysis workflow described in Chapter 3 were used to compare the composition of lipid droplets of *C. elegans* at Day

1, Day 4, and Day 7 of age. This nematode has been successfully used as a model of aging, but knowledge of its LD lipid and protein compositions are still rather limited.[144] Our findings suggest that lipid droplets have increased TG content and decreased phospholipid (PC, PG) content with age. Metabolomic studies of *C. elegans* have contributed significantly to the understanding of the biology of aging of other organisms.[142,183] Aging in *C. elegans* share many similar characteristics with aging in humans including general decline in cellular function, and reducing the capability to respond to internal and external stress. However, it is still unknown how aging affects lipid droplet composition and fat storage in different model organisms. Our lipidomic analysis revealed distinct lipid compositions specific to each age group. Further validation of these results will open new avenues to understand how lipid droplets impinge on lifespan regulation in *C. elegans* and possibly humans.

Our workflow was also used to compare the lipid droplet compositions of liver in young and geriatric mice. The lipid composition of lipid droplets had previously not been determined in this context by any non-targeted methods including LC/MS. Preliminary identifications were assigned to features enriched or unique to lipid droplets in young and old mouse models (Chapter 4). Comparison of lipid profiles enriched from mouse liver resulted in 416 features that are significantly altered from young to old lipid droplets in positive ESI. This number was 12 in negative ESI. Many of the preliminary identifications made, such as PE(16:0/0:0) and sphinganine, have previously been associated with aging indicating that the preliminary identifications made may be of high relevance to age related diseases.[184] In the future, identifications will be validated and investigated for their specific

role in lipid droplet biology and aging.

The findings described in this thesis suggest age associated changes in the lipidomic profiles of lipid droplets in two different model organisms. These preliminary identifications may lead to additional follow-up experiments to further increase our understanding of how lipid droplet composition changes and contributes to aging.

6.2. Future Work

The reconstruction of lipid metabolism pathways requires novel strategies for the mapping of lipid data at the molecular species levels instead of at lipid class/subclass levels.[185] This reconstitution also requires the integration of comprehensive lipidomic data with genetic, transcriptional, and enzyme data to perform metabolic pathway and flux analyses.[37] Defining lipid identities is a challenging task because of the large structural diversity of lipid classes and lipid species. This task requires a combination of novel and existing bioinformatics resources. Additional developments of those reported in this thesis could provide new insights into the biology of lipids. These developments include: validating the preliminary identifications using standards and making additional database entries (Section 6.2.1.), isolating high purity subcellular organelles (Section 6.2.2.), and improving lipid analysis using ion mobility mass spectrometry (Section 6.2.3.).

6.2.1. Improve and Validate Preliminary Identifications

As described throughout this thesis, LC/MS was used to make preliminary

identifications of metabolites from enriched lipid droplets in two different model organisms. Using the workflow[91], of the 82 features detected in all D1D4 comparisons 12 compounds were not identified with online database searches (the work described in Chapter 4). Of the 95 features detected in all D1D7 comparisons 17 compounds were not identified. Of the 16 features detected in all D4D4 comparisons 2 compounds were not identified with online database searches. Of the 343 features detected in lipid droplet fractions of old and young mouse liver in positive ESI, 181 were not identified with online database searches (the work described in Chapter 5). This number is 3 out of 12 for the data collected in negative ESI. Searching in a molecular structure database is clearly limited to those compounds present in the database.[186] Thus, there is a need to enrich the mass spectrometry databases to improve the number of identifications and decrease the experimental time needed to validate preliminary identifications. Various databases have been developed to aid in assigning structures to spectral peaks observed in metabolomics experiments. Several recent reviews have discussed the general capabilities of various MS-based databases and software tools.[187] Additional database entries produced by the LC/MS community could also lower the risk of false positive identifications and increase the confidence in the results.[188]

The work described in Chapters 4 and 5 made several preliminary identifications of features enriched in lipid droplets of different age groups. Validation of preliminary identifications is always needed to confirm their identification and is relatively straightforward if high quality commercial standards are available. Future validation will require acquisition of high quality commercially available standards that are analyzed by

LC/MS using the exact same methodology applied to lipid samples. This includes comparison of extracted ion chromatograms, low energy mass spectra, and high energy mass spectra. The standard will need to be run neat/in solution, spiked in biological matrix, and spiked and extracted in biological matrix for the full structural elucidation.[143] Information would also need to be collected on targeted precursor ion and neutral loss scans, as well as MS/MS spectra to help validate the data. If the preliminary identification is correct, the mass spectra of the biological feature and the commercial standard should be very similar. In summary, having lipid standards will help strengthen tentative identifications.

6.2.2. Improving Purification of Subcellular Organelle Enrichment

An isolation procedure which enriches a specific organelle and minimizes contaminations by membranes from other organelles is beneficial to reliable profiling of lipids and assignation of biological function. It is also known that employing inadequate purification methods when performing lipidomics analyses may lead to inaccurate selection of tentative biomarkers.[51,53]

To improve and adapt the method discussed in Chapters 4 and 5 to other subcellular organelles in different model organisms, new methodologies could be utilized to increase the purity and yield of subcellular organelle isolation. Alternative methods such as immunoisolation techniques could be developed to overcome the problems with other techniques such as density gradient centrifugation. A major advantage of antibody-based separation techniques is the specificity that antibodies bring to the separation, enabling an

organelle type to be selectively isolated from the complex biological system.[189]

Generally, a molecular target unique to an organelle type that is usually found on the surface of such organelles would be identified and an antibody that binds specifically to that target would be selected. Organelles will be captured with magnetic beads coated with such antibodies against the desired targets by using a magnet (Figure 6.1).[190]

.

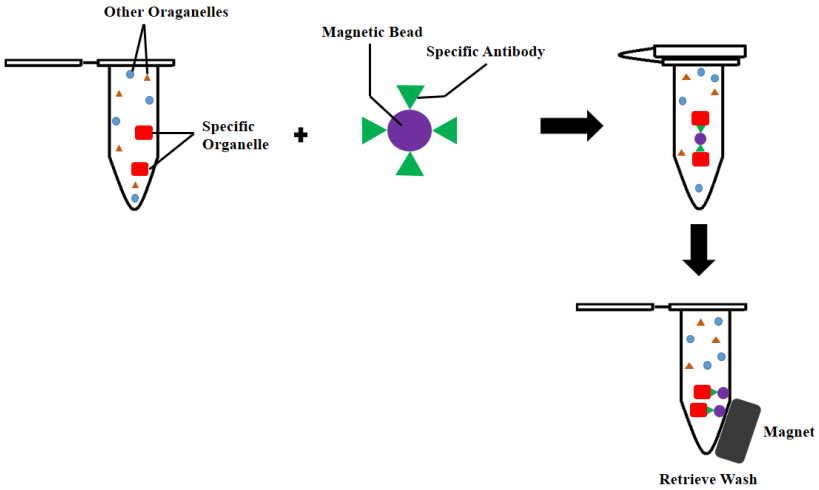

Figure 6.24. Diagram of an immunoisolation experiment using magnetic beads. The sample contains both the desired organelle with the molecular target of the antibody and other organelles. Magnetic beads with conjugated antibody against the molecular target are added to the sample. Organelles bound by antibodies conjugated to the magnetic beads are retrieved using a small magnet at the side of the tube and the unbound organelles are washed away.

6.2.3. Improving Lipid Analysis by Ion Mobility Mass Spectrometry

Detection of cis/trans isomerism is an important aspect in current biological and medical lipid research.[132] The change from cis to trans geometry is evoked by peroxidation

and involvement in electrophilic free radical reactions. Alterations in the geometry of lipids severely impacts their membrane functions and signaling properties and are thought to play a major role in aging and health impairments.[191]

Due to the complexity of the lipidome and the significant amount of isobaric and isomeric overlap, the detailed examination of lipids is challenging. High throughput structural analysis of lipids has been recently demonstrated through the use of rapid gas phase separation on the basis of the ion mobility (IM) combined with mass spectrometry (IM/MS).[132,192] The Synapt G2 instrument described in Chapter 2 has T-Wave ion mobility to significantly enhance the peak capacity, specificity, and sensitivity of biomolecule analysis.

The most straightforward method of measuring the ion mobility is the drift time method in which the arrival time of a distribution of ions is recorded under the influence of a weak electric field.[71] Drift time ion mobility methods have been successfully used to investigate the mobility-mass (drift time and *m/z*) correlation profiles of signals obtained from phosphatidyl-choline (PC), -ethanolamine (PE), -serine (PS), -inositol (PI), -glycerol (PG), phosphatidic acid (PA), and sphingomyelin (SM) lipid containing standards.[193] IM/MS is also able to distinguish fatty acid (FA) isomers with cis- and trans-orientations for the monounsaturated FAs. Therefore, further advances in lipidomic analysis of the lipid droplets and other organelles should consider the use of IM/MS.

6.2.4. Concluding Remarks

This chapter points to future approaches to advance the work described in this thesis, which contributes to our fundamental understanding of lipid droplets and how their lipidomic profile changes in aging.

In general, the findings in this thesis add significantly to the field of lipidomic analysis and opens up opportunities for new studies to determine the role of aging in lipid droplet biology.

Bibliography

References

(1) Perry, D. P. Introduction to Aging, Cancer, and Age-related Diseases. *Annals of the New York Academy of Sciences* **2010**, *1197*, vii-x.

(2) Kirkwood, T. B. Understanding the odd science of aging. *Cell* **2005**, *120*, 437-447.

(3) World Health Organization. US National Institute of Aging,. **2011**.

(4) Nakagawa, Y.; Hattori, M.; Harada, K.; Shirase, R.; Bando, M.; Okano, G. Age-related changes in intramyocellular lipid in humans by in vivo H-MR spectroscopy. *Gerontology* **2007**, *53*, 218-223.

(5) Partridge, G. J.; Creeper, J. Skeletal myopathy in juvenile barramundi, Lates calcarifer (Bloch), cultured in potassium-deficient saline groundwater. *Journal of fish diseases* **2004**, *27*, 523-530.

(6) Bartz, R.; Zehmer, J. K.; Zhu, M.; Chen, Y.; Serrero, G.; Zhao, Y.; Liu, P. Dynamic activity of lipid droplets: protein phosphorylation and GTP-mediated protein translocation. *Journal of proteome research* **2007**, *6*, 3256-3265.

(7) Cermelli, S.; Guo, Y.; Gross, S. P.; Welte, M. A. The lipid-droplet proteome reveals that droplets are a protein-storage depot. *Current biology : CB* **2006**, *16*, 1783-1795.

(8) Welte, M. A. Expanding roles for lipid droplets. *Current biology : CB* **2015**, *25*, R470-481.

(9) Welte, M. A. Proteins under new management: lipid droplets deliver. *Trends in cell biology* **2007**, *17*, 363-369.

(10) Goldberg, A. A.; Bourque, S. D.; Kyryakov, P.; Boukh-Viner, T.; Gregg, C.; Beach, A.; Burstein, M. T.; Machkalyan, G.; Richard, V.; Rampersad, S.; Titorenko, V. I. A novel function of lipid droplets in regulating longevity. *Biochemical Society transactions* **2009**, *37*, 1050-1055.

(11) Farese, R. V., Jr.; Walther, T. C. Lipid droplets finally get a little R-E-S-P-E-C-T. *Cell* **2009**, *139*, 855-860.

(12) Moldavski, O.; Amen, T.; Levin-Zaidman, S.; Eisenstein, M.; Rogachev, I.; Brandis, A.; Kaganovich, D.; Schuldiner, M. Lipid Droplets Are Essential for Efficient Clearance of Cytosolic Inclusion Bodies. *Developmental cell* **2015**, *33*, 603-610.

(13) Ohsaki, Y.; Cheng, J.; Fujita, A.; Tokumoto, T.; Fujimoto, T. Cytoplasmic lipid droplets are sites of convergence of proteasomal and autophagic degradation of apolipoprotein B. *Molecular biology of the cell* **2006**, *17*, 2674-2683.

(14) Blanksby, S. J.; Mitchell, T. W. Advances in mass spectrometry for lipidomics. *Annual review of analytical chemistry* **2010**, *3*, 433-465.

(15) Putri, S. P.; Yamamoto, S.; Tsugawa, H.; Fukusaki, E. Current metabolomics: technological advances. *Journal of bioscience and bioengineering* **2013**, *116*, 9-16.

(16) Griffiths, W. J.; Wang, Y. Mass spectrometry: from proteomics to metabolomics and lipidomics. *Chemical Society reviews* **2009**, *38*, 1882-1896.

(17) Beger, R. D. A review of applications of metabolomics in cancer. *Metabolites* **2013**, *3*, 552-574.

(18) Mishur, R. J.; Rea, S. L. Applications of mass spectrometry to metabolomics and metabonomics: detection of biomarkers of aging and of age-related diseases. *Mass spectrometry reviews* **2012**, *31*, 70-95.

(19) Cambiaghi, A.; Ferrario, M.; Masseroli, M. Analysis of metabolomic data: tools, current strategies and future challenges for omics data integration. *Briefings in bioinformatics* **2017**, *18*, 498-510.

(20) Patti, G. J.; Yanes, O.; Siuzdak, G. Innovation: Metabolomics: the apogee of the omics trilogy. *Nature reviews. Molecular cell biology* **2012**, *13*, 263-269.

(21) Beale, D. J.; Barratt, R.; Marlow, D. R.; Dunn, M. S.; Palombo, E. A.; Morrison, P. D.; Key, C. Application of metabolomics to understanding biofilms in water distribution systems: a pilot study. *Biofouling* **2013**, *29*, 283-294.

(22) Kotze, H. L.; Armitage, E. G.; Sharkey, K. J.; Allwood, J. W.; Dunn, W. B.; Williams, K. J.; Goodacre, R. A novel untargeted metabolomics correlation-based network analysis incorporating human metabolic reconstructions. *BMC systems biology* **2013**, *7*, 107.

(23) Bou Khalil, M.; Hou, W.; Zhou, H.; Elisma, F.; Swayne, L. A.; Blanchard, A. P.; Yao, Z.; Bennett, S. A.; Figeys, D. Lipidomics era: accomplishments and challenges. *Mass spectrometry reviews* **2010**, *29*, 877-929.

(24) Fahy, E.; Subramaniam, S.; Murphy, R. C.; Nishijima, M.; Raetz, C. R.; Shimizu, T.; Spener, F.; van Meer, G.; Wakelam, M. J.; Dennis, E. A. Update of the LIPID MAPS comprehensive classification system for lipids. *Journal of lipid research* **2009**, *50 Suppl*, S9-14.

(25) Heerklotz, H.; Seelig, J. Detergent-like action of the antibiotic peptide surfactin on lipid membranes. *Biophysical journal* **2001**, *81*, 1547-1554.

(26) Piomelli, D.; Astarita, G.; Rapaka, R. A neuroscientist's guide to lipidomics. *Nature reviews. Neuroscience* **2007**, *8*, 743-754.

(27) Han, X.; Gross, R. W. Global analyses of cellular lipidomes directly from crude extracts of biological samples by ESI mass spectrometry: a bridge to lipidomics. *Journal of lipid research* **2003**, *44*, 1071-1079.

(28) Dowhan, W. Molecular genetic approaches to defining lipid function. *Journal of lipid research* **2009**, *50 Suppl*, S305-310.

(29) Mc Auley, M. T.; Mooney, K. M. Computationally Modeling Lipid Metabolism and Aging: A Mini-review. *Computational and structural biotechnology journal* **2015**, *13*, 38-46.

(30) Mc Auley, M. T.; Mooney, K. M. Computational systems biology for aging research. *Interdisciplinary topics in gerontology* **2015**, *40*, 35-48.

(31) German, J. B.; Gillies, L. A.; Smilowitz, J. T.; Zivkovic, A. M.; Watkins, S. M. Lipidomics and lipid profiling in metabolomics. *Current opinion in lipidology* **2007**, *18*, 66-71.

(32) Alvarez, E.; Ruiz-Gutierrez, V.; Sobrino, F.; Santa-Maria, C. Age-related changes in membrane lipid composition, fluidity and respiratory burst in rat peritoneal neutrophils. *Clinical and experimental immunology* **2001**, *124*, 95-102.

(33) Cohen, R.; Barenholz, Y.; Gatt, S.; Dagan, A. Preparation and characterization of well defined D-erythro sphingomyelins. *Chemistry and physics of lipids* **1984**, *35*, 371-384.

(34) Shinitzky, M. Membrane fluidity in malignancy. Adversative and recuperative. *Biochimica et biophysica acta* **1984**, *738*, 251-261.

(35) Shinitzky, M.; Skornick, Y.; Gorelik, E.; Sindelar, W. Regulation of membrane function by lipids; implications for tumor development. *Progress in clinical and biological research* **1983**, *132B*, 425-433.

(36) Shinitzky, M. Patterns of lipid changes in membranes of the aged brain. *Gerontology* **1987**, *33*, 149-154.

(37) Yang, K.; Han, X. Lipidomics: Techniques, Applications, and Outcomes Related to Biomedical Sciences. *Trends in biochemical sciences* **2016**, *41*, 954-969.

(38) Schuldiner, M.; Bohnert, M. A different kind of love - lipid droplet contact sites. *Biochimica et biophysica acta* **2017**, *1862*, 1188-1196.

(39) Krahmer, N.; Farese, R. V., Jr.; Walther, T. C. Balancing the fat: lipid droplets and human disease. *EMBO molecular medicine* **2013**, *5*, 973-983.

(40) Singh, R.; Cuervo, A. M. Lipophagy: connecting autophagy and lipid metabolism. *International journal of cell biology* **2012**, *2012*, 282041.

(41) Liu, K.; Czaja, M. J. Regulation of lipid stores and metabolism by lipophagy. *Cell death and differentiation* **2013**, *20*, 3-11.

(42) Schweiger, M.; Lass, A.; Zimmermann, R.; Eichmann, T. O.; Zechner, R. Neutral lipid storage disease: genetic disorders caused by mutations in adipose triglyceride lipase/PNPLA2 or CGI-58/ABHD5. *American journal of physiology. Endocrinology and metabolism* **2009**, *297*, E289-296.

(43) Morales, P. E.; Bucarey, J. L.; Espinosa, A. Muscle Lipid Metabolism: Role of Lipid Droplets and Perilipins. *Journal of diabetes research* **2017**, *2017*, 1789395.

(44) Horn, P. J.; Ledbetter, N. R.; James, C. N.; Hoffman, W. D.; Case, C. R.; Verbeck, G. F.; Chapman, K. D. Visualization of lipid droplet composition by direct organelle mass spectrometry. *The Journal of biological chemistry* **2011**, *286*, 3298-3306.

(45) Horn, P. J.; Chapman, K. D. Organellar lipidomics. *Plant signaling & behavior* **2011**, *6*, 1594-1596.

(46) Rupasinghe, T. W. Lipidomics: extraction protocols for biological matrices. *Methods in molecular biology* **2013**, *1055*, 71-80.

(47) Chen, X.; Morris, R.; Lawrence, M. J.; Quinn, P. J. The isolation and structure of membrane lipid rafts from rat brain. *Biochimie* **2007**, *89*, 192-196.

(48) Kikuchi, M.; Hatano, N.; Yokota, S.; Shimozawa, N.; Imanaka, T.; Taniguchi, H. Proteomic analysis of rat liver peroxisome: presence of peroxisome-specific isozyme of Lon protease. *The Journal of biological chemistry* **2004**, *279*, 421-428.

(49) Zhang, L.; Wang, X.; Peng, X.; Wei, Y.; Cao, R.; Liu, Z.; Xiong, J.; Ying, X.; Chen, P.; Liang, S. Immunoaffinity purification of plasma membrane with secondary antibody superparamagnetic beads for proteomic analysis. *Journal of proteome research* **2007**, *6*, 34-43.

(50) Otieno, A. C.; Mwongela, S. M. Capillary electrophoresis-based methods for the determination of lipids--a review. *Analytica chimica acta* **2008**, *624*, 163-174.

(51) Cajka, T.; Fiehn, O. Comprehensive analysis of lipids in biological systems by liquid chromatography-mass spectrometry. *Trends in analytical chemistry : TRAC* **2014**, *61*, 192-206.

(52) Fuchs, B.; Suss, R.; Teuber, K.; Eibisch, M.; Schiller, J. Lipid analysis by thin-layer chromatography--a review of the current state. *Journal of chromatography. A* **2011**, *1218*, 2754-2774.

(53) Cajka, T.; Vaclavikova, M.; Dzuman, Z.; Vaclavik, L.; Ovesna, J.; Hajslova, J. Rapid LC-MS-based metabolomics method to study the Fusarium infection of barley. *Journal of separation science* **2014**, *37*, 912-919.

(54) Wenk, M. R. The emerging field of lipidomics. *Nature reviews. Drug discovery* **2005**, *4*, 594-610.

(55) Gutnikov, G. Fatty acid profiles of lipid samples. *Journal of chromatography. B, Biomedical applications* **1995**, *671*, 71-89.

(56) Kuksis, A.; Marai, L.; Gornall, D. A. Direct gas chromatographic examination of total lipid extracts. *Journal of lipid research* **1967**, *8*, 352-358.

(57) Adosraku, R. K.; Choi, G. T.; Constantinou-Kokotos, V.; Anderson, M. M.; Gibbons, W. A. NMR lipid profiles of cells, tissues, and body fluids: proton NMR analysis of human erythrocyte lipids. *Journal of lipid research* **1994**, *35*, 1925-1931.

(58) Schiller, J.; Arnold, K. Application of high resolution 31P NMR spectroscopy to the characterization of the phospholipid composition of tissues and body fluids - a methodological

review. *Medical science monitor : international medical journal of experimental and clinical research* **2002**, *8*, MT205-222.

(59) Mahrous, E. A.; Lee, R. B.; Lee, R. E. A rapid approach to lipid profiling of mycobacteria using 2D HSQC NMR maps. *Journal of lipid research* **2008**, *49*, 455-463.

(60) Taguchi, R.; Houjou, T.; Nakanishi, H.; Yamazaki, T.; Ishida, M.; Imagawa, M.; Shimizu, T. Focused lipidomics by tandem mass spectrometry. *Journal of chromatography. B, Analytical technologies in the biomedical and life sciences* **2005**, *823*, 26-36.

(61) Houjou, T.; Yamatani, K.; Imagawa, M.; Shimizu, T.; Taguchi, R. A shotgun tandem mass spectrometric analysis of phospholipids with normal-phase and/or reverse-phase liquid chromatography/electrospray ionization mass spectrometry. *Rapid communications in mass spectrometry : RCM* **2005**, *19*, 654-666.

(62) Cai, S. S.; Syage, J. A. Comparison of atmospheric pressure photoionization, atmospheric pressure chemical ionization, and electrospray ionization mass spectrometry for analysis of lipids. *Analytical chemistry* **2006**, *78*, 1191-1199.

(63) Cai, X.; Dong, J.; Liu, J.; Zheng, H.; Kaweeteerawat, C.; Wang, F.; Ji, Z.; Li, R. Multi-hierarchical profiling the structure-activity relationships of engineered nanomaterials at nano-bio interfaces. *Nature communications* **2018**, *9*, 4416.

(64) Knittelfelder, O. L.; Weberhofer, B. P.; Eichmann, T. O.; Kohlwein, S. D.; Rechberger, G. N. A versatile ultra-high performance LC-MS method for lipid profiling. *Journal of chromatography. B, Analytical technologies in the biomedical and life sciences* **2014**, *951-952*, 119-128.

(65) Pulfer, M.; Murphy, R. C. Electrospray mass spectrometry of phospholipids. *Mass spectrometry reviews* **2003**, *22*, 332-364.

(66) Wolf, C.; Quinn, P. J. Lipidomics: practical aspects and applications. *Progress in lipid research* **2008**, *47*, 15-36.

(67) Brugger, B.; Erben, G.; Sandhoff, R.; Wieland, F. T.; Lehmann, W. D. Quantitative analysis of biological membrane lipids at the low picomole level by nano-electrospray ionization tandem mass spectrometry. *Proceedings of the National Academy of Sciences of the United States of America* **1997**, *94*, 2339-2344.

(68) Han, X.; Cheng, H. Characterization and direct quantitation of cerebroside molecular species from lipid extracts by shotgun lipidomics. *Journal of lipid research* **2005**, *46*, 163-175.

(69) Karas, M.; Hillenkamp, F. Laser desorption ionization of proteins with molecular masses exceeding 10,000 daltons. *Analytical chemistry* **1988**, *60*, 2299-2301.

(70) Rujoi, M.; Estrada, R.; Yappert, M. C. In situ MALDI-TOF MS regional analysis of neutral phospholipids in lens tissue. *Analytical chemistry* **2004**, *76*, 1657-1663.

(71) Woods, A. S.; Ugarov, M.; Egan, T.; Koomen, J.; Gillig, K. J.; Fuhrer, K.; Gonin, M.; Schultz, J. A. Lipid/peptide/nucleotide separation with MALDI-ion mobility-TOF MS. *Analytical chemistry* **2004**, *76*, 2187-2195.

(72) Cornett, D. S.; Reyzer, M. L.; Chaurand, P.; Caprioli, R. M. MALDI imaging mass spectrometry: molecular snapshots of biochemical systems. *Nature methods* **2007**, *4*, 828-833.

(73) Harkewicz, R.; Dennis, E. A. Applications of mass spectrometry to lipids and membranes. *Annual review of biochemistry* **2011**, *80*, 301-325.

(74) Kofeler, H. C.; Fauland, A.; Rechberger, G. N.; Trotzmuller, M. Mass spectrometry based lipidomics: an overview of technological platforms. *Metabolites* **2012**, *2*, 19-38.

(75) Ekroos, K.; Chernushevich, I. V.; Simons, K.; Shevchenko, A. Quantitative profiling of phospholipids by multiple precursor ion scanning on a hybrid quadrupole time-of-flight mass spectrometer. *Analytical chemistry* **2002**, *74*, 941-949.

(76) Rainville, P. D.; Stumpf, C. L.; Shockcor, J. P.; Plumb, R. S.; Nicholson, J. K. Novel application of reversed-phase UPLC-oaTOF-MS for lipid analysis in complex biological mixtures: a new tool for lipidomics. *Journal of proteome research* **2007**, *6*, 552-558.

(77) Schwudke, D.; Hannich, J. T.; Surendranath, V.; Grimard, V.; Moehring, T.; Burton, L.; Kurzchalia, T.; Shevchenko, A. Top-down lipidomic screens by multivariate analysis of high-resolution survey mass spectra. *Analytical chemistry* **2007**, *79*, 4083-4093.

(78) Ivanova, P. T.; Cerda, B. A.; Horn, D. M.; Cohen, J. S.; McLafferty, F. W.; Brown, H. A. Electrospray ionization mass spectrometry analysis of changes in phospholipids in RBL-2H3 mastocytoma cells during degranulation. *Proceedings of the National Academy of Sciences of the United States of America* **2001**, *98*, 7152-7157.

(79) Yu, Z.; Chen, H.; Ai, J.; Zhu, Y.; Li, Y.; Borgia, J. A.; Yang, J. S.; Zhang, J.; Jiang, B.; Gu, W.; Deng, Y. Global lipidomics identified plasma lipids as novel biomarkers for early detection of lung cancer. *Oncotarget* **2017**, *8*, 107899-107906.

(80) Trimpin, S.; Clemmer, D. E.; McEwen, C. N. Charge-remote fragmentation of lithiated fatty acids on a TOF-TOF instrument using matrix-ionization. *Journal of the American Society for Mass Spectrometry* **2007**, *18*, 1967-1972.

(81) Jackson, S. N.; Wang, H. Y.; Woods, A. S. Direct profiling of lipid distribution in brain tissue using MALDI-TOFMS. *Analytical chemistry* **2005**, *77*, 4523-4527.

(82) Larsen, A.; Uran, S.; Jacobsen, P. B.; Skotland, T. Collision-induced dissociation of glycero phospholipids using electrospray ion-trap mass spectrometry. *Rapid communications in mass spectrometry : RCM* **2001**, *15*, 2393-2398.

(83) Schwartz, J. C.; Senko, M. W.; Syka, J. E. A two-dimensional quadrupole ion trap mass spectrometer. *Journal of the American Society for Mass Spectrometry* **2002**, *13*, 659-669.

(84) Dong, Y.; Wang, H.; Zhang, Y.; An, N.; Zhang, Y.; Shou, D. Ultra high performance liquid chromatography with synapt high-definition mass spectrometry and a pattern recognition approach to characterize chemical constituents and rat metabolites after the oral administration of Phellinus igniarius. *Journal of separation science* **2015**, *38*, 1137-1148.

(85) Makarov, A.; Denisov, E.; Lange, O.; Horning, S. Dynamic range of mass accuracy in LTQ Orbitrap hybrid mass spectrometer. *Journal of the American Society for Mass Spectrometry* **2006**, *17*, 977-982.

(86) Sugimoto, M.; Kawakami, M.; Robert, M.; Soga, T.; Tomita, M. Bioinformatics Tools for Mass Spectroscopy-Based Metabolomic Data Processing and Analysis. *Current bioinformatics* **2012**, *7*, 96-108.

(87) Scalbert, A.; Brennan, L.; Fiehn, O.; Hankemeier, T.; Kristal, B. S.; van Ommen, B.; Pujos-Guillot, E.; Verheij, E.; Wishart, D.; Wopereis, S. Mass-spectrometry-based metabolomics: limitations and recommendations for future progress with particular focus on nutrition research. *Metabolomics : Official journal of the Metabolomic Society* **2009**, *5*, 435-458.

(88) Christin, C.; Bischoff, R.; Horvatovich, P. Data processing pipelines for comprehensive profiling of proteomics samples by label-free LC-MS for biomarker discovery. *Talanta* **2011**, *83*, 1209-1224.

(89) Katajamaa, M.; Oresic, M. Data processing for mass spectrometry-based metabolomics. *Journal of chromatography. A* **2007**, *1158*, 318-328.

(90) Aretz, I.; Meierhofer, D. Advantages and Pitfalls of Mass Spectrometry Based Metabolome Profiling in Systems Biology. *International journal of molecular sciences* **2016**, *17*.

(91) Satori, C. P.; Ramezani, M.; Koopmeiners, J. S.; Meyer, A. F.; Rodriguez-Navarro, J. A.; Kuhns, M. M.; Taylor, T. H.; Haynes, C. L.; Dalluge, J. J.; Arriaga, E. A. Checkpoints for Preliminary Identification of Small Molecules found Enriched in Autophagosomes and Activated Mast Cell Secretions Analyzed by Comparative UPLC/MS(e). *Analytical methods : advancing methods and applications* **2017**, *9*, 46-54.

(92) Spicer, R.; Salek, R. M.; Moreno, P.; Canueto, D.; Steinbeck, C. Navigating freely-available software tools for metabolomics analysis. *Metabolomics : Official journal of the Metabolomic Society* **2017**, *13*, 106.

(93) Chitraju, C.; Trotzmuller, M.; Hartler, J.; Wolinski, H.; Thallinger, G. G.; Lass, A.; Zechner, R.; Zimmermann, R.; Kofeler, H. C.; Spener, F. Lipidomic analysis of lipid droplets from murine hepatocytes reveals distinct signatures for nutritional stress. *Journal of lipid research* **2012**, *53*, 2141-2152.

(94) Zhang, J.; Yang, W.; Li, S.; Yao, S.; Qi, P.; Yang, Z.; Feng, Z.; Hou, J.; Cai, L.; Yang, M.; Wu, W.; Guo, D. A. An intelligentized strategy for endogenous small molecules characterization and quality evaluation of earthworm from two geographic origins by ultra-high performance HILIC/QTOF MS(E) and Progenesis QI. *Analytical and bioanalytical chemistry* **2016**, *408*, 3881-3890.

(95) Wilcoxen, K. M.; Uehara, T.; Myint, K. T.; Sato, Y.; Oda, Y. Practical metabolomics in drug discovery. *Expert opinion on drug discovery* **2010**, *5*, 249-263.

(96) Gorrochategui, E.; Casas, J.; Porte, C.; Lacorte, S.; Tauler, R. Chemometric strategy for untargeted lipidomics: biomarker detection and identification in stressed human placental cells. *Analytica chimica acta* **2015**, *854*, 20-33.

(97) Denery, J. R.; Nunes, A. A.; Hixon, M. S.; Dickerson, T. J.; Janda, K. D. Metabolomics-based discovery of diagnostic biomarkers for onchocerciasis. *PLoS neglected tropical diseases* **2010**, *4*.

(98) Gowda, G. A.; Djukovic, D. Overview of mass spectrometry-based metabolomics: opportunities and challenges. *Methods in molecular biology* **2014**, *1198*, 3-12.

(99) Dettmer, K.; Aronov, P. A.; Hammock, B. D. Mass spectrometry-based metabolomics. *Mass spectrometry reviews* **2007**, *26*, 51-78.

(100) Matsuda, F. Technical Challenges in Mass Spectrometry-Based Metabolomics. *Mass spectrometry* **2016**, *5*, S0052.

(101) Ubaida Mohien, C.; Colquhoun, D. R.; Mathias, D. K.; Gibbons, J. G.; Armistead, J. S.; Rodriguez, M. C.; Rodriguez, M. H.; Edwards, N. J.; Hartler, J.; Thallinger, G. G.; Graham, D. R.; Martinez-Barnetche, J.; Rokas, A.; Dinglasan, R. R. A bioinformatics approach for integrated transcriptomic and proteomic comparative analyses of model and non-sequenced anopheline vectors of human malaria parasites. *Molecular & cellular proteomics : MCP* **2013**, *12*, 120-131.

(102) Nielen, M. W.; van Engelen, M. C.; Zuiderent, R.; Ramaker, R. Screening and confirmation criteria for hormone residue analysis using liquid chromatography accurate mass time-of-flight, Fourier transform ion cyclotron resonance and orbitrap mass spectrometry techniques. *Analytica chimica acta* **2007**, *586*, 122-129.

(103) Dunn, W. B. Current trends and future requirements for the mass spectrometric investigation of microbial, mammalian and plant metabolomes. *Physical biology* **2008**, *5*, 011001.

(104) Dunn, W. B.; Broadhurst, D.; Brown, M.; Baker, P. N.; Redman, C. W.; Kenny, L. C.; Kell, D. B. Metabolic profiling of serum using Ultra Performance Liquid Chromatography and the LTQ-Orbitrap mass spectrometry system. *Journal of chromatography. B, Analytical technologies in the biomedical and life sciences* **2008**, *871*, 288-298.

(105) Tautenhahn, R.; Patti, G. J.; Rinehart, D.; Siuzdak, G. XCMS Online: a web-based platform to process untargeted metabolomic data. *Analytical chemistry* **2012**, *84*, 5035-5039.

(106) Glauser, G.; Veyrat, N.; Rochat, B.; Wolfender, J. L.; Turlings, T. C. Ultra-high pressure liquid chromatography-mass spectrometry for plant metabolomics: a systematic comparison of high-resolution quadrupole-time-of-flight and single stage Orbitrap mass spectrometers. *Journal of chromatography. A* **2013**, *1292*, 151-159.

(107) Eichhorn, P.; Perez, S.; Acena, J.; Gardinali, P.; Abad, J. L.; Barcelo, D. Identification of phototransformation products of sildenafil (Viagra) and its N-demethylated human metabolite under simulated sunlight. *Journal of mass spectrometry : JMS* **2012**, *47*, 701-711.

(108) Bligh, E. G.; Dyer, W. J. A rapid method of total lipid extraction and purification. *Canadian journal of biochemistry and physiology* **1959**, *37*, 911-917.

(109) Smith, C. A.; Want, E. J.; O'Maille, G.; Abagyan, R.; Siuzdak, G. XCMS: processing mass spectrometry data for metabolite profiling using nonlinear peak alignment, matching, and identification. *Analytical chemistry* **2006**, *78*, 779-787.

(110) Cappadona, S.; Baker, P. R.; Cutillas, P. R.; Heck, A. J.; van Breukelen, B. Current challenges in software solutions for mass spectrometry-based quantitative proteomics. *Amino acids* **2012**, *43*, 1087-1108.

(111) Paglia, G.; Stocchero, M.; Cacciatore, S.; Lai, S.; Angel, P.; Alam, M. T.; Keller, M.; Ralser, M.; Astarita, G. Unbiased Metabolomic Investigation of Alzheimer's Disease Brain Points to Dysregulation of Mitochondrial Aspartate Metabolism. *Journal of proteome research* **2016**, *15*, 608-618.

(112) Chen, Y. X.; Zhang, X. J.; Huang, J.; Zhou, S. J.; Liu, F.; Jiang, L. L.; Chen, M.; Wan, J. B.; Yang, D. Z. UHPLC/Q-TOFMS-based plasma metabolomics of polycystic ovary syndrome patients with and without insulin resistance. *Journal of pharmaceutical and biomedical analysis* **2016**, *121*, 141-150.

(113) Patti, G. J.; Tautenhahn, R.; Rinehart, D.; Cho, K.; Shriver, L. P.; Manchester, M.; Nikolskiy, I.; Johnson, C. H.; Mahieu, N. G.; Siuzdak, G. A view from above: cloud plots to visualize global metabolomic data. *Analytical chemistry* **2013**, *85*, 798-804.

(114) Saoi, M.; Percival, M.; Nemr, C.; Li, A.; Gibala, M.; Britz-McKibbin, P. Characterization of the Human Skeletal Muscle Metabolome for Elucidating the Mechanisms of Bicarbonate Ingestion on Strenuous Interval Exercise. *Analytical chemistry* **2019**, *91*, 4709-4718.

(115) Bristow, A. W.; Webb, K. S. Intercomparison study on accurate mass measurement of small molecules in mass spectrometry. *Journal of the American Society for Mass Spectrometry* **2003**, *14*, 1086-1098.

(116) Jonsson, P.; Johansson, A. I.; Gullberg, J.; Trygg, J.; A, J.; Grung, B.; Marklund, S.; Sjostrom, M.; Antti, H.; Moritz, T. High-throughput data analysis for detecting and identifying differences between samples in GC/MS-based metabolomic analyses. *Analytical chemistry* **2005**, *77*, 5635-5642.

(117) O'Connor, A.; Brasher, C. J.; Slatter, D. A.; Meckelmann, S. W.; Hawksworth, J. I.; Allen, S. M.; O'Donnell, V. B. LipidFinder: A computational workflow for discovery of lipids identifies eicosanoid-phosphoinositides in platelets. *JCI insight* **2017**, *2*, e91634.

(118) Yang, K.; Han, X. Accurate quantification of lipid species by electrospray ionization mass spectrometry - Meet a key challenge in lipidomics. *Metabolites* **2011**, *1*, 21-40.

(119) Murphy, R. C.; Gaskell, S. J. New applications of mass spectrometry in lipid analysis. *The Journal of biological chemistry* **2011**, *286*, 25427-25433.

(120) Makarov, A.; Denisov, E. Dynamics of ions of intact proteins in the Orbitrap mass analyzer. *Journal of the American Society for Mass Spectrometry* **2009**, *20*, 1486-1495.

(121) Makarov, A.; Denisov, E.; Kholomeev, A.; Balschun, W.; Lange, O.; Strupat, K.; Horning, S. Performance evaluation of a hybrid linear ion trap/orbitrap mass spectrometer. *Analytical chemistry* **2006**, *78*, 2113-2120.

(122) Auley, M. T.; Mooney, K. M.; Angell, P. J.; Wilkinson, S. J. Mathematical modelling of metabolic regulation in aging. *Metabolites* **2015**, *5*, 232-251.

(123) Kalli, A.; Smith, G. T.; Sweredoski, M. J.; Hess, S. Evaluation and optimization of mass spectrometric settings during data-dependent acquisition mode: focus on LTQ-Orbitrap mass analyzers. *Journal of proteome research* **2013**, *12*, 3071-3086.

(124) Tabb, D. L.; Vega-Montoto, L.; Rudnick, P. A.; Variyath, A. M.; Ham, A. J.; Bunk, D. M.; Kilpatrick, L. E.; Billheimer, D. D.; Blackman, R. K.; Cardasis, H. L.; Carr, S. A.; Clauser, K. R.; Jaffe, J. D.; Kowalski, K. A.; Neubert, T. A.; Regnier, F. E.; Schilling, B.; Tegeler, T. J.; Wang, M.; Wang, P.; Whiteaker, J. R.; Zimmerman, L. J.; Fisher, S. J.; Gibson, B. W.; Kinsinger, C. R.; Mesri, M.; Rodriguez, H.; Stein, S. E.; Tempst, P.; Paulovich, A. G.; Liebler, D. C.; Spiegelman, C. Repeatability and reproducibility in proteomic identifications by liquid chromatography-tandem mass spectrometry. *Journal of proteome research* **2010**, *9*, 761-776.

(125) Scigelova, M.; Makarov, A. Orbitrap mass analyzer--overview and applications in proteomics. *Proteomics* **2006**, *6 Suppl 2*, 16-21.

(126) Zubarev, R. A.; Makarov, A. Orbitrap mass spectrometry. *Analytical chemistry* **2013**, *85*, 5288-5296.

(127) Makarov, A. Electrostatic axially harmonic orbital trapping: a high-performance technique of mass analysis. *Analytical chemistry* **2000**, *72*, 1156-1162.

(128) Coles, J. N.; Guilhaus, M. Resolution limitations from detector pulse width and jitter in a linear orthogonal-acceleration time-of-flight mass spectrometer. *Journal of the American Society for Mass Spectrometry* **1994**, *5*, 772-778.

(129) Park, E. S.; Wallace, W. E.; Guttman, C. M.; Flynn, K. M.; Richardson, M. C.; Holmes, G. A. A general method for quantitative measurement of molecular mass distribution by mass spectrometry. *Journal of the American Society for Mass Spectrometry* **2009**, *20*, 1638-1644.

(130) Kaufmann, A. Strategy for the elucidation of elemental compositions of trace analytes based on a mass resolution of 100,000 full width at half maximum. *Rapid communications in mass spectrometry : RCM* **2010**, *24*, 2035-2045.

(131) Kaufmann, A.; Widmer, M.; Maden, K. Post-interface signal suppression, a phenomenon observed in a single-stage Orbitrap mass spectrometer coupled to an electrospray interfaced liquid chromatograph. *Rapid communications in mass spectrometry : RCM* **2010**, *24*, 2162-2170.

(132) Campbell, J. L.; Baba, T.; Liu, C.; Lane, C. S.; Le Blanc, J. C. Y.; Hager, J. W. Analyzing Glycopeptide Isomers by Combining Differential Mobility Spectrometry with Electron- and Collision-Based Tandem Mass Spectrometry. *Journal of the American Society for Mass Spectrometry* **2017**, *28*, 1374-1381.

(133) Walther, T. C.; Farese, R. V., Jr. Lipid droplets and cellular lipid metabolism. *Annual review of biochemistry* **2012**, *81*, 687-714.

(134) Patterson, N. H.; Alabdulkarim, B.; Lazaris, A.; Thomas, A.; Marcinkiewicz, M. M.; Gao, Z. H.; Vermeulen, P. B.; Chaurand, P.; Metrakos, P. Assessment of pathological response to therapy using lipid mass spectrometry imaging. *Scientific reports* **2016**, *6*, 36814.

(135) Williams, M. L. Lipids in normal and pathological desquamation. *Advances in lipid research* **1991**, *24*, 211-262.

(136) Ackerman, D.; Gems, D. The mystery of C. elegans aging: an emerging role for fat. Distant parallels between C. elegans aging and metabolic syndrome? *BioEssays : news and reviews in molecular, cellular and developmental biology* **2012**, *34*, 466-471.

(137) Tissenbaum, H. A. Using C. elegans for aging research. *Invertebrate reproduction & development* **2015**, *59*, 59-63.

(138) Welte, M. A. As the fat flies: The dynamic lipid droplets of Drosophila embryos. *Biochimica et biophysica acta* **2015**, *1851*, 1156-1185.

(139) Walther, T. C.; Farese, R. V., Jr. The life of lipid droplets. *Biochimica et biophysica acta* **2009**, *1791*, 459-466.

(140) Yu, Y.; Li, T.; Wu, N.; Jiang, L.; Ji, X.; Huang, H. The Role of Lipid Droplets in Mortierella alpina Aging Revealed by Integrative Subcellular and Whole-Cell Proteome Analysis. *Scientific reports* **2017**, *7*, 43896.

(141) Thiam, A. R.; Foret, L. The physics of lipid droplet nucleation, growth and budding. *Biochimica et biophysica acta* **2016**, *1861*, 715-722.

(142) Hou, N. S.; Taubert, S. Function and Regulation of Lipid Biology in Caenorhabditis elegans Aging. *Frontiers in physiology* **2012**, *3*, 143.

(143) Prasain, J. K.; Wilson, L.; Hoang, H. D.; Moore, R.; Miller, M. A. Comparative Lipidomics of Caenorhabditis elegans Metabolic Disease Models by SWATH Non-Targeted Tandem Mass Spectrometry. *Metabolites* **2015**, *5*, 677-696.

(144) Vrablik, T. L.; Petyuk, V. A.; Larson, E. M.; Smith, R. D.; Watts, J. L. Lipidomic and proteomic analysis of Caenorhabditis elegans lipid droplets and identification of ACS-4 as a lipid droplet-associated protein. *Biochimica et biophysica acta* **2015**, *1851*, 1337-1345.

(145) Listenberger, L. L.; Han, X.; Lewis, S. E.; Cases, S.; Farese, R. V., Jr.; Ory, D. S.; Schaffer, J. E. Triglyceride accumulation protects against fatty acid-induced lipotoxicity. *Proceedings of the National Academy of Sciences of the United States of America* **2003**, *100*, 3077-3082.

(146) Lynn, K. S.; Cheng, M. L.; Chen, Y. R.; Hsu, C.; Chen, A.; Lih, T. M.; Chang, H. Y.; Huang, C. J.; Shiao, M. S.; Pan, W. H.; Sung, T. Y.; Hsu, W. L. Metabolite identification for mass spectrometry-based metabolomics using multiple types of correlated ion information. *Analytical chemistry* **2015**, *87*, 2143-2151.

(147) Lee, D. Y.; Bowen, B. P.; Northen, T. R. Mass spectrometry-based metabolomics, analysis of metabolite-protein interactions, and imaging. *BioTechniques* **2010**, *49*, 557-565.

(148) Benton, H. P.; Ivanisevic, J.; Mahieu, N. G.; Kurczy, M. E.; Johnson, C. H.; Franco, L.; Rinehart, D.; Valentine, E.; Gowda, H.; Ubhi, B. K.; Tautenhahn, R.; Gieschen, A.; Fields, M. W.; Patti, G. J.; Siuzdak, G. Autonomous metabolomics for rapid metabolite identification in global profiling. *Analytical chemistry* **2015**, *87*, 884-891.

(149) McMahon, A.; Lu, H.; Butovich, I. A. The spectrophotometric sulfo-phospho-vanillin assessment of total lipids in human meibomian gland secretions. *Lipids* **2013**, *48*, 513-525.

(150) Cheng, Y. S.; Zheng, Y.; VanderGheynst, J. S. Rapid quantitative analysis of lipids using a colorimetric method in a microplate format. *Lipids* **2011**, *46*, 95-103.

(151) Hur, M.; Campbell, A. A.; Almeida-de-Macedo, M.; Li, L.; Ransom, N.; Jose, A.; Crispin, M.; Nikolau, B. J.; Wurtele, E. S. A global approach to analysis and interpretation of metabolic data for plant natural product discovery. *Natural product reports* **2013**, *30*, 565-583.

(152) Brunius, C.; Shi, L.; Landberg, R. Large-scale untargeted LC-MS metabolomics data correction using between-batch feature alignment and cluster-based within-batch signal intensity drift correction. *Metabolomics : Official journal of the Metabolomic Society* **2016**, *12*, 173.

(153) Feng, Q.; Liu, Z.; Zhong, S.; Li, R.; Xia, H.; Jie, Z.; Wen, B.; Chen, X.; Yan, W.; Fan, Y.; Guo, Z.; Meng, N.; Chen, J.; Yu, X.; Zhang, Z.; Kristiansen, K.; Wang, J.; Xu, X.; He, K.; Li, G. Integrated metabolomics and metagenomics analysis of plasma and urine identified microbial metabolites associated with coronary heart disease. *Scientific reports* **2016**, *6*, 22525.

(154) Shi, X.; Li, J.; Zou, X.; Greggain, J.; Rodkaer, S. V.; Faergeman, N. J.; Liang, B.; Watts, J. L. Regulation of lipid droplet size and phospholipid composition by stearoyl-CoA desaturase. *Journal of lipid research* **2013**, *54*, 2504-2514.

(155) Copes, N.; Edwards, C.; Chaput, D.; Saifee, M.; Barjuca, I.; Nelson, D.; Paraggio, A.; Saad, P.; Lipps, D.; Stevens, S. M., Jr.; Bradshaw, P. C. Metabolome and proteome changes with aging in Caenorhabditis elegans. *Experimental gerontology* **2015**, *72*, 67-84.

(156) Gao, A. W.; Chatzispyrou, I. A.; Kamble, R.; Liu, Y. J.; Herzog, K.; Smith, R. L.; van Lenthe, H.; Vervaart, M. A. T.; van Cruchten, A.; Luyf, A. C.; van Kampen, A.; Pras-Raves, M. L.; Vaz, F. M.; Houtkooper, R. H. A sensitive mass spectrometry platform identifies metabolic changes of life history traits in C. elegans. *Scientific reports* **2017**, *7*, 2408.

(157) Shpilka, T.; Welter, E.; Borovsky, N.; Amar, N.; Mari, M.; Reggiori, F.; Elazar, Z. Lipid droplets and their component triglycerides and steryl esters regulate autophagosome biogenesis. *The EMBO journal* **2015**, *34*, 2117-2131.

(158) Tucker, M. Z.; Turcotte, L. P. Aging is associated with elevated muscle triglyceride content and increased insulin-stimulated fatty acid uptake. *American journal of physiology. Endocrinology and metabolism* **2003**, *285*, E827-835.

(159) Gluchowski, N. L.; Becuwe, M.; Walther, T. C.; Farese, R. V., Jr. Lipid droplets and liver disease: from basic biology to clinical implications. *Nature reviews. Gastroenterology & hepatology* **2017**, *14*, 343-355.

(160) Tosato, M.; Zamboni, V.; Ferrini, A.; Cesari, M. The aging process and potential interventions to extend life expectancy. *Clinical interventions in aging* **2007**, *2*, 401-412.

(161) van Meer, G. Cellular lipidomics. *The EMBO journal* **2005**, *24*, 3159-3165.

(162) Thiam, A. R.; Farese, R. V., Jr.; Walther, T. C. The biophysics and cell biology of lipid droplets. *Nature reviews. Molecular cell biology* **2013**, *14*, 775-786.

(163) Ohsaki, Y.; Suzuki, M.; Fujimoto, T. Open questions in lipid droplet biology. *Chemistry & biology* **2014**, *21*, 86-96.

(164) Wilfling, F.; Wang, H.; Haas, J. T.; Krahmer, N.; Gould, T. J.; Uchida, A.; Cheng, J. X.; Graham, M.; Christiano, R.; Frohlich, F.; Liu, X.; Buhman, K. K.; Coleman, R. A.; Bewersdorf, J.; Farese, R. V., Jr.; Walther, T. C. Triacylglycerol synthesis enzymes mediate lipid droplet growth by relocalizing from the ER to lipid droplets. *Developmental cell* **2013**, *24*, 384-399.

(165) Atshaves, B. P.; Storey, S. M.; McIntosh, A. L.; Petrescu, A. D.; Lyuksyutova, O. I.; Greenberg, A. S.; Schroeder, F. Sterol carrier protein-2 expression modulates protein and lipid composition of lipid droplets. *The Journal of biological chemistry* **2001**, *276*, 25324-25335.

(166) Ding, Y.; Zhang, S.; Yang, L.; Na, H.; Zhang, P.; Zhang, H.; Wang, Y.; Chen, Y.; Yu, J.; Huo, C.; Xu, S.; Garaiova, M.; Cong, Y.; Liu, P. Isolating lipid droplets from multiple species. *Nature protocols* **2013**, *8*, 43-51.

(167) Slawik, M.; Vidal-Puig, A. J. Lipotoxicity, overnutrition and energy metabolism in aging. *Ageing research reviews* **2006**, *5*, 144-164.

(168) Chan, R. B.; Oliveira, T. G.; Cortes, E. P.; Honig, L. S.; Duff, K. E.; Small, S. A.; Wenk, M. R.; Shui, G.; Di Paolo, G. Comparative lipidomic analysis of mouse and human brain with Alzheimer disease. *The Journal of biological chemistry* **2012**, *287*, 2678-2688.

(169) Penno, A.; Hackenbroich, G.; Thiele, C. Phospholipids and lipid droplets. *Biochimica et biophysica acta* **2013**, *1831*, 589-594.

(170) Kim, S.; Cheon, H. S.; Song, J. C.; Yun, S. M.; Park, S. I.; Jeon, J. P. Aging-related Changes in Mouse Serum Glycerophospholipid Profiles. *Osong public health and research perspectives* **2014**, *5*, 345-350.

(171) Nicolson, G. L.; Ash, M. E. Membrane Lipid Replacement for chronic illnesses, aging and cancer using oral glycerolphospholipid formulations with fructooligosaccharides to restore phospholipid function in cellular membranes, organelles, cells and tissues. *Biochimica et biophysica acta* **2017**, *1859*, 1704-1724.

(172) Krahmer, N.; Guo, Y.; Wilfling, F.; Hilger, M.; Lingrell, S.; Heger, K.; Newman, H. W.; Schmidt-Supprian, M.; Vance, D. E.; Mann, M.; Farese, R. V., Jr.; Walther, T. C. Phosphatidylcholine synthesis for lipid droplet expansion is mediated by localized activation of CTP:phosphocholine cytidylyltransferase. *Cell metabolism* **2011**, *14*, 504-515.

(173) Guijas, C.; Rodriguez, J. P.; Rubio, J. M.; Balboa, M. A.; Balsinde, J. Phospholipase A2 regulation of lipid droplet formation. *Biochimica et biophysica acta* **2014**, *1841*, 1661-1671.

(174) Mok, H. J.; Shin, H.; Lee, J. W.; Lee, G. K.; Suh, C. S.; Kim, K. P.; Lim, H. J. Age-Associated Lipidome Changes in Metaphase II Mouse Oocytes. *PloS one* **2016**, *11*, e0148577.

(175) Brocard, L.; Immel, F.; Coulon, D.; Esnay, N.; Tuphile, K.; Pascal, S.; Claverol, S.; Fouillen, L.; Bessoule, J. J.; Brehelin, C. Proteomic Analysis of Lipid Droplets from Arabidopsis Aging Leaves Brings New Insight into Their Biogenesis and Functions. *Frontiers in plant science* **2017**, *8*, 894.

(176) Pollard, A. K.; Ortori, C. A.; Stoger, R.; Barrett, D. A.; Chakrabarti, L. Mouse mitochondrial lipid composition is defined by age in brain and muscle. *Aging* **2017**, *9*, 986-998.

(177) Johri, A.; Beal, M. F. Mitochondrial dysfunction in neurodegenerative diseases. *The Journal of pharmacology and experimental therapeutics* **2012**, *342*, 619-630.

(178) Chan, D. C. Mitochondria: dynamic organelles in disease, aging, and development. *Cell* **2006**, *125*, 1241-1252.

(179) Zhao, L.; Zou, X.; Feng, Z.; Luo, C.; Liu, J.; Li, H.; Chang, L.; Wang, H.; Li, Y.; Long, J.; Gao, F.; Liu, J. Evidence for association of mitochondrial metabolism alteration with lipid accumulation in aging rats. *Experimental gerontology* **2014**, *56*, 3-12.

(180) Brugger, B. Lipidomics: analysis of the lipid composition of cells and subcellular organelles by electrospray ionization mass spectrometry. *Annual review of biochemistry* **2014**, *83*, 79-98.

(181) Ivanova, P. T.; Milne, S. B.; Myers, D. S.; Brown, H. A. Lipidomics: a mass spectrometry based systems level analysis of cellular lipids. *Current opinion in chemical biology* **2009**, *13*, 526-531.

(182) Hardisty, A.; Roberts, D.; Biodiversity Informatics, C.; Addink, W.; Aelterman, B.; Agosti, D.; Amaral-Zettler, L.; Arino, A. H.; Arvanitidis, C.; Backeljau, T.; Bailly, N.; Belbin, L.; Berendsohn, W.; Bertrand, N.; Caithness, N.; Campbell, D.; Cochrane, G.; Conruyt, N.; Culham, A.; Damgaard, C.; Davies, N.; Fady, B.; Faulwetter, S.; Feest, A.; Field, D.; Garnier, E.; Geser, G.; Gilbert, J.; Grosche; Grosser, D.; Hardisty, A.; Herbinet, B.; Hobern, D.; Jones, A.; de Jong, Y.; King, D.; Knapp, S.; Koivula, H.; Los, W.; Meyer, C.; Morris, R. A.; Morrison, N.; Morse, D.; Obst, M.; Pafilis, E.; Page, L. M.; Page, R.; Pape, T.; Parr, C.; Paton, A.; Patterson, D.; Paymal, E.; Penev, L.; Pollet, M.; Pyle, R.; von Raab-Straube, E.; Robert, V.; Roberts, D.; Robertson, T.; Rovellotti, O.; Saarenmaa, H.; Schalk, P.; Schaminee, J.; Schofield, P.; Sier, A.; Sierra, S.; Smith, V.; van Spronsen, E.; Thornton-Wood, S.; van Tienderen, P.; van Tol, J.; Tuama, E. O.; Uetz, P.; Vaas, L.; Vignes Lebbe, R.; Vision, T.; Vu, D.; De Wever, A.; White, R.; Willis, K.; Young, F. A decadal view of biodiversity informatics: challenges and priorities. *BMC ecology* **2013**, *13*, 16.

(183) Hou, L.; Huang, J.; Green, C. D.; Boyd-Kirkup, J.; Zhang, W.; Yu, X.; Gong, W.; Zhou, B.; Han, J. D. Systems biology in aging: linking the old and the young. *Current genomics* **2012**, *13*, 558-565.

(184) Rockenfeller, P.; Koska, M.; Pietrocola, F.; Minois, N.; Knittelfelder, O.; Sica, V.; Franz, J.; Carmona-Gutierrez, D.; Kroemer, G.; Madeo, F. Phosphatidylethanolamine positively regulates autophagy and longevity. *Cell death and differentiation* **2015**, *22*, 499-508.

(185) Hyotylainen, T.; Oresic, M. Systems biology strategies to study lipidomes in health and disease. *Progress in lipid research* **2014**, *55*, 43-60.

(186) Duhrkop, K.; Shen, H.; Meusel, M.; Rousu, J.; Bocker, S. Searching molecular structure databases with tandem mass spectra using CSI:FingerID. *Proceedings of the National Academy of Sciences of the United States of America* **2015**, *112*, 12580-12585.

(187) Kind, T.; Fiehn, O. Advances in structure elucidation of small molecules using mass spectrometry. *Bioanalytical reviews* **2010**, *2*, 23-60.

(188) Schrimpe-Rutledge, A. C.; Codreanu, S. G.; Sherrod, S. D.; McLean, J. A. Untargeted Metabolomics Strategies-Challenges and Emerging Directions. *Journal of the American Society for Mass Spectrometry* **2016**, *27*, 1897-1905.

(189) Hornig-Do, H. T.; Gunther, G.; Bust, M.; Lehnartz, P.; Bosio, A.; Wiesner, R. J. Isolation of functional pure mitochondria by superparamagnetic microbeads. *Analytical biochemistry* **2009**, *389*, 1-5.

(190) Ru, Y.; Yin, L.; Sun, H.; Yin, S.; Pan, Q.; Wei, H.; Wu, L.; Liu, S. A micropreparation of mitochondria from cells using magnetic beads with immunoaffinity. *Analytical biochemistry* **2012**, *421*, 219-226.

(191) Chatgilialoglu, C.; Ferreri, C.; Melchiorre, M.; Sansone, A.; Torreggiani, A. Lipid geometrical isomerism: from chemistry to biology and diagnostics. *Chemical reviews* **2014**, *114*, 255-284.

(192) Ruotolo, B. T.; Benesch, J. L.; Sandercock, A. M.; Hyung, S. J.; Robinson, C. V. Ion mobility-mass spectrometry analysis of large protein complexes. *Nature protocols* **2008**, *3*, 1139-1152.

(193) Groessl, M.; Graf, S.; Knochenmuss, R. High resolution ion mobility-mass spectrometry for separation and identification of isomeric lipids. *The Analyst* **2015**, *140*, 6904-6911.

Appendices

Appendix A

Supplementary Material to Chapter 4

Comparative Lipidomic Analysis of lipid droplets from *C. elegans* at Different Age.

ID	Fold	p-value	Change	*m/z*	Rt	Name
2	263.24	0.0029	UP	922.7871	10.5	TG(18:3/18:3/20:1)
4	240.82	0.0032	UP	923.791	10.5	TG(18:0/18:2/19:0)
88	110.59	0.0399	UP	948.8024	10.56	TG(18:2/20:3/20:3)
223	98.26	0.0254	UP	888.9749	10.73	TG(17:1/18:1/18:1)
102	96.17	0.0046	UP	927.8213	10.73	TG(18:3/18:3/20:1)
47	92.19	0.0089	UP	920.771	10.34	TG(17:0/17:1/18:0)
32	88.59	0.0036	UP	943.8519	11.01	TG(17:0/20:2/20:2)
71	86.08	0.0035	UP	904.834	10.99	TG(16:1/16:1/22:0)
287	84.39	0.0066	UP	925.8055	10.59	TG(18:3/18:3/20:2)
49	83.55	0.0106	UP	942.756	10.17	TG(17:2/20:1/20:1)
493	82.78	0.0246	UP	944.8647	11.15	TG(17:1/20:1/20:1)
123	81.28	0.0485	UP	946.7866	10.42	TG(18:3/20:3/20:3)
443	78.78	0.0145	UP	943.7589	10.17	TG(17:0/20:2/20:2)
24	62.94	0.0289	UP	926.8174	10.72	TG(18:2/18:3/20:0)
82	59.11	0.0074	UP	952.8334	10.79	TG(18:2/20:2/20:2)
166	53.61	0.0113	UP	944.7704	10.27	TG(18:2/20:4/20:4)
33	52.96	0.0033	UP	928.835	10.89	TG(18:1/18:3/20:0)
143	51.26	0.0119	UP	954.848	10.91	TG(18:3/20:1/20:1)
363	37.28	0.0057	UP	927.742	10.49	TG(18:3/18:3/20:1)
55	32.77	0.0468	UP	918.8411	10.94	TG(18:3/18:3/20:3)
105	31.73	0.0365	UP	889.8065	10.73	TG(16:1/17:0/20:1)
158	30.81	0.0304	UP	968.7704	10.24	TG(20:4/20:4/20:4)
61	30.76	0.0216	UP	910.7875	10.53	TG(17:2/18:3/20:1)
283	29.02	0.0276	UP	889.9777	10.73	TG(16:1/17:0/20:1)
63	28.45	0.0065	UP	866.7243	10.05	TG(12:0/18:1/22:6)
22	26.98	0.0428	UP	960.8962	11.38	TG(18:2/20:0/20:0)
372	26.85	0.0092	UP	928.7447	10.49	TG(18:1/18:3/20:0)
67	25.42	0.0291	UP	905.8374	10.98	TG(17:1/18:3/19:0)
95	22.67	0.0109	UP	942.8489	11	TG(17:2/20:1/20:1)
119	22.14	0.0363	UP	888.8036	10.74	TG(17:1/18:1/18:1)
56	21.72	0.0010	UP	890.8097	10.73	TG(16:1/17:0/20:1)
135	21.38	0.0369	UP	887.7909	10.59	TG(17:2/18:2/18:2)
58	21.10	0.0088	UP	906.8407	10.98	TG(16:1/17:0/21:0)
172	20.36	0.0210	UP	918.7551	10.19	TG(18:3/18:3/20:3)
484	18.10	0.0071	UP	888.7942	10.58	TG(17:2/18:0/18:1)
6	17.72	0.0018	UP	880.7398	10.18	TG(16:1/17:2/20:4)

280	16.99	0.0214	UP	948.713	10.17	TG(18:2/20:3/20:3)
43	16.02	0.0194	UP	914.7233	9.92	TG(18:3/18:3/20:5)
399	15.61	0.0090	UP	858.7554	10.36	TG(15:0/16:0/20:4)
252	13.44	0.0144	UP	854.7231	10.14	TG(17:2/17:2/17:2)
131	12.56	0.0408	UP	933.786	10.87	TG(18:0/18:2/20:0)
10	11.87	0.0103	UP	940.7392	10	TG(18:2/20:5/20:5)
319	11.84	0.0218	UP	980.8641	11.11	TG(20:0/20:3/20:3)
200	10.88	0.0034	UP	663.4964	7.74	1-dodecanoyl-2-heneicosanoyl-glycero-3-phosphate
78	9.89	0.0084	UP	860.7618	10.36	TG(13:0/18:3/20:0)
434	9.35	0.0215	UP	892.8344	11.02	TG(17:1/18:0/18:0)
45	9.04	0.0070	UP	830.7238	10.13	TG(12:0/15:0/22:4
110	8.69	0.0114	UP	792.7085	10.11	TG(16:1/14:0/16:1)
69	8.24	0.0000	UP	920.864	11.23	TG(18:3/18:3/20:2)
322	7.99	0.0022	UP	966.754	10.09	TG(20:3/20:5/20:5)
17	7.63	0.0050	UP	900.8032	10.65	TG(16:0/18:0/20:4)
100	6.74	0.0002	UP	988.9273	11.53	TG(20:0/20:1/20:1)
186	6.71	0.0414	UP	857.7417	10.27	TG(17:0/17:2/17:2)
246	6.50	0.0098	UP	851.781	10.56	TG(14:0/14:0/22:0)
176	6.32	0.0098	UP	888.7084	9.86	TG(17:1/18:1/18:1)
207	6.14	0.0134	UP	940.8329	10.88	TG(18:2/20:5/20:5)
170	5.80	0.0078	UP	894.8407	11.02	TG(18:3/18:3/20:3)
487	5.73	0.0330	UP	921.7744	10.34	TG(17:0/18:3/20:0)
44	5.45	0.0027	DOWN	868.7396	10.22	TG(16:0/16:1/20:5)
220	4.62	0.0168	DOWN	796.6345	9.97	N-(tricosanoyl)-hexadecasphing-4-enine-1-phosphocholine
31	4.54	0.0121	DOWN	840.7078	9.96	TG(18:3/14:0/18:3)
37	4.38	0.0204	UP	805.7113	10.09	TG(14:0/14:0/19:1)
209	4.29	0.0011	DOWN	855.7267	10.13	TG(16:0/16:0/18:1)
249	4.21	0.0252	UP	962.723	9.81	TG(20:5/20:5/20:5)
241	3.89	0.0040	DOWN	841.725	10.58	TG(16:0/16:1/17:0)
495	3.62	0.0160	DOWN	839.7094	10.48	TG(13:0/18:1/18:1)
272	2.43	0.0096	DOWN	834.2399	8.86	N-(tetracosanoyl)-sphinganine-1-phosphocholine
415	2.37	0.0015	DOWN	813.6942	10.35	TG(15:0/15:0/17:1)
274	159.73	0.0422	UP	949.8058	10.56	NA
168	123.91	0.0018	UP	951.8207	10.68	NA
254	93.59	0.0269	UP	902.9913	10.81	NA
149	85.14	0.0240	UP	945.7744	10.27	NA
1	80.72	0.0045	UP	929.8376	10.89	NA
60	71.78	0.0139	UP	955.8523	10.91	NA

144	49.10	0.0459	UP	895.7591	10.32	NA
234	47.76	0.0082	UP	950.8091	10.56	NA
76	45.97	0.0092	UP	911.7906	10.53	NA
80	37.05	0.0357	UP	917.7424	10.13	NA
351	34.61	0.0442	UP	909.7752	10.43	NA
21	22.06	0.0047	UP	902.809	10.65	NA
16	20.73	0.0017	UP	901.8063	10.65	NA
425	19.60	0.0089	UP	947.7094	10.17	NA
367	18.03	0.0124	UP	925.7254	10.34	NA
364	16.76	0.0202	UP	893.7422	10.1	NA
479	15.85	0.0140	UP	949.7249	10.26	NA
222	15.74	0.0048	UP	591.5699	11.29	NA
121	14.98	0.0186	UP	967.7578	10.09	NA
9	13.86	0.0158	UP	941.7425	10	NA
489	9.06	0.0068	UP	945.8688	11.14	NA
229	7.73	0.0118	UP	861.7757	10.6	NA
297	7.21	0.0093	UP	931.7584	10.22	NA
451	5.20	0.0166	UP	197.0819	9.97	NA
127	4.22	0.0149	UP	907.845	10.99	NA
463	4.12	0.0445	DOWN	793.7121	10.07	NA
500	3.83	0.0001	UP	685.2045	8.1	NA

Table A.9. Meta analysis of Day 1 and Day 7 samples. A list of corresponding *m/z* and retention time values along with potential matches to the METLIN database for the shared dysregulated metabolic features that are significantly altered in all of the technical replicates. NA: Not Assigned, PC: Phophatidylcholine, PE: Phophatidylethanolamine, TG: Triglyceride, DG: Diacylglycerol, SM: Sphingomyelin, CE: Cholesteryl ester, PA: Phophatidic acid, PS: Phophatidylserine, PI: Phosphatidylinositol.

ID	Fold	p-value	Change	*m/z*	Rt	Name
317	97.3	0.0057	UP	922.787	10.5	TG(18:3/18:3/20:1)
312	86.4	0.0064	UP	923.791	10.5	TG(18:0/18:2/19:0)
294	44.7	0.0095	UP	920.7706	10.34	TG(18:3/18:3/20:2)
133	42.4	0.0054	UP	926.817	10.73	TG(18:2/18:3/20:0)
5	40	0.0026	UP	916.8342	10.96	TG(17:0/18:3/20:0)
95	38.6	0.008	UP	928.8339	10.89	TG(18:1/18:3/20:0)
238	38.6	0.008	UP	928.8243	10.73	TG(18:1/18:3/20:0)
430	34.2	0.0107	UP	948.8026	10.56	TG(18:2/20:3/20:3)
125	33.1	0.0277	UP	942.8486	11.01	TG(17:2/20:1/20:1)
121	30.3	0.0007	UP	850.7783	10.56	TG(16:0/16:0/18:1)
43	28.5	0.0126	UP	942.7556	10.17	TG(17:2/20:1/20:1)
209	28.1	0.0284	UP	954.8475	10.92	TG(18:3/20:1/20:1)
54	26.8	0.0148	UP	943.7585	10.17	TG(17:0/20:2/20:2)
355	23.3	0.0008	UP	888.9745	10.74	TG(17:1/18:1/18:1)
76	23.3	0.00086	UP	888.8033	10.75	TG(17:2/18:0/18:1)
69	22.5	0.0475	UP	887.7907	10.59	TG(17:2/18:2/18:2)
32	19.7	0.0174	UP	859.7587	10.36	TG(16:1/17:2/18:0)
161	19.4	0.0029	UP	927.8208	10.73	TG(18:3/18:3/20:1)
275	19.4	0.0029	UP	927.741	10.5	TG(18:3/18:3/20:1)
232	16.7	0.082	UP	910.7871	10.53	TG(17:2/18:3/20:1)
399	16.5	0.0156	UP	918.842	10.96	TG(18:3/18:3/20:3)
10	16.1	0.0472	UP	886.7875	10.59	TG(17:2/18:1/18:1)
20	15	0.0031	UP	877.8062	10.78	TG(17:2/17:2/18:0)
416	12.6	0.0314	UP	904.8339	10.99	TG(16:1/16:1/22:0)
200	12.5	0.0021	UP	849.7749	10.56	TG(16:0/17:1/17:1)
332	12.4	0.0157	UP	908.7718	10.43	TG(17:2/18:3/20:2)
27	12	0.0399	UP	933.8683	11.19	TG(18:0/18:2/20:0)
213	12	0.0399	UP	932.8647	11.19	TG(18:0/18:2/20:0)
51	11.4	0.0074	UP	860.7626	10.4	TG(13:0/18:3/20:0)
93	11.3	0.0184	DOWN	663.4958	7.74	1-dodecanoyl-2-heneicosanoyl-glycero-3-phosphate
217	10.9	0.0132	UP	892.8333	11.02	TG(17:1/18:0/18:0)
82	9.9	0.0137	DOWN	834.7471	10.33	N-(tetracosanoyl)-sphinganine-1-phosphocholine
109	9.2	0.0123	UP	899.79	10.52	TG(17:2/17:2/20:3)
250	9.2	0.0132	UP	899.7091	10.35	TG(17:2/17:2/20:3)
211	8.7	0.0045	UP	844.7394	10.23	TG(16:0/17:2/17:2)
123	8.4	0.0221	UP	960.896	11.39	TG(18:2/20:0/20:0)
181	8.1	0.0044	UP	854.723	10.14	TG(17:2/17:2/17:2)
4	7.4	0.024	UP	920.8555	11.13	TG(18:0/18:1/19:0)

87	7.3	0.0154	UP	940.7387	10	TG(18:2/20:5/20:5)
282	6.9	0.0129	UP	921.7741	10.34	TG(17:0/18:3/20:0)
122	6.7	0.0061	DOWN	795.7274	10.27	N-(tricosanoyl)-hexadecasphing-4-enine-1-phosphocholine
163	6.7	0.0061	DOWN	795.6317	9.97	N-(tricosanoyl)-hexadecasphing-4-enine-1-phosphocholine
11	6.3	0.0153	UP	889.8064	10.75	TG(16:1/17:0/20:1)
49	6.3	0.0153	UP	891.8216	10.92	TG(16:1/17:0/20:1)
428	6.3	0.0153	UP	890.8142	10.84	TG(16:1/17:0/20:1)
129	5.9	0.0098	UP	806.7241	10.24	TG(13:0/17:1(9Z)/17:1(9Z))
319	5.3	0.0118	UP	937.8185	11.19	TG(18:0/18:2/20:0)
144	5.3	0.0396	UP	840.7072	9.96	TG(18:3/14:0/18:3)
182	5.2	0.0033	UP	769.6311	9.81	TG(12:0/12:0/20:2(11Z,14Z))
33	5.2	0.0272	UP	906.8492	11.16	TG(16:1/17:0/21:0)
21	4.8	0.0117	UP	766.6917	10.01	TG(13:0/13:0/18:1)
151	4.7	0.0165	UP	752.6768	9.84	TG(12:0/12:0/19:1(9Z))
306	4.7	0.0143	UP	797.6625	10.08	TG(16:1/14:0/16:1)
120	4.5	0.0057	UP	878.8165	10.87	TG(17:0/17:1/18:0)
141	4.2	0.0036	UP	794.7245	10.27	TG(16:0/14:0/16:1)
91	2.5	0.0015	DOWN	855.7269	10.13	TG(16:0/16:0/18:1)
260	2.3	0.0282	UP	823.7575	10.43	beta-hydroarchaetidylglyerol
102	2.3	0.0073	UP	822.7537	10.42	TG(16:0/16:0/16:1)
373	2.1	0.0106	DOWN	841.7233	10.59	TG(16:0/16:1/17:0)
45	49	0.0059	UP	929.8373	10.89	NA
67	15.6	0.0077	UP	883.7586	10.3	NA
68	17.6	0.0007	UP	861.7748	10.61	NA
99	19.6	0.207	UP	944.7623	10.22	NA
105	15	0.0299	UP	846.7554	10.39	NA
166	8.3	0.0213	UP	941.742	10.01	NA
169	3.6	0.0073	UP	197.0817	9.97	NA
185	13.8	0.0208	UP	947.7903	10.42	NA
190	6.5	0.0015	UP	907.8436	10.99	NA
216	26.6	0.0165	UP	930.8399	10.86	NA
237	5.1	0.0057	UP	894.8401	11.02	NA
259	11.2	0.0155	UP	915.7264	9.92	NA
265	10.9	0.0095	UP	884.763	10.35	NA
307	39.2	0.0363	UP	902.991	10.81	NA
327	16.4	0.0055	UP	909.7749	10.43	NA
331	5.5	0.0124	UP	765.6798	9.86	NA
345	56.9	0.0885	UP	949.8055	10.56	NA
347	18.4	0.095	UP	896.7635	10.31	NA

350	6.1	0.0108	UP	781.7113	10.1	NA
384	3.2	0.0068	UP	864.7942	10.73	NA
389	4.2	0.0288	UP	798.666	10.07	NA

Table A.10. Meta analysis of Day 1 and Day 4 samples. A list of corresponding *m/z* and retention time values along with potential matches to the METLIN database for the shared dysregulated metabolic features that are significantly altered in all of the technical replicates.

ID	Fold	p-value	Change	*m/z*	Rt	Name
53	9.4	0.0242	UP	944.7704	10.27	TG(16:1/20:5/22:4)
131	7	0.047	UP	931.7581	10.22	TG(17:2/20:4/20:4)
5	3.1	0.0146	UP	942.756	10.17	TG(18:3/20:4/20:4)
13	3	0.1365	UP	955.8519	10.91	TG(17:1/19:0/22:3)
50	3	0.027	UP	950.8091	10.56	TG(18:2/20:1/20:4)
65	2.8	0.0096	UP	952.8326	10.79	TG(18:1/20:2/20:3)
19	2.7	0.0291	DOWN	967.7574	10.09	PI(d20:0/26:0)
51	2.5	0.0088	UP	911.791	10.53	TG(17:0/18:2/20:4)
75	2.5	0.0088	UP	910.7879	10.53	TG(17:0/18:3/20:3)
136	2.3	0.018	DOWN	767.6953	10.01	TG(13:0/13:0/18:1(9Z))
14	2.1	0.0202	UP	954.8477	10.91	TG(16:0/20:4/22:1)
87	2.1	0.0018	UP	966.7546	10.09	TG(20:4/20:4/20:5)
143	2	0.0146	UP	945.7741	10.27	TG(20:2/18:3/20:2)
140	4.6	0.0404	UP	591.5689	11.29	NA
77	3	0.0019	UP	953.836	10.79	NA
71	2.1	0.0016	DOWN	1148.326	7.45	NA

Table A.3. Meta analysis of Day 4 and Day 7 samples. A list of corresponding m/z and retention time values along with potential matches to the METLIN database for the shared dysregulated metabolic features that are significantly altered in all of the technical replicates.

Appendix B
Supplementary Material to Chapter 5
Lipidomic Analysis of Enriched Lipid Droplets from Young and Geriatric Mice Reveals Distinct Signatures of Aging

ID	Fold	p-value	Change	*m/z*	Rt	Name
5	44.07	0.0000	UP	850.6753	9.52	TG(16:1/14:0/18:1)
3	37.31	0.0000	UP	849.6723	9.52	PS(O-18:0/22:1(11Z))
11	30.79	0.0001	UP	555.4562	10.29	Demethylspheroidene
30	20.48	0.0005	UP	812.7000	10.29	TG(16:0/14:0/16:1)
25	20.23	0.0004	UP	351.3052	11.10	PA(20:0/22:0)
6	17.31	0.0000	UP	791.6700	11.10	PC(16:0/22:5)
8	13.32	0.0001	UP	809.6800	9.52	TG(12:0/17:0/20:3(8Z,11Z,14 Z))
47	11.71	0.0016	UP	811.6963	10.29	TG(16:0/14:0/16:1(9Z))
19	11.55	0.0002	UP	792.6736	11.10	TG(16:0/14:0/16:1(9Z))
109	11.25	0.0070	UP	931.7710	10.79	TG(18:2/18:3/20:3)
15	9.73	0.0001	UP	501.0962	1.25	2-(Diphenylphosphorothioyl)-3-methyl-5,6-diphenylphosphinine
113	9.72	0.0072	DOWN	682.6494	11.52	18:1 Campesteryl ester
100	9.12	0.0064	UP	992.9237	11.14	TG(18:3/20:2/20:2)
16	8.27	0.0002	UP	828.6941	9.53	PC(22:6/18:2)
92	7.82	0.0056	DOWN	311.2556	7.94	1-[1,1-Bis(pentyloxy)ethoxy]pentane
110	7.77	0.0072	DOWN	758.7304	7.06	PC(16:0/18:3(6Z,9Z,12Z))
87	7.67	0.0051	DOWN	383.3678	11.53	PC (17:0-17:0)
281	7.66	0.0260	DOWN	640.6031	11.14	Cholesteryl palmitelaidate
28	7.60	0.0005	UP	827.6914	9.53	TG(12:0/17:0/20:3(8Z,11Z,14 Z))
357	7.01	0.0380	DOWN	760.7466	7.45	PE(18:1(11Z)/18:1(9Z))
86	6.64	0.0049	DOWN	384.3709	11.52	PC(20:4/18:1)
359	6.20	0.0383	DOWN	782.5694	6.81	PC(18:2/22:5)
366	5.91	0.0403	UP	892.7403	10.12	TG(17:1/18:2/20:0)
111	5.79	0.0072	DOWN	369.3521	11.65	(5Z,7E)-9,10-seco-5,7,10(19)-cholestatriene
363	5.76	0.0393	UP	177.1650	11.98	1,2-Dihydro-1,1,6-trimethylnaphthalene
68	5.65	0.0031	DOWN	675.6048	11.65	Cholesteryl stearate
267	5.34	0.0237	UP	845.0954	10.28	TG(16:1/17:1/17:2)
346	5.21	0.0364	DOWN	641.6061	11.14	Cer(d18:1/23:0)
268	4.99	0.0242	UP	1080.9680	12.33	TG(17:1/17:1/17:1)
234	4.75	0.0195	DOWN	813.6845	8.49	SM(d18:2/24:0)
303	4.64	0.0288	UP	517.3864	4.56	TG(16:1/18:3/20:5)
233	4.57	0.0193	DOWN	849.1276	10.62	PS(O-18:0/22:1(11Z))
217	4.43	0.0172	DOWN	847.1120	10.45	PC(18:1/20:5)

130	4.42	0.0092	DOWN	833.5888	7.13	PA(22:1(11Z)/22:2(13Z,16Z))
283	4.41	0.0261	DOWN	845.9101	10.28	PC(18:3/22:4)
361	4.36	0.0388	DOWN	856.7398	10.24	TG(14:0/15:0/15:0)
254	4.30	0.0222	DOWN	848.1136	10.45	PS(20:0/20:1(11Z))
127	4.27	0.0088	DOWN	807.5732	6.78	PC(20:4/18:1)
285	4.16	0.0266	DOWN	844.9082	10.28	PC(20:4/16:0)
331	4.05	0.0340	DOWN	780.5536	6.72	PC(16:0/22:4)
152	4.04	0.0106	DOWN	831.5730	6.74	PC(20:4/20:4)
194	4.03	0.0145	DOWN	670.6488	11.66	18:0 Cholesteryl ester
150	4.01	0.0105	DOWN	832.5854	7.13	PC(20:3(8Z,11Z,14Z)/16:0)
161	3.98	0.0113	DOWN	830.5695	6.74	PC(22:6/18:2)
91	3.86	0.0055	UP	202.0339	1.39	[6-(Methanesulfonyl)pyridin-3-yl]boronic acid
222	3.81	0.0175	UP	844.7403	10.28	TG(16:0/17:2/17:2)
76	3.81	0.0037	UP	470.3106	5.03	TG(16:0/14:0/16:1)
409	3.80	0.0483	DOWN	756.5545	6.61	PC(15:1(9Z)/20:1(11Z))
173	3.79	0.0121	DOWN	806.5697	6.79	PC(18:1/22:6)
210	3.79	0.0167	UP	882.7550	10.30	TG(17:2/18:2/18:2)
314	3.79	0.0304	DOWN	766.5384	7.00	PC(22:6/18:1)
408	3.75	0.0482	DOWN	894.7466	10.11	PC(22:6/18:2)
232	3.70	0.0193	DOWN	812.6159	7.90	PC(18:1/20:4)
274	3.69	0.0251	DOWN	767.5418	7.00	PE(20:2(11Z,14Z)/16:0)
242	3.68	0.0206	DOWN	847.9253	10.45	PC(16:0/22:6)
145	3.67	0.0102	UP	595.4699	8.07	DG(16:0/16:0/0:0)
247	3.67	0.0213	DOWN	849.9413	10.62	PS(18:0/22:0)
367	3.65	0.0403	DOWN	787.6689	8.45	SM(d18:1/22:0)
371	3.59	0.0406	UP	929.7541	10.63	TG(18:0/14:0/16:1(9Z))
105	3.59	0.0068	DOWN	1020.9890	12.06	TG(20:2/22:0/22:0)
297	3.51	0.0283	UP	883.7589	10.30	TG(17:2/19:0/20:4)
209	3.51	0.0166	DOWN	809.5890	7.17	SM(d18:1/22:0)
414	3.51	0.0494	DOWN	669.6381	11.39	PC(15:0/19:3(9Z,12Z,15Z))
243	3.49	0.0206	DOWN	814.6234	7.90	TG(16:1/16:1/18:0)
258	3.47	0.0227	DOWN	810.5919	7.17	PA(22:1(11Z)/22:0)
72	3.47	0.0033	UP	422.2726	4.24	Ammonium diheptylnaphthalenesulphonate
94	3.45	0.0057	DOWN	911.6528	9.94	TG(17:2/17:2/20:5)
413	3.43	0.0490	DOWN	871.1178	10.35	PE(19:0/0:0)
378	3.42	0.0423	DOWN	668.6349	11.39	CE(18:1/0:0)
266	3.40	0.0235	UP	596.4731	8.06	TG(17:0/18:2/20:1)
190	3.37	0.0140	DOWN	830.5667	7.17	PC(20:5(5Z,8Z,11Z,14Z,17Z)/15:0)
332	3.37	0.0346	DOWN	813.6200	7.90	N-(15Z-tetracosenoyl)-sphing-4-enine-1-phosphocholine
265	3.36	0.0234	UP	845.7438	10.28	TG(16:1/16:1/18:2)
187	3.35	0.0137	DOWN	834.5917	7.13	PA(20:0/22:0)
102	3.34	0.0064	UP	157.1017	9.98	2,2-Dimethyl-2H-indene
405	3.27	0.0476	DOWN	940.7394	10.06	TG(20:0/20:0/22:0)

159	3.26	0.0112	DOWN	893.8359	11.11	PC(18:1/22:6)
156	3.24	0.0110	DOWN	870.5402	7.13	PC(18:3(6Z,9Z,12Z)/18:0)
193	3.22	0.0144	DOWN	808.5856	7.17	PC(16:0/22:5)
164	3.21	0.0115	DOWN	854.5668	7.13	PC(20:5(5Z,8Z,11Z,14Z,17Z)
396	3.21	0.0465	UP	1098.9430	11.53	TG(14:0/18:4(6Z,9Z,12Z,15Z)/22:4(7Z,10Z,13Z,16Z))
306	3.21	0.0293	UP	1095.9870	12.18	TG(15:0/15:0/16:1(9Z))
141	3.19	0.0100	DOWN	645.5601	11.15	Cholesteryl palmitelaidate
174	3.17	0.0123	DOWN	855.5701	7.13	PC(16:0/22:5(4Z,7Z,10Z,13Z,16Z))
280	3.17	0.0260	DOWN	772.5848	7.39	PE(20:2(5Z,8Z)/18:0)
148	3.17	0.0104	DOWN	892.8322	11.11	TG(16:1(9Z)/17:1(9Z)/17:2(9Z,12Z))
368	3.16	0.0404	UP	1103.8950	11.34	TG(13:0/13:0/22:1(11Z))
279	3.14	0.0258	UP	1099.9470	11.55	TG(17:1/17:2/18:3)
301	3.13	0.0285	UP	846.7465	10.28	TG(18:0/18:2/19:0)
160	3.12	0.0113	DOWN	831.5703	7.17	PC(16:0/22:5)
333	3.11	0.0347	DOWN	870.9271	10.35	PC(18:2/18:2)
375	3.10	0.0416	DOWN	745.5579	7.40	PC(14:0/20:3(5Z,8Z,11Z))
269	3.09	0.0244	UP	918.8478	11.14	TG(14:1(9Z)/18:2(9Z,12Z)/22:5(7Z,10Z,13Z,16Z,19Z))
125	3.08	0.0087	UP	145.1016	9.98	2,2-Dimethyl-2H-indene
155	3.07	0.0109	DOWN	646.5632	11.15	CE(16:1)
321	3.07	0.0311	DOWN	667.6221	11.20	PE(18:2(9Z,12Z)/19:1(9Z))
178	3.04	0.0129	UP	847.5424	7.17	TG(18:0/14:0/16:1)
251	3.04	0.0220	DOWN	811.6196	9.94	PA(O-16:0/14:0)
246	3.04	0.0206	DOWN	832.7400	10.33	PC(20:1(11Z)/20:1(11Z))
61	3.03	0.0025	UP	928.7446	10.62	TG(16:1/20:5/22:6)
93	3.02	0.0056	UP	927.7419	10.62	TG(18:3/20:2/20:2)
89	3.00	0.0052	UP	443.2820	4.24	Diethylene glycol monooleate
206	3.00	0.0163	UP	892.8246	10.95	TG(17:2/17:2/20:5)
182	2.99	0.0133	DOWN	822.5409	7.19	PC(18:0/20:3)
202	2.98	0.0158	UP	643.3635	9.44	Cholesteryl palmitelaidate
298	2.97	0.0283	DOWN	727.5671	9.48	Cholesteryl 11-hydroperoxy-eicosatetraenoate
60	2.97	0.0024	UP	563.4440	8.43	1-tetradecanyl-2-(8-[3]-ladderane-octanyl)-sn-glycerol
134	2.96	0.0096	UP	1065.9210	11.27	Tricyclo(4.4.2.0(1,6))dodeca-2,4,7,9-tetraene
129	2.95	0.0091	UP	564.4469	8.59	1-tetradecyl-2-acetyl-sn-glycero-3-phosphocholine
257	2.93	0.0226	DOWN	852.5515	6.74	PC(20:4/22:6)
290	2.90	0.0271	DOWN	858.7553	10.40	PC(16:0/18:3(6Z,9Z,12Z))
271	2.90	0.0248	UP	890.8183	10.95	TG(13:0/18:4(6Z,9Z,12Z,15Z)/20:1(11Z))
62	2.89	0.0026	UP	307.2614	9.98	2,6-dimethyl-hexadecanoic acid

239	2.86	0.0204	UP	941.6986	10.46	TG(12:0/21:0/22:3(10Z,13Z,16Z))
77	2.86	0.0038	UP	472.3115	5.04	octadecyldimethylsilanol
347	2.84	0.0367	UP	916.8337	10.98	TG(17:0/19:1(9Z)/19:1(9Z))
275	2.83	0.0252	DOWN	534.2960	2.96	LPC(16:0/0:0)
349	2.81	0.0372	DOWN	846.9242	10.45	PC(16:1/22:6)
308	2.80	0.0297	UP	917.8362	10.98	TG(17:2/17:2/20:4)
168	2.78	0.0119	DOWN	863.7896	10.75	PC(18:1/22:6)
330	2.76	0.0340	DOWN	744.5540	6.76	PS(18:0/22:0)
13	2.74	0.0001	UP	753.4884	6.52	DG(22:5/22:6/0:0)
307	2.73	0.0296	DOWN	891.8212	10.95	TG(17:1/17:2/18:3)
390	2.72	0.0455	DOWN	804.5543	6.55	PC(16:0/20:4)
244	2.69	0.0206	DOWN	786.5917	7.21	SM(d18:1/24:1(15Z))
97	2.68	0.0061	UP	442.2793	4.24	TG(12:0/15:1(9Z)/22:2(13Z,16Z))
328	2.68	0.0335	DOWN	822.7554	10.58	PE(18:1(11Z)/20:4(8Z,11Z,14Z,17Z))
221	2.68	0.0175	DOWN	778.5362	6.59	PC(16:0/20:4(5E,8E,11E,14E))
18	2.67	0.0002	UP	725.4567	5.80	DG(20:5/22:6/0:0)
203	2.65	0.0159	DOWN	627.4958	7.86	DG(17:1/20:5/0:0)
133	2.64	0.0096	DOWN	895.6791	9.94	TG(17:2/17:2/20:5)
310	2.63	0.0300	UP	945.7745	10.45	TG(14:0/20:2(11Z,14Z)/21:0)
295	2.61	0.0280	UP	185.1333	9.98	Chamazulene
397	2.60	0.0467	UP	859.7585	10.40	TG(13:0/13:0/22:4(7Z,10Z,13Z,16Z))
398	2.57	0.0468	DOWN	884.7706	10.45	PE(20:1(11Z)/16:1(9Z))
112	2.55	0.0072	DOWN	864.8022	10.91	TG(17:0/17:0/17:1)
115	2.55	0.0075	UP	865.8049	10.91	TG(17:0/17:2/17:2)
343	2.54	0.0359	DOWN	868.7407	10.19	PE(18:0/18:2)
196	2.51	0.0148	UP	796.7309	10.33	TG(16:0/14:0/16:1)
374	2.50	0.0416	UP	794.7241	10.33	TG(16:0/16:1/18:3)
394	2.48	0.0463	DOWN	733.5575	6.88	DG(22:6/20:5)
299	2.48	0.0284	DOWN	860.7709	10.57	TG(17:1/17:1/17:1)
294	2.46	0.0280	UP	861.7738	10.57	TG(13:0/18:2(9Z,12Z)/22:0)
341	2.44	0.0357	DOWN	795.7268	10.33	PE(21:0/20:3(8Z,11Z,14Z))
237	2.44	0.0197	UP	623.5004	8.56	TG(18:2/20:5/20:5)
322	2.44	0.0322	UP	862.7772	10.57	TG(16:0/17:2/17:2)
389	2.43	0.0451	UP	820.7401	10.40	TG(16:1/16:1/18:2)
406	2.43	0.0480	DOWN	826.7767	10.76	PC(17:1(9Z)/18:4(6Z,9Z,12Z,15Z))
315	2.39	0.0304	DOWN	824.7614	10.58	PC(16:1/22:6)
377	2.37	0.0419	UP	617.5866	11.40	TG(13:0/18:2(9Z,12Z)/20:1(11Z))
63	2.34	0.0028	UP	561.5246	10.99	1-tetradecanyl-2-(8-[3]-ladderane-octanyl)-sn-glycerol
215	2.34	0.0170	UP	955.7716	10.78	TG(18:3/20:4/20:5)
407	2.31	0.0482	DOWN	823.7584	10.58	PE(22:2/14:0)

325	2.30	0.0331	DOWN	750.5516	9.49	PC(17:2(9Z,12Z)/19:1(9Z))
404	2.29	0.0475	UP	596.4741	7.44	TG(17:0/17:0/17:1)
352	2.28	0.0373	DOWN	658.6108	8.78	Cer(d18:1/23:0)
230	2.28	0.0190	UP	891.7756	11.09	TG(16:1/17:1/18:1)
340	2.27	0.0357	UP	862.7864	10.75	TG(16:0/18:1/19:0)
403	2.27	0.0475	UP	935.8765	11.24	TG(18:3/18:3/20:1)
410	2.27	0.0486	UP	595.4704	7.28	TG(18:3/18:3/18:3)
344	2.25	0.0363	DOWN	749.5483	9.49	DG(21:0/22:6/0:0)
108	2.22	0.0070	DOWN	991.9198	11.14	TG(18:3/20:2/20:2)
393	2.21	0.0461	DOWN	864.6562	10.12	PC(20:2/20:5)
355	2.21	0.0375	UP	444.2796	4.24	Diethylene glycol monooleate
379	2.19	0.0425	DOWN	459.3295	1.22	2,5-Bis(octyloxy)-4-[(trimethylsilyl)ethynyl]benzaldehyde
384	2.19	0.0439	DOWN	837.6352	10.03	PA(22:1(11Z)/22:2(13Z,16Z))
391	2.19	0.0455	DOWN	768.7081	10.29	TG(14:0/17:2(9Z,12Z)/22:3(10Z,13Z,16Z))
188	2.18	0.0137	UP	918.7028	10.42	TG(18:2/18:3/18:3)
386	2.16	0.0442	DOWN	371.3594	11.37	Neomethymycin
416	2.16	0.0495	DOWN	769.7112	10.29	PE(20:2(5Z,8Z)/18:0)
311	2.14	0.0301	UP	897.6947	10.11	TG(17:0/18:0/18:2)
376	2.14	0.0417	DOWN	922.6975	10.09	TG(18:2/18:3/20:0)
334	2.12	0.0347	UP	898.6977	10.12	TG(17:1/17:1/17:2)
387	2.11	0.0447	DOWN	823.7488	10.39	PC(16:1/22:6)
320	2.11	0.0308	DOWN	872.6811	10.05	SM (d18:1/12:0)
189	2.11	0.0139	UP	921.8233	11.41	TG(17:2/18:1/18:3)
382	2.09	0.0430	DOWN	257.2271	11.36	1,4a-dimethyl-7-(propan-2-yl)-1,2,3,4,4a,9,10,10a-octahydrophenanthrene
201	2.08	0.0153	DOWN	784.7234	10.93	PC(16:0/20:5)
48	2.08	0.0017	UP	486.4159	5.74	12-[Bis(2-hydroxyethyl)amino]-12-oxododecyl dodecanoate
211	2.08	0.0170	UP	783.7199	10.93	TG(17:2/18:2/18:2)
123	2.07	0.0084	DOWN	550.5931	10.43	PE(19:0/18:3(9Z,12Z,15Z))
336	2.02	0.0350	UP	575.5047	10.68	TG(17:1/17:2/20:5)
329	2.02	0.0338	DOWN	588.4687	7.48	PC(16:1/22:6)
54	28.8	0.002	DOWN	1102.055	12.308	NA
65	26.5	0.003	DOWN	1139.065	12.293	NA
55	23	0.002	DOWN	1101.052	12.301	NA
58	18.7	0.002	DOWN	1100.041	12.16	NA
59	16.8	0.002	DOWN	1140.07	12.293	NA
2	15.7	2E-06	UP	1048.913	11.102	NA
1	14.8	1E-06	UP	1047.91	11.098	NA
83	14.4	0.005	DOWN	1099.037	12.16	NA
184	12.4	0.013	UP	1123.015	12.644	NA
179	12.1	0.013	UP	1124.018	12.647	NA

66	10.9	0.003	DOWN	1126.055	12.182	NA
158	10.4	0.011	DOWN	1128.07	12.331	NA
95	9.89	0.006	UP	1099.94	12.438	NA
120	9.58	0.008	UP	1100.942	12.43	NA
140	9.45	0.01	DOWN	1155.098	12.529	NA
116	8.89	0.008	UP	1095.988	12.434	NA
99	8.74	0.006	UP	1094.984	12.432	NA
227	8.7	0.019	UP	1080.932	11.401	NA
176	8.58	0.013	DOWN	1127.067	12.333	NA
153	8.53	0.011	DOWN	1156.101	12.529	NA
181	8.11	0.013	UP	1078.961	12.438	NA
69	7.93	0.003	DOWN	1151.066	12.26	NA
229	7.64	0.019	UP	1077.957	12.434	NA
137	7.54	0.01	DOWN	1154.086	12.389	NA
106	7.4	0.007	DOWN	1153.082	12.389	NA
273	7.03	0.025	DOWN	680.634	11.329	NA
12	6.68	1E-04	UP	471.0857	1.2465	NA
121	6.67	0.008	UP	1081.972	12.331	NA
50	6.64	0.002	UP	1122.003	12.464	NA
96	6.58	0.006	UP	1096.991	12.432	NA
44	6.47	0.001	UP	1120.999	12.468	NA
27	6.43	5E-04	UP	1097.993	12.434	NA
79	6.34	0.004	UP	1137.022	12.434	NA
32	6.32	6E-04	UP	1195.123	11.721	NA
46	6.19	0.001	UP	1139.032	12.434	NA
10	6.08	7E-05	UP	1076.945	11.846	NA
24	6.03	3E-04	UP	1196.125	11.721	NA
98	5.99	0.006	UP	1082.976	12.335	NA
162	5.86	0.011	UP	1071.907	12.226	NA
114	5.83	0.007	DOWN	1182.116	12.59	NA
64	5.53	0.003	UP	1067.142	12.234	NA
17	5.49	2E-04	UP	1096.991	12.177	NA
20	5.49	2E-04	UP	1138.027	12.43	NA
124	5.46	0.009	DOWN	397.3832	11.61	NA
175	5.3	0.012	DOWN	381.3523	11.321	NA
70	5.13	0.003	UP	1136.011	12.427	NA
250	4.99	0.022	UP	199.1488	9.2729	NA
126	4.92	0.009	DOWN	370.3555	11.65	NA
56	4.92	0.002	UP	1052.936	12.149	NA
34	4.9	7E-04	UP	1118.984	12.312	NA
52	4.9	0.002	UP	1053.941	12.147	NA
33	4.89	6E-04	UP	1048.913	11.666	NA
183	4.82	0.013	DOWN	383.3678	11.321	NA
39	4.8	9E-04	UP	1119.987	12.309	NA
195	4.75	0.015	DOWN	384.371	11.327	NA
132	4.72	0.009	DOWN	1181.113	12.597	NA

21	4.71	2E-04	UP	1068.96	12.234	NA
45	4.67	0.001	UP	1047.909	11.666	NA
278	4.56	0.026	UP	213.1647	9.2663	NA
37	4.52	8E-04	UP	1021.895	11.632	NA
4	4.5	2E-05	UP	1079.964	11.985	NA
9	4.48	6E-05	UP	1077.958	11.982	NA
7	4.47	3E-05	UP	1078.961	11.982	NA
23	4.45	2E-04	UP	1075.939	11.846	NA
49	4.31	0.002	UP	1080.968	12.167	NA
53	4.18	0.002	UP	1066.954	12.233	NA
74	4.18	0.003	UP	1098.996	12.434	NA
40	4.15	0.001	UP	1022.898	11.632	NA
107	4.06	0.007	UP	178.1679	11.985	NA
26	4.02	4E-04	UP	492.2923	5.0213	NA
84	4	0.005	UP	1049.927	12.23	NA
149	4	0.01	UP	1050.929	12.23	NA
136	3.93	0.01	DOWN	1125.05	12.182	NA
35	3.93	7E-04	UP	1118.98	12.147	NA
14	3.83	1E-04	UP	1049.926	11.807	NA
177	3.82	0.013	DOWN	1017.936	11.192	NA
287	3.8	0.027	DOWN	1018.939	11.192	NA
142	3.8	0.01	DOWN	1020.956	11.387	NA
36	3.77	7E-04	UP	1066.954	12.069	NA
90	3.73	0.005	UP	1091.956	12.123	NA
71	3.72	0.003	UP	1090.953	12.121	NA
167	3.71	0.012	UP	1069.892	11.658	NA
192	3.69	0.014	UP	159.1172	9.2654	NA
78	3.69	0.004	UP	1067.957	12.232	NA
131	3.68	0.009	UP	143.0856	9.9803	NA
169	3.66	0.012	DOWN	1021.959	11.387	NA
42	3.64	0.001	UP	1092.966	12.114	NA
200	3.62	0.015	UP	145.1015	9.2654	NA
67	3.61	0.003	UP	1050.929	12.063	NA
236	3.58	0.02	DOWN	688.6094	11.526	NA
104	3.58	0.007	UP	1051.933	12.237	NA
214	3.57	0.017	DOWN	1019.952	11.389	NA
29	3.55	5E-04	UP	1107.98	12.232	NA
276	3.48	0.025	UP	1126.972	11.693	NA
122	3.46	0.008	UP	1116.962	12.154	NA
381	3.43	0.043	DOWN	1130.012	11.299	NA
22	3.37	2E-04	UP	1050.929	11.804	NA
73	3.29	0.003	UP	1092.969	12.275	NA
80	3.29	0.004	UP	1109.998	12.234	NA
88	3.28	0.005	UP	158.107	9.9823	NA
228	3.27	0.019	UP	1070.894	11.659	NA
82	3.23	0.005	UP	1066.924	11.269	NA

163	3.21	0.011	UP	119.0857	9.9893	NA
219	3.2	0.017	UP	595.4702	7.4417	NA
51	3.14	0.002	UP	1051.933	11.807	NA
165	3.07	0.012	UP	554.3315	5.9481	NA
43	3.05	0.001	UP	1093.972	12.269	NA
38	3.02	9E-04	UP	1051.933	12.059	NA
101	2.99	0.006	UP	172.1222	9.9781	NA
75	2.95	0.003	UP	1108.992	12.07	NA
399	2.93	0.047	UP	1039.925	11.629	NA
135	2.91	0.01	UP	1094.984	12.241	NA
380	2.91	0.043	UP	596.4736	7.2838	NA
362	2.9	0.039	UP	1140.978	11.529	NA
57	2.89	0.002	UP	1049.926	12.056	NA
348	2.87	0.037	UP	1108.992	12.233	NA
171	2.81	0.012	UP	307.2041	8.5588	NA
191	2.8	0.014	DOWN	687.6074	11.526	NA
41	2.79	0.001	UP	1135.006	12.286	NA
253	2.77	0.022	DOWN	618.619	8.7756	NA
146	2.75	0.01	UP	471.3133	5.0384	NA
316	2.74	0.031	DOWN	351.2273	4.464	NA
241	2.74	0.021	UP	641.3656	9.4436	NA
286	2.74	0.027	UP	536.8963	7.6779	NA
170	2.67	0.012	UP	563.4438	8.5972	NA
81	2.66	0.005	UP	1107.98	12.066	NA
213	2.62	0.017	UP	159.1174	9.982	NA
118	2.59	0.008	UP	464.261	4.2408	NA
264	2.59	0.023	UP	171.1173	9.9832	NA
144	2.53	0.01	UP	508.7142	7.0944	NA
147	2.52	0.01	UP	1093.971	11.849	NA
345	2.52	0.036	UP	417.0752	1.2502	NA
289	2.51	0.027	UP	555.3347	5.9481	NA
365	2.47	0.04	UP	213.1648	9.9821	NA
335	2.46	0.035	DOWN	295.0924	1.391	NA
360	2.45	0.038	UP	173.133	9.3987	NA
317	2.43	0.031	DOWN	1112.035	12.093	NA
245	2.42	0.021	UP	147.1173	9.9821	NA
154	2.41	0.011	DOWN	550.6283	8.1677	NA
277	2.41	0.025	DOWN	370.3561	11.391	NA
260	2.4	0.023	UP	199.149	9.9848	NA
288	2.4	0.027	DOWN	369.3527	11.389	NA
103	2.37	0.007	UP	1097.923	11.849	NA
128	2.36	0.009	UP	1071.907	12.068	NA
358	2.36	0.038	DOWN	519.3255	2.9611	NA
263	2.33	0.023	DOWN	149.0237	5.2268	NA
208	2.31	0.016	DOWN	394.3014	5.0542	NA
259	2.28	0.023	UP	576.3129	5.9481	NA

342	2.25	0.036	DOWN	129.0547	5.0571	NA
31	2.23	5E-04	DOWN	116.9678	12.012	NA
386	2.16	0.044	DOWN	371.3594	11.375	NA
282	2.14	0.026	UP	173.1331	9.9931	NA
351	2.14	0.037	UP	105.0699	9.5956	NA
302	2.12	0.029	DOWN	393.298	5.0571	NA
172	2.11	0.012	UP	536.7489	7.6779	NA
356	2.11	0.038	UP	1109.998	12.066	NA
224	2.09	0.018	UP	1098.924	11.845	NA
261	2.08	0.023	UP	1072.91	12.072	NA
262	2.08	0.023	DOWN	428.3056	1.22	NA
337	2.01	0.035	UP	91.05358	9.5957	NA

Table B.11. Summary of significant features of enriched lipid droplets from young and old mouse liver observed in positive electrospray ionization. NA: Not Assigned, PC: Phophatidylcholine, PE: Phophatidylethanolamine, SM: Sphingomyelin, CE: Cholesteryl ester, PA: Phophatidic acid, PS: Phophatidylserine, TG: Triglyceride, DG: Diacylglycerol.

ID	Fold	p-value	Change	*m/z*	Rt	Name
2	93.96	0.0009	UP	983.4781	1.51	Lanatoside
6	3.45	0.0089	DOWN	473.2378	5.95	PC(22:6/15:0)
8	3.24	0.0139	DOWN	772.5848	6.39	PE(18:1/20:4)
1	3.05	0.0005	UP	254.2486	4.24	Palmitamide
9	2.54	0.014	DOWN	182.1185	1.39	Ethyl 3-(piperidin-1-yl) prop-2-enoate
7	2.31	0.013	DOWN	764.523	7.01	PC(15:0/20:5)
12	2.05	0.0417	UP	790.5383	7.38	PE(18:0/22:6)
10	2	0.021	DOWN	605.4539	6.56	PA(16:0/14:1)
3	3.29	0.0015	UP	553.319	5.95	NA
4	3.23	0.0031	UP	245.0398	1.39	NA
5	2.98	0.0059	UP	552.3158	1.79	NA
11	2.06	0.0407	UP	791.5418	7.38	NA

Table B.12. Summary of significant features of enriched lipid droplets from young and old mouse liver observed in negative electrospray ionization.